DISORDER, ITINERANT FERROMAGNETISM, AND THE ANOMALOUS HALL EFFECT IN TWO DIMENSIONS

By

PARTHA MITRA

A DISSERTATION PRESENTED TO THE GRADUATE SCHOOL
OF THE UNIVERSITY OF FLORIDA IN PARTIAL FULFILLMENT
OF THE REQUIREMENTS FOR THE DEGREE OF
DOCTOR OF PHILOSOPHY

UNIVERSITY OF FLORIDA

2006

To my parents for all their sacrifices to provide me the best education.

ACKNOWLEDGMENTS

I am grateful to Art Hebard for giving me the wonderful opportunity to be a part of his lab, which for the last five years was my home away from home. I deeply appreciate the freedom I enjoyed while working under him, nicely balanced by the much needed guidance and support. I have always (secretly) admired his unadulterated enthusiasm, willingness to learn and elegant but simple approach to understanding fundamental physics. I have met some wonderful researchers with diverse personalities during my stay at the Hebard lab and I am proud to be able to collaborate and be a part of the team. In particular I am thankful to Steve for the guidance and training he provided during my early days in the lab.

I thank Khandelkar Muttalib and Peter Wolfle for their interest in the theoretical aspects of my research. In particular I thank K.M. for the numerous discussions we had in the past couple of months. I am thankful to Dimitrii Maslov for teaching the best solid state course and for his useful theoretical insights regarding my research during the few discussions we had. I am thankful to the members of the departmental cryogenic facility, Greg and John, for the wonderful support in the form of an unlimited supply of liquid He, which was indispensable for my research. I also thank the members of the machine shop, the electronic shop and graduate student office for the excellent standards they have maintained over the years.

I am indebted to my parents for their support, encouragement and for always believing in me. I appreciate the sacrifices they made over all these years to provide me

the best education. I could not have come this far without their blessings. I appreciate the warmth and affection of my little sister Mala and is thankful for her understandings while I was not there for her as a big brother for the last several years. I thank my loving wife Shweta for being a part of my life and for her unconditional love and affection. I appreciate her support at the home front while I was busy with my work during the past several months. I am also grateful for the warmth and affection that I received from her family. I am thankful for having a large and wonderful supportive family and appreciate the love and encouragement that I have received, especially from my cousin brothers and sisters. In the end I thank all my friends, roommates, tennis buddies etc. who have touched my life in many ways over the years and apologize for not being able to list everybody's name in here.

TABLE OF CONTENTS

LIST OF TABLES

LIST OF FIGURES

Abstract of Dissertation Presented to the Graduate School
of the University of Florida in Partial Fulfillment of the
Requirements for the Degree of Doctor of Philosophy

DISORDER, ITINERANT FERROMAGNETISM, AND
THE ANOMALOUS HALL EFFECT IN TWO DIMENSIONS

By

Partha Mitra

May 2006

Chair: Arthur F. Hebard
Major Department: Physics

In this dissertation we address the unsettled issue of how long-range magnetic order in band ferromagnetic metals like iron or cobalt is affected by localization of itinerant conduction electrons due to increasing disorder. We study a series of polycrystalline iron films in the thickness range of 2nm to 10nm. The sheet resistances of the films at T=5K is considered to be a measure of disorder and varies over a wide range from 100Ω to 1,000,000Ω. To protect these ultra-thin air sensitive films from oxidation, the experiments were performed in a special homemade high vacuum system, capable of *in-situ* magnetotransport measurement on thin films at low temperatures. To characterize the magnetism in the films, we monitor the anomalous Hall (AH) effect, which refers to the transverse electric potential that develops in magnetic materials in response to an applied charge current, proportional to the volume magnetization.

Our experiments reveal a crossover in the magneto-transport properties for film resistances on the order of $\hbar / e^2 \approx 4.1k\Omega$. Surprisingly, in the high resistance regime

where the samples were found to systematically cross over from a weakly disordered metal to a Mott insulator, the magnitude and temperature dependence of AH resistance does not show a pronounced change. We attribute this so called "anomalous Hall insulating" behavior to the granular morphology of the films, where inter-grain tunneling processes dominate the longitudinal resistance, and the anomalous Hall resistance is determined by the intrinsic ferromagnetic nature of the grains. In the insulating phase long-range ferromagnetic order appears to be absent in the films and we demonstrate the existence of a new resistance scale much greater than $\hbar / e^2$ where correlation between localized magnetic moments as measured by AH effect, disappears. We also demonstrate how the granular morphology of the films allows the two different quantum transport mechanisms in metals, namely weak localization and the Coulomb anomaly, to be distinguished from each other as they have a different effect on the longitudinal and anomalous Hall conductivity. We present a preliminary understanding of the results on the basis of existing theories and some new calculations done in collaboration with theorists.

CHAPTER 1
INTRODUCTION

Recently there has been considerable activity in the field of spintronic devices [1], which rely on the manipulation of spin of conduction electrons in solids and promise to revolutionize microelectronics once spin-polarized electrons can be injected efficiently into semiconductors at room temperatures. Currently, the most widely used spintronic device based on metallic multilayers is the giant magnetoresistive (GMR) spin-valve head for magnetic hard-disk drives. The GMR effect is based on large changes in electrical resistance due to variations in the relative magnetic orientation of layers on either side of a thin spacer layer. Spintronic structures are also at the heart of the proposed magnetic random access memory (MRAM), a fast non-volatile new generation of memory. From a more fundamental point, spintronics studies involve understanding spin transport and spin interaction with the solid-state environment under the influence of applied electromagnetic fields and rely heavily on the results obtained in other branches of physics including magnetism, semiconductor physics, optics and mesoscopic physics. However, there are several major challenges in building a useful spintronic device. These challenges include finding an effective way to polarize a spin system, understanding how long the spins are able to remember their orientation and finding a way for spins to be detected.

Perhaps the simplest way to generate a spin-polarized current is to apply an electric field to the ferromagnetic transition metals, namely iron, cobalt or nickel. The spontaneous magnetization in these band ferromagnets is due to the unequal population

of up (majority) and down (minority) spin electrons in the conduction band. The difference in the spin population results in a spin current coupled with the charge current that flows in response to an applied electric field. This spin current generates a transverse voltage due to spin-dependent asymmetric scattering of electrons from impurities or phonons, a phenomenon known as the anomalous Hall (AH) effect [2] as shown schematically in Fig. 1-1 . The AH effect (AHE) is observed in all ferromagnetic materials regardless of the nature of the exchange mechanism and also in superparamagnetic systems comprising weakly-coupled localized moments. Unlike the ordinary or normal Hall effect, which depends only on the effective carrier density in the material, the AH effect is a transport process that couples the volume magnetization in the material to motion of the itinerant carriers via the spin-orbit interaction. The transverse AH voltage relies on itinerant charge carriers and is directly proportional to the volume magnetization. Thus a thorough characterization of the AH effect is useful for studying magnetic properties in materials especially when direct magnetization measurements via SQUID are not possible.

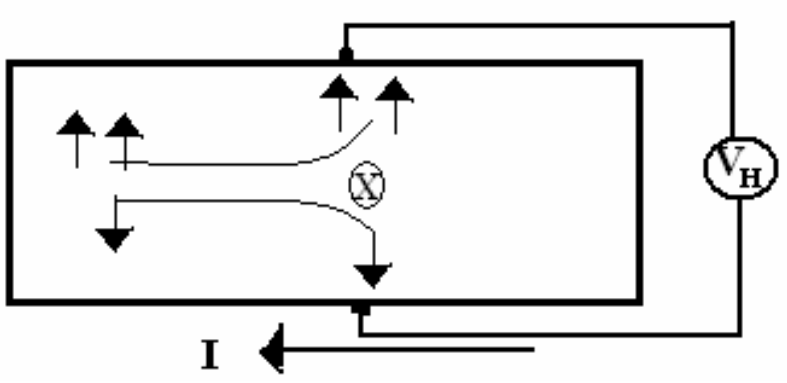

Figure 1-1: A cartoon describing the origin of the anomalous Hall effect in an itinerant ferromagnet with unequal number of spin-up and spin down conduction electrons due to spin dependent scattering of electrons from an impurity X. A transverse electric potential V_H is developed due to accumulation of charges at the edge of the sample.

A related phenomenon, which recently has generated considerable interest, is the spin Hall effect (SHE) [3] where an electric field applied across a doped semiconductor generates a transverse spin current that in equilibrium leads to an accumulation of opposite spins at the film boundaries [4] as shown schematically in Fig. 1-2. This accumulation of spins results in a gradient of spin population in the transverse direction and is not associated with an electric potential because the total number of electrons irrespective of spin orientation remains the same along the transverse direction. Since there is no electronic device that can directly detect spin accumulation potential, it is not possible to directly determine the spin conductivity from any simple scheme analogous to that of the normal or anomalous Hall effect.

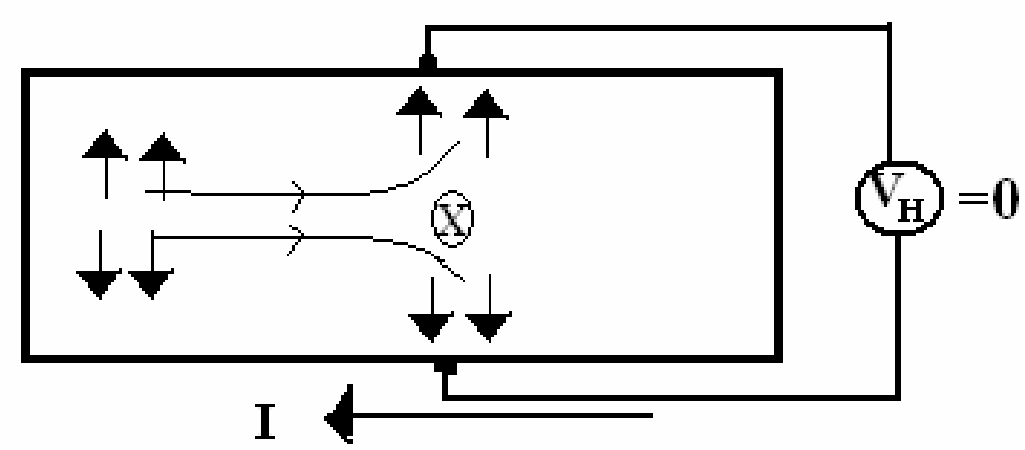

Figure 1-2: A cartoon describing the origin of the spin Hall effect in a paramagnetic conductor due to spin dependent scattering of electrons from an impurity X. There is a gradient of spin potential in the transverse direction but no net electric potential.

The importance of the AH effect and the SH effect lies in the fact that both effects provide a unique way of manipulating electron spins with external electric fields and hence have potential for application in the development of novel spintronic devices. Both the AH effect and the SH effect in itinerant systems result from similar spin dependent

microscopic scattering mechanisms due to the presence of spin-orbit coupling. Phenomenologically, the two effects are complements of each other: in the AHE an electric potential due to the separation of electric charge develops transverse to a spin polarized current, while in the SHE a spin potential due to spin accumulation develops transverse to a charge current with equal spin populations. Quantitatively, the AH effect will be similar to the inverse spin Hall effect (ISHE) in which a longitudinal spin current carrying no net charge generates a transverse polarization voltage. In other words there is no electric field associated with static spin accumulation but a real electric field associated with spin currents. Recently it was shown theoretically that by redefining the spin current [5], one can demonstrate an Onsager relation that relates the spin Hall conductivity to the anomalous Hall conductivity. Thus the AH effect can provide an important route for making quantitative estimates of spin dependent transport coefficients in magnetic materials.

In this dissertation we study the AH effect by addressing a fundamental and unsettled question regarding magnetism in the transition metal elements (iron, cobalt and nickel). Ferromagnetsim in these materials is known to be due to mobile (itinerant) electrons that are also responsible for electrical conduction. The balance between the kinetic energy and exchange interaction energy of the conduction electrons determines whether a metal with a spin-split band becomes a ferromagnet with long rang order or a paramagnet with enhanced susceptibility. If an inequality known as Stoner criterion [6] is satisfied, then the material is a band ferromagnet. Band structure calculations for the transition metals show that indeed the conditions are favorable for ferromagnetism with the magnetic properties determined by spin polarized itinerant carriers. We are

investigating whether quenching the itinerancy of the conduction electrons with increasing disorder can violate the Stoner criterion. In this regard we grow a series of Fe, Co and Fe/C_{60} films in a very clean environment and systematically reduce the film thickness, thereby increasing resistance. The air-sensitive nature of these films rules out the possibility of a magnetization measurement using a SQUID magnetometer. As we will show in the following chapters, the AH effect is an alternative and effective tool to probe magnetic ordering in conducting materials. We will show that with decreasing thickness, long range ferromagnetic order in thicker films gradually disappears and passes over to a system of weakly coupled magnetic clusters. Eventually at very high resistances there is an unexpected and pronounced disappearance of magnetic ordering as measured by the AH effect. We also demonstrate that morphology plays an important role in governing the magnetic and electrical properties in thin films. Our experiments also shed light on another unsettled issue concerning the extent to which weak localization corrections are important in ferromagnetic films.

In chapter 2, we describe in detail the SHIVA apparatus capable of *in situ* magnetotransport measurements, which proved to be indispensable for this project. In chapter 3 we demonstrate the usefulness of the SHIVA apparatus by describing a short project that studies the effect of low energy ion beam irradiation on the conductivity of metal films. In chapter 4 we describe the phenomenology of the AH effect and discuss various microscopic mechanisms that are responsible for this effect. Chapter 5 provides a brief review of the various quantum corrections to the transport properties in disordered metals. A detailed account of our experimental result and discussions based on the

existing theoretical understanding is provided in chapter 6. Finally, in chapter 7 we summarize and discuss some possible future experiments related to this dissertation..

CHAPTER 2
EXPERIMENTAL SETUP: SHIVA APPARATUS

In this section we describe a unique custom built high vacuum system that was designed for *in situ* characterization of air sensitive films. This apparatus, shown schematically in Fig. 2-1,was given a pet name SHIVA, which is the acronym for Sample Handling In VAcuum. SHIVA has a clever design that combines a growth chamber, a cryostat and a load lock into one single vacuum system and has mechanical "arms" for transferring samples between the compartments without breaking vacuum. The load lock LL is a small chamber used to mount and unmount samples from the system and is separated from the growth chamber and cryostat by gate valves V1 and V2 respectively. This arrangement allows the growth chamber and the cryostat to be under high vacuum all the time, and the sample is introduced by opening the gate valves only when the load lock is pumped down to a suitable base pressure.

The mechanical "arms" A1, A2 and A3 consist of a strong magnet sliding on the outside of a long hollow stainless steel tube attached to the vacuum chamber, and another solid rod inside the tube magnetically coupled. Hence by sliding the outside magnet, one can translate and rotate the rod with a thruster attached to its end, inside the vacuum chamber. Sample holders or pucks are specially designed such that substrates are loaded on one of its faces and slots on other faces where the thruster on the "arms" can be inserted and locked onto the puck by a twisting motion. The puck is first mounted on A3 inside the load lock and then pushed inside the growth chamber. Thruster A1 then comes

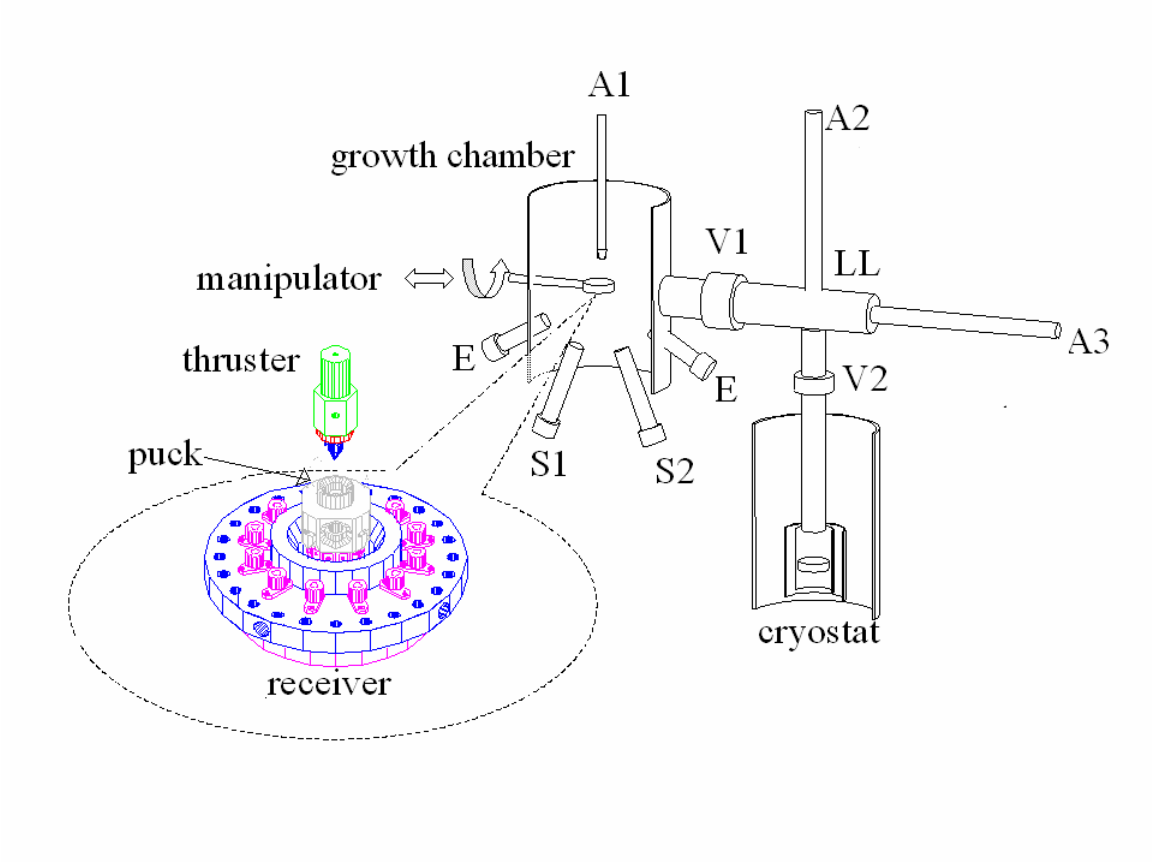

Figure 2-1:Schematic representation of the SHIVA apparatus and a blowup (in color) of the receiver platform showing how a puck can be locked in with the help of thruster. LL: Load lock; A1,A2,A3: transfer arms with thruster mounted at each end; V1,V2: gate valves separating the growth chamber from load lock and load lock from cryostat respectively; E: Optical ports for ellipsometry.

down and locks into the puck so that A3 can be disconnected from the puck by untwisting and taken out of the chamber. The puck, which is now secured on A1, is then delivered to a receiver platform, and the design is such that the puck engages in the receiver and disengages from A1 in one twist, so that A1 can be taken out of the way. Once the sample is grown on the substrate, A1 comes down and locks into the puck and disengages it from the receiver. The next step is to bring A3 back into the growth chamber , lock into the puck, and then disengage A1. The puck is then brought back into the load lock where thruster A2 engages on it and then A3 is disengaged. Now the sample can be pushed

inside the cryostat and delivered to a receiver platform similar to that in the growth chamber. If necessary, the sample can be transferred back to the growth chamber from the cryostat for further processing, by reversing the steps described above. The point to note here is that during the whole procedure, there is no need to break vacuum, the importance of which cannot be overemphasized.

Samples are usually grown through shadow masks on a set of electrodes made of thick films of gold pre deposited on the substrate. Inside the body of the pucks a set of wires are soldered from inside on to small hemispherical copper "heads" attached firmly on the outside of the puck. The other ends of the wires emerge from the sample side of the puck and are connected to the electrodes on the substrate before the puck is loaded in the vacuum chamber. Thus the electrodes on the substrate are electrically connected to different copper heads. The receiver also has a set of spring loaded copper heads on the inside, such that when the puck is placed inside the receiver and engaged, the two sets of heads press firmly against each other and make good electrical contact. Another set of wires connect each of the copper heads on the receiver, run via vacuum feed-throughs out of the vacuum chamber to a break-out panel. Thus when a puck is engaged properly in the receiver, each of the electrodes on the substrate is electrically accessible outside the chamber at the break out panel. This allows us to monitor the resistance of the sample during deposition in the growth chamber and also after the puck is delivered into the cryostat and engaged with an identical receiver in the cryostat.

The growth chamber can be pumped down to a base pressure ~10^{-9} Torr and is equipped with a variety of deposition sources, namely two AJA magnetron sputter guns, two RADAK thermal evaporation furnaces and an ion beam gun. The receiver in the

growth chamber is mounted on a manipulator that allows us to position the substrate so that it faces the appropriate deposition source. The thickness of the films can be monitored with a quartz crystal oscillator firmly attached on the receiver close to the sample. The growth chamber also has two optical ports specially designed for attaching a Woolam M44 fixed angle ellipsometer, which adds the capability of *in situ* monitoring of the optical constants and/or thickness of the thin films during deposition.

The cryostat is housed inside a CRYOFAB liquid helium dewar with a liquid nitrogen outer jacket. When the dewar is cold the cryostat can reach a base pressure $\sim 10^{-8}$ Torr. The cryostat has an AMI superconducting magnet, which allows magnetotransport measurement at low temperatures down to 4.5K and magnetic field upto 7T. The temperature of the sample is measured accurately with a Cernox thermometer glued on the puck right underneath the substrate. The temperature of the sample is controlled within a fraction of a Kelvin by a Lakeshore 332 temperature controller connected to a second Cernox thermometer and resistive heater mounted on the receiver.

CHAPTER 3
NANO SMOOTHENING DUE TO ION IRRADIATION

Ion-assisted deposition refers to the technique in which a beam of noble gas ions, usually argon, with energies less than 1 keV, is simultaneously incident on a thin film during growth. The most prominent consequences of ion-assisted film growth include densification, modification of nucleation and growth, interface mixing, defect generation, and changes in topography and surface roughness [7]. In contrast to this general technique of ion-assisted deposition, some investigators have reported on the use of a sequential technique in which thin films are first deposited and then, after deposition, exposed to an ion beam. Results of this approach include ion bombardment induced nanostructuring of Cu(001) surfaces [8], the formation of reproducible ripple structures on Si(001) and Ag(110) and (001) surfaces [9] and the roughening or smoothing of Si(001) and SiO_2 surfaces [10, 11] where the result depends on ion type, energy and angle of incidence. At the moderately higher energies of a few keV, interlayer exchange coupling in Fe/Cr/Fe trilayers can be controlled with He ion bombardment [12], and microscopic holes can be filled using pulsed Ar ion beams in a process called "ion-beam sculpting" [13]. Many of these experiments thus provide strong evidence of ion beam induced nanoscale matter transport on solid-state surfaces, a process that promises to be useful in applications requiring nano-textured surfaces and interfaces. We are going to present a systematic study of the effect of low energy (~200eV) ion beam exposure on the room temperature resistance of polycrystalline metallic films.

Experimental Details

Sample Fabrication

Using the SHIVA apparatus described in chapter 2, we have grown a series of iron films on glass substrates at room temperature, using r.f. magnetron sputtering source. We used an r.f. power of 35W and Ar gas flow of 10sccm that resulted in a chamber pressure ~10^{-4} Torr and a d.c. bias in the sputter gun ~145V. Under these conditions the Iron films grows at a rate of 4Å/minute. We have also grown a few copper films by thermal evaporation using a RADAK source at a temperature of 1100^{o}C. Film thickness was measured by a calibrated quartz crystal thickness monitor placed in close proximity to the sample and varies from 15-45Å for the Fe films and 75-130Å for the Cu films. The samples were grown on square substrates with pre deposited gold leads at the four corners and used van der Pauw technique [14] to measure sheet resistances of these films. The use of van der Pauw technique on square shaped samples allowed us to avoid using any shadow mask during growth, thus eliminating the possibility of contamination due to re-sputtering from the mask during subsequent ion beam exposure. Immediately after growth, the samples were exposed to a beam of Ar^{+} ion beam generated by 8cm Advanced Energy Kauffman type broad beam ion source. Following are the parameters used to run the ion gun: Ar gas flow ~10sccm, beam voltage =200V, beam current =2mA, accelerator voltage= 45V.

The experiments are performed in ultra high vacuum (UHV) conditions, and the sheet resistance of the films is monitored *in situ* without breaking vacuum between the film growth and subsequent ion beam exposure steps. The incident noble gas ions are chemically unreactive and simply transfer a fraction of their kinetic energy to the atoms in the film, a process which, as discussed above [8-13], can result in a significant

modification of the surface morphology of the film and hence its physical properties. Using atomic force microscopy (AFM) we confirm an ion beam induced smoothening of our films and find that there is a reproducible correlation of the reduction in sheet resistance with ion beam parameters (beam voltage and current density) and initial starting sheet resistance.

Measurement Setup

In a classic paper published in *Phillips Technical Review* (1958), van der Pauw [14] proposed a novel method based on a mapping theorem for measuring sheet resistance and Hall constant of an arbitrary shaped uniform film. Consider a flat lamellar square film free of holes with four small contacts A, B, C and D at its corners (see Fig. 3-1). Apply a current I_{AB} at contact A and take it off at contact B. Measure the potential difference between C and D and define

$$R_1 = \frac{V_D - V_C}{I_{AB}} \tag{3-1}$$

Similarly, apply a current I_{CB} and measure the potential difference between D and A define

$$R_2 = \frac{V_A - V_D}{I_{CB}} \tag{3-2}$$

The sheet resistance R is determined from a mathematical relation between the above measurements as given by

$$\exp(-\pi \frac{R_1}{R}) + \exp(-\pi \frac{R_2}{R}) = 1 \tag{3-3}$$

The solution of the above equation can be written in a simplified form

$$R = \frac{\pi}{\ln 2} \frac{R_1 + R_2}{2} f(\frac{R_1}{R_2}) \tag{3-4}$$

where f is a numerical factor that depends only on the ratio R_1/R_2 and is given by the following transcendental equation

$$\cosh\left(\frac{R_1/R_2-1}{R_1/R_2+1}\frac{\ln 2}{f}\right)=\frac{1}{2}\exp\left(\frac{\ln 2}{f}\right) \qquad (3\text{-}5)$$

which can be easily estimated to any degree of accuracy by numerical methods. Thus the van der Pauw method involves two independent measurements in different electrical configurations. A closer look reveal that the two configurations for measuring R_1 and R_2 can be switched from one to other by simply interchanging any one of the diagonal contacts keeping the other fixed. Usually one uses a mechanical or electronic switching system to change the electrical configuration for the two measurements.

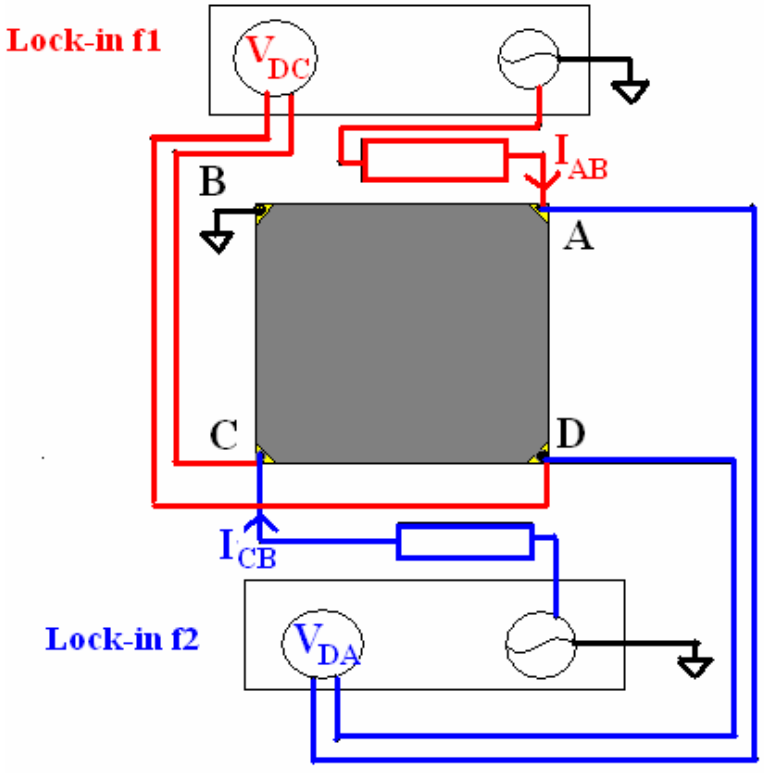

Figure 3-1: A setup for non-switching van der Pauw technique to measure sheet resistance of a sample (shaded square ABCD) using two SR830 lock-in amplifiers operating at different frequencies *f1* and *f2*. Different colors are used to represent electrical connections for each lock-in.

We have used a nonswitching technique [15] where the two measurements can be made simultaneously without changing configurations, by using a.c. excitations instead of d.c. currents as described above. With contact B of the sample connected to ground, we apply two independent ac currents I_{AB} and I_{CB} with different modulating frequencies. This can be achieved by using lockin amplifiers, which can be used as a constant current source by using a ballast resistor at the voltage source. The same lock in amplifiers can also be used to measure the corresponding voltages V_{DC} and V_{AD}. We have operated two SR830 lock-in amplifiers at frequencies of f_1=17Hz and f_2=27Hz, and using 1MΩ ballast resistors, we were able to source 1μA of a.c. current into our samples. This arrangement, shown schematically in Fig. 3-1, allows us to simultaneously measure both components, R_1 and R_2, of the resistance and assess film homogeneity ($|R_1-R_2|$) during growth and subsequent ion exposure. We also simultaneously measured the reading of a quartz crystal monitor as a measure of film thickness. However, due to lack of calibration of crystal monitor output as a ion beam is incident on it, we quote our thickness in arbitrary units.

Experimental Results

We report [16] on an additional and unexpected effect of ion milling on the resistance of ultra thin films. As shown in Fig.3-2 the resistance of a Cu (top panel) and Fe (bottom panel) film undergoes a pronounced decrease which is initiated at time $t = 0$ when the beam is first directed onto the sample. The resistance reaches a broad minimum and then begins to rise after about 50 s. The initial resistance decreases have been measured to be as large as a factor of ~25 for Cu and ~2 for Fe. This is an unusual result because the ion beam is expected to erode the film at a constant rate, as indicated by the linear decrease

of the accumulated thickness of the material deposited onto the thickness monitor (right hand axes). Apparently, during initial stages of milling, the resistance decreases as material is being removed. As discussed later, we attribute this decrease to an ion beam induced smoothening of the film.

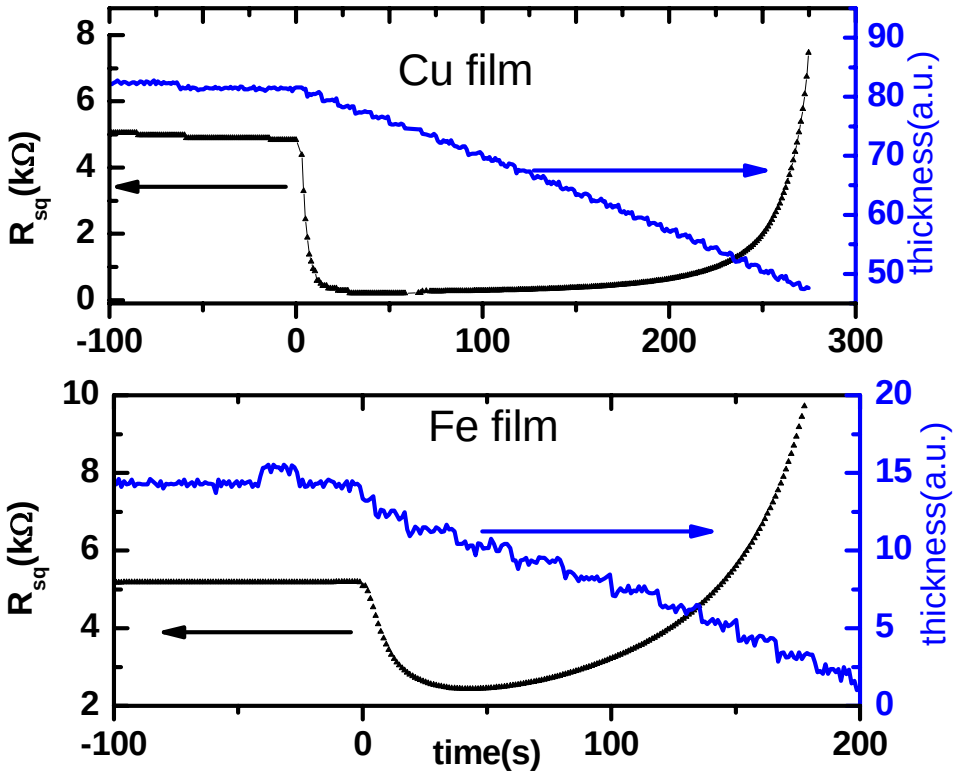

Figure 3-2: Plot of sheet resistance (left hand axis) and thickness (right hand axis) as a function of time for an ultra thin Cu (upper panel) and Fe (lower panel) film. At time t =0 the ion beam is turned on. The resistance and thickness, measured simultaneously, show that as material is being steadily removed the resistance initially decreases to a minimum and then increases.

We checked the stability of the minimum resistances achieved due to ion exposure is stable and is not an experimental artifact. We turned off the ion beam when the resistance is near the broad minimum (Fig. 3-3). The resistance remains stable with no significant drift at the minimum value during the time ion beam was off. The resistance starts to rise as soon as the ion beam exposure is started again.

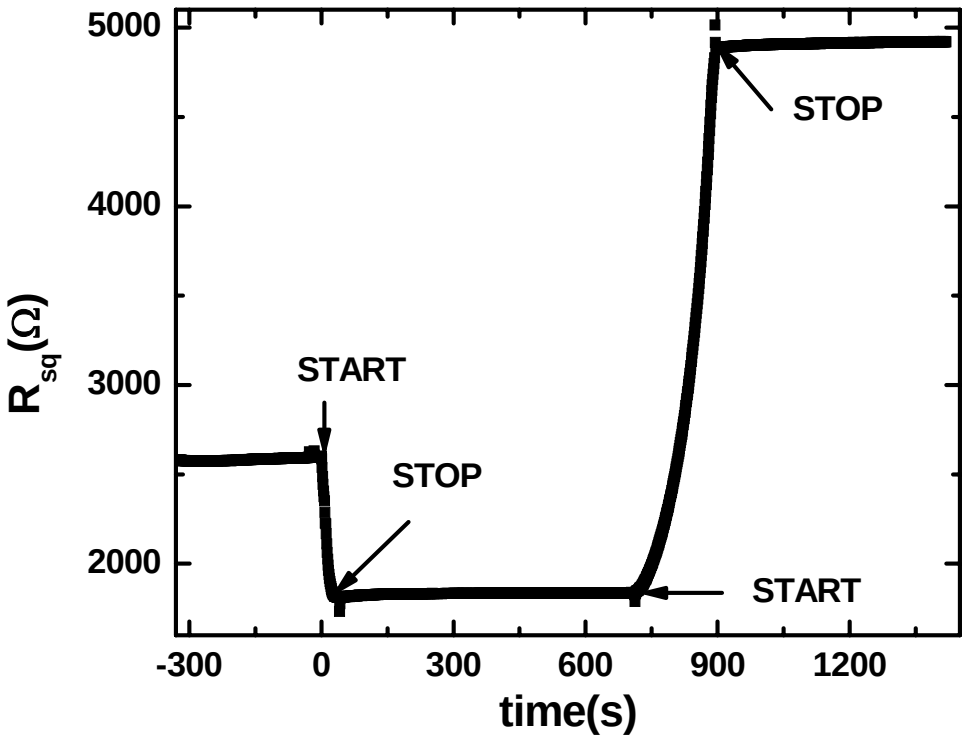

Figure 3-3:Check of stability of the reduced resistance due to ion beam irradiation. START and STOP refers to ion beam exposure. During the time the ion beam is off the resistance remains stable and does not show any significant drift.

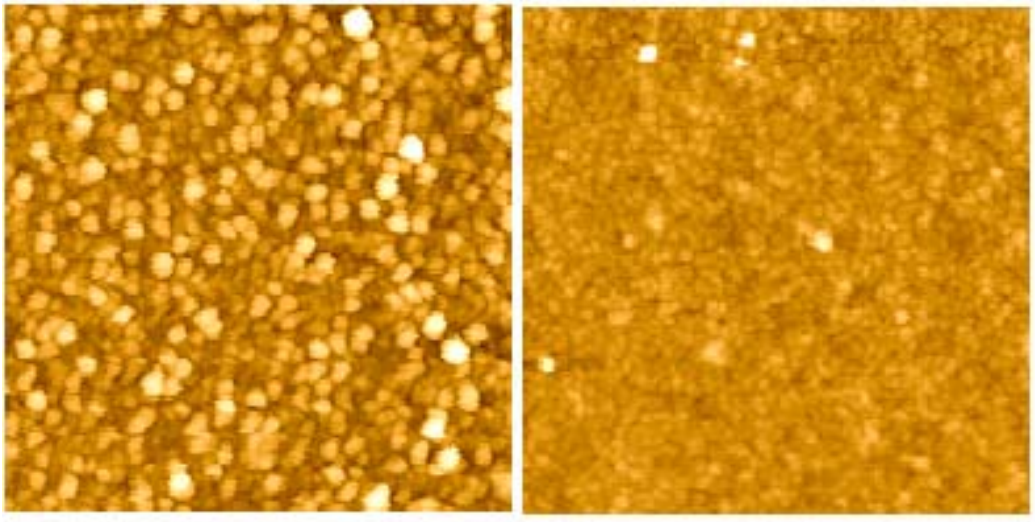

Figure 3-4:AFM surface topography of two 120 Å thick Cu films with $R_i \approx 2$ kΩ. The unmilled film (left panel) has a rms average roughness of 30 Å compared to the 10 Å roughness of the film (right panel) which was milled to its minimum resistance $R = R_m$.

Auger electron spectroscopy of an ion-milled film compared with that of a pure film does not show the presence of impurity contaminants that might be inadvertently sputtered on the film by the ion beam and thus lower its resistance.

The relative decrease in the resistance of our ultra-thin films due to ion milling is strongly correlated with their initial surface roughness. Fig. 3-2 shows that for a Cu and a Fe film with similar initial sheet resistances near 5 kΩ, the minimum resistance reached during the ion milling process is more than a factor of ten lower for Cu (~200 Ω) than it is for Fe (~2.5 kΩ). An important insight into the cause of this difference is provided by our *ex situ* AFM studies, which show that Cu films grown by thermal sublimation have an rms roughness larger by a factor of ~3 than Fe films grown by sputtering. We have also compared the roughness of films not exposed to an ion beam with films ion milled close to the resistance minimum. As shown in Fig. 3-4, this comparison for a typical Cu film reveals that the ion-milled film (right panel) has an rms roughness of 10 Å compared to 30 Å for an unmilled film (left panel). The smoothening effect is also confirmed in AFM images of Fe films, which, with their initially smoother topography, exhibit a smaller reduction (factor of 1.2) in rms roughness. For even smoother films such as Gd and Pd, which become conducting almost immediately after deposition begins, we do not observe an initial resistance decrease.

There is also a pronounced increase in homogeneity associated with ion milling. If the films are homogeneous, then R_1 and R_2 should both show the same time dependence and have similar magnitudes. However, a thin film grows through various stages, starting with nucleation of isolated grains, then coalescence of the grains and finally formation of a homogeneous system of well-connected grains. At the early stages of growth the local

resistance is extremely sensitive to local variations in temperature, incident flux and pressure. Any gradients in these quantities can give rise to long length scale anisotropies in the electrical resistance and hence significant differences in R_1 and R_2. In our experiments, R_1 and R_2 can differ by factors as large as 3 for Fe and 20 for Cu films. However, when these "inhomogeneous" films are exposed to the ion beam, both R_1 and R_2 individually decrease to approximately the same minimum. Thus the anisotropy measured by $|R_1 - R_2|$ and the total sheet resistance as measured by the van der Pauw combination of R_1 and R_2 [15] simultaneously decrease.

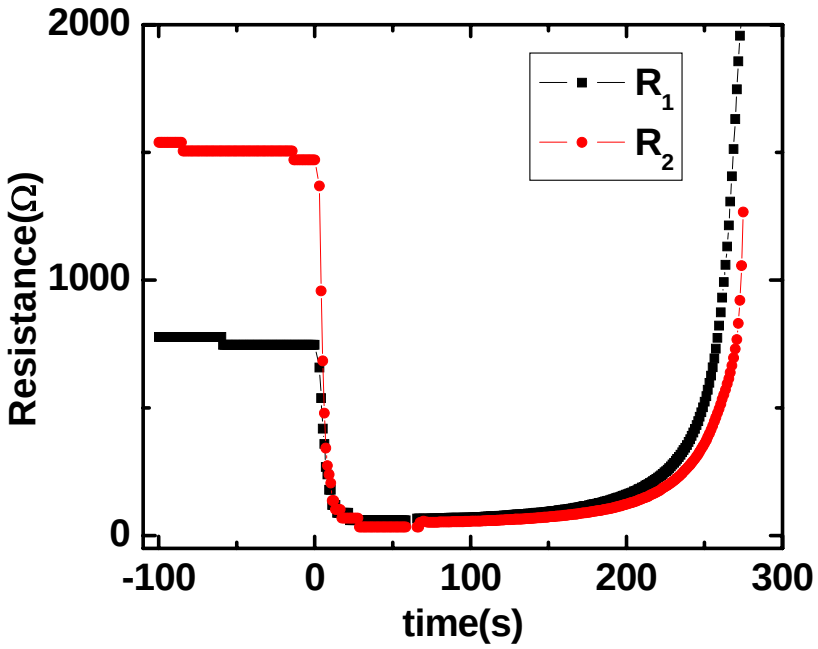

Figure 3-5: The two van der Pauw component R_1 and R_2 plotted separately for the copper film shown in Fig. 3-2.

We model the ion beam induced decrease in sheet resistance from an initial value $R = R_i$ to a minimum value $R = R_m$ as equivalent to connecting a shunt resistance R_s in parallel with R_i. We use the parallel resistance formula to calculate R_s as follows:

$$\frac{1}{R_i} + \frac{1}{R_s} = \frac{1}{R_m} \qquad (3\text{-}6)$$

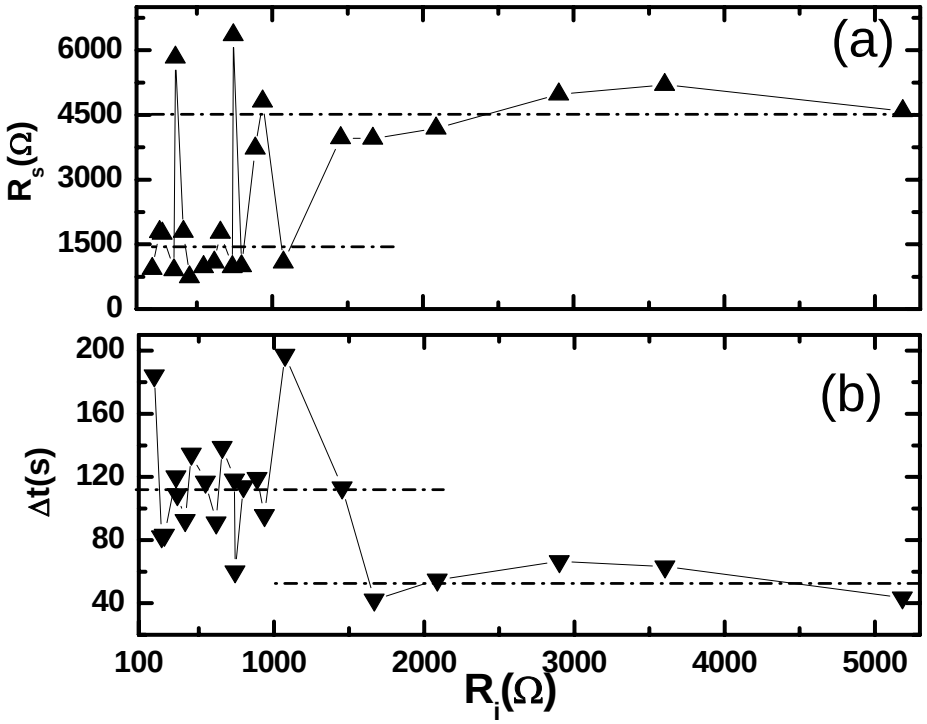

Figure 3-6: Plot of the shunting resistance R_s (panel a) and the time Δt required for the ion beam to mill the film to its resistance minimum R_m (panel b) as a function of the initial resistance R_i. The horizontal dashed lines represent the nominally constant values of R_s and Δt over the indicated ranges of R_i. The crossover to different plateaus near $R_i = 1500\ \Omega$ represents a change in film morphology in which a smaller ion dose ($\propto \Delta t$) gives rise to a larger shunt resistance.

In Fig. 3-6(a) we plot the calculated values of R_s versus R_i for twenty-two different Fe films. We note the interesting result that R_s (indicated by the horizontal dashed lines) is constant and on the order of 4500 Ω for ultra thin films with $R_i > 1500\ \Omega$ and constant and on the order of 1400 Ω for thicker films with $R_i < 1500\ \Omega$. Fig. 3-6(b) shows the dependence on R_i of the ion exposure time Δt, needed to reach the minimum resistance R_m. Since the beam flux is constant for all the experiments, Δt is proportional to the total number of ions incident on the films or, equivalently, the ion dose. We find that Δt behaves similarly to R_s. The crossover in both plots near $R_i = 1500\ \Omega$, corresponding to a thickness of around 25Å, most likely reflects a change in film morphology in which a

smaller ion dose ($\propto \Delta t$) gives rise to a larger shunt resistance. Thus for ultra thin films with $R_i > 1500\ \Omega$ the shunt resistance increases by a factor of ~3 and the dose needed to achieve the resistance minimum decreases by a factor of ~2. The relative constancy of the shunt resistance values for a wide range of initial resistances implies that the ion milling is primarily a surface modification effect in which the rearranged surface atoms can be thought of as providing a shunting resistance that is independent of film thickness. Similar data are found for the Cu films where Δt ~75 s and the shunting path resistance R_s = 200 Ω is more than an order of magnitude lower than for Fe. If the initial film is very thick, then its conductance dominates and $R_i << R_s$. Under these conditions the resistance decrease, $R_i - R_m \approx R_i(R_i / R_s)$, due to nano smoothening is negligible as is in fact verified for iron films of thickness greater than 50Å ($R_i > 200\ \Omega$) when the resistance decrease is not observed as shown in Fig. 3-7.

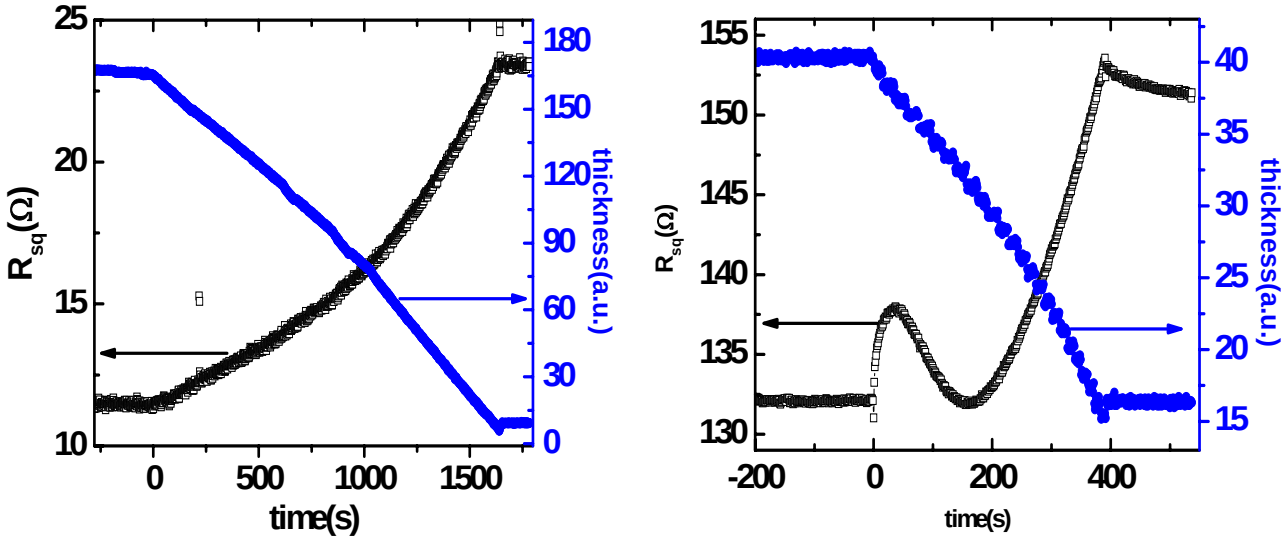

Figure 3-7: Effect of ion-beam exposure on thicker iron films (d>50Å). Note that resistance does not go below its initial value at t=0, when the beam was started.

The minimum resistance reached during ion milling is not sensitive to small variations in the incident ion energy. The resistance minima of Fe films, having almost identical initial sheet resistances, separately exposed to beam energies varying from 50 eV to 250 eV do not show any pronounced dependence on beam energy. However at 50 eV, Δt was larger by a factor of 10 and the resistance minimum was broader.

Discussion

We surmise that two competing processes are occurring during the ion irradiation process: (1) sputter erosion by the impinging ions preferentially removes atoms from the film at high points where they have less coordination with neighbors and hence less binding energy and (2) the nanoscale transport of material from high points (peaks) near grain centers to low points (valleys) between adjacent grains. The resulting nano smoothening process dominates in the initial stages of the ion exposure, resulting in a decrease in resistance and an increase in homogeneity. From a microscopic point of view, the decrease in resistance can be attributed to a variety of mechanisms including: a transition from the diffuse surface scattering of rough films to specular surface scattering of smooth surfaces [17, 18], the removal of foreign surface absorbates [19] and the filling in of high resistivity weak spots at grain boundaries. Equivalently, one can interpret the results in terms of percolation where the ion milling gives rise to a restructuring of the grains and a concomitantly lower critical thickness for the onset of conductivity. Ion beam induced grain growth [20] is probably not relevant because our incident ion energies are too low. At all stages of milling, the erosion of the film at a constant rate is occurring and, as shown in Fig. 3-2, this process eventually dominates over the smoothening process when the resistance starts to rise.

Our results for Fe and Cu films are reminiscent of experiments in which it was found that C_{60} monolayers deposited onto thin Cu films give rise to a shunting path with R_s independent of R_i over a similar range [21]. In this case the physics is different, since the charge transferred across the Cu/C_{60} interface begins to fill the lowest unoccupied band in the C_{60} monolayer, thus causing the monolayer to become conducting.

In conclusion, we have shown that post deposition ion milling of ultra thin Fe and Cu films gives rise to a pronounced initial decrease in resistance and a concomitant improvement of electrical homogeneity and film smoothness. The observation of a constant shunt resistance that is independent of the underlying film implies that the initial resistance decrease is due primarily to surface modification. In the initial stages of ion bombardment, in which pronounced resistance decreases are observed, the lateral transport of material and the associated nano-smoothening dominates over the removal of material. With continued milling the film is uniformly etched away and the resistance increases. While these techniques are clearly applicable to fundamental studies of thin films where the resistance can advantageously be externally tuned with an ion beam, they may also have applicability to the preparation of polycrystalline surfaces prior to the formation of tunnel barriers or the improvement of interfaces in metallic bilayers or superlattices.

CHAPTER 4
THE ANOMALOUS HALL EFFECT IN MAGNETIC MATERIALS

Itinerant Ferromagnetism

Ferromagnetism in metals arises from unpaired *d*- or *f*-electrons in the atoms. The experimentally observed values of the magnetic moment per atom for the ferromagnetic transition elements iron, cobalt and nickel are 2.22,1.78 and 0.60 respectively in units of Bohr magneton [22, 23], that is the magnetic moment of one electron. These non-integral values cannot be explained in terms of models where the magnetic electrons are localized at the core of the atoms forming the lattice. Instead, the magnetic electrons are believed to be itinerant, and are free to move within the crystal and participate in conduction. The magnetization in this case is due to spontaneously spin-split bands. In 1934, Stoner derived a condition [6] under which a gas of electrons with exchange interaction between them becomes a ferromagnet.

In a normal metal, in the absence of a magnetic field, there are equal numbers of up and down spins in the conduction band. Imagine a situation when spin-down electrons within an energy range δE of the Fermi energy E_F are placed in the spin-up band. The number of electrons moved is $g(E_F)\delta E/2$, where $g(E_F)$ is the density of states at the Fermi level and the increase in energy is δE. Hence the change in kinetic energy is

$$\Delta E_{K.E} = \frac{1}{2} g(E_F) \cdot (\delta E)^2 \qquad (4\text{-}1)$$

This increase in energy is compensated if there is an exchange interaction *J* between electrons that lowers the energy if two spins are parallel. This will lead to a potential energy given by

$$\Delta E_{P.E.} = -\frac{1}{2} J(g(E_F)\delta E)^2 \tag{4-2}$$

Thus the total change in energy is given by

$$\Delta E = \frac{1}{2} g(E_F)\delta E^2 (1 - Jg(E_F)) \tag{4-3}$$

and spontaneous ferromagnetism is possible if $\Delta E < 0$ which implies :

$$Jg(E_F) \geq 1 \tag{4-4}$$

This inequality is the Stoner criterion for ferromagnetic instability that requires the exchange energy to be strong and the density of states at Fermi level to be large. This theory is very successful in explaining the ferromagnetic behavior of the three transition metal elements iron, cobalt and nickel. Band structure calculations for crystals of the transition elements show that the Fermi energy crosses the unoccupied *d*-bands, which has an imbalance of spins. The calculated values of magnetic moment per atom from band structure are in good agreement with experimental values. If the Stoner criterion is not satisfied, there will not be any spontaneous long range magnetic order but rather a paramagnet with renormalized susceptibility given by.

$$\chi = \frac{M}{H} \approx \frac{\chi_P}{1 - J \cdot g(E_F)} \tag{4-5}$$

where χ_P is the Pauli paramagnetic susceptibility. Thus there will be a large increase in magnetic susceptibility is known as Stoner enhancement as is experimentally observed for Pd and Pt which are materials where $Jg(E_F)$ is close to but less than unity.

Anomalous Hall Effect

The anomalous Hall (AH) effect [2] in magnetic materials refers to the phenomenon when a transverse electric potential proportional to the volume magnetization develops in response to an applied charge current. This transverse electric potential is different from that due to the normal Hall effect, which is a result of Lorentz force acting on the charge carriers due to an applied magnetic field leading to accumulation of charges at the transverse edges. The AH effect results from spin-dependent scattering of the conduction electrons due to spin-orbit coupling with scattering centers. In principle the AH effect can manifest itself in the absence of any external magnetic field if the sample is a single magnetic domain. However macroscopic ferromagnetic samples in zero magnetic fields consist of randomly oriented multiple magnetic moments with net moment of zero. An external magnetic field has to be applied to line up domains along its direction, in order to observe a finite AH effect. The magnitude of the AH potential due to a certain applied magnetic field is at least 10^2-10^3 times higher than that of the normal Hall effect, in most ferromagnetic materials, which makes it easier to separate the two effects. A typical Hall curve for a ferromagnetic sample of iron is shown in Fig. 4-1. The initial steep increase in the hall resistance at low fields is due to the increasing alignment of magnetic domains along the field direction until some characteristic field when all the moments are lined up. Thereafter, the Hall resistance rises with a much smaller rate that is due to normal Hall effect. This typical behavior can be described using a phenomenological expression [2]

$$\rho_{xy} = R_s M + R_n B \tag{4-6}$$

where the Hall resistivity is described as the sum of the anomalous Hall resistivity proportional to magnetization and the normal Hall resistivity proportional to the magnetic

field. R_o is the normal Hall coefficient and depends only on the effective carrier density in the material. R_s is the AH coefficient and depends on the microscopic parameters that describe the scattering mechanism. For years, theoretical studies of the AH effect has generated considerable debate and controversy. We present here a brief account of theoretical understandings, which are relevant to our experimental work.

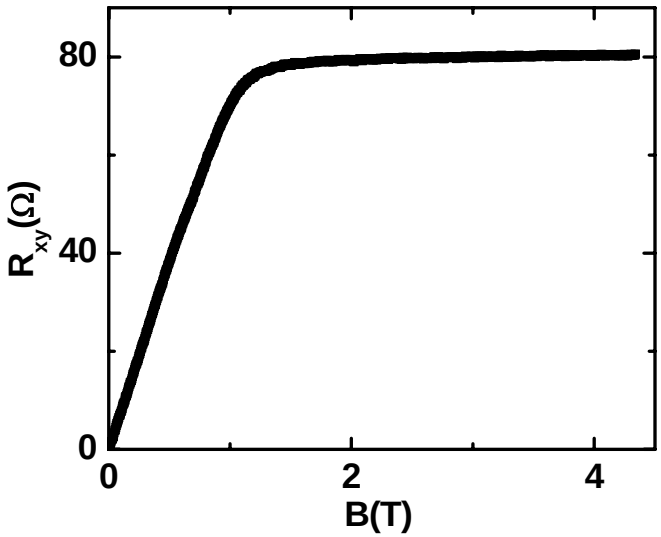

Figure 4-1:The Hall curve for a 20Å thick iron film of resistance R_o=2700Ω at T=5K, showing anomalous behavior.

Anomalous Hall Effect for Itinerant Carriers

We consider models where a transverse voltage arises due to spin-orbit interaction of the spin polarized current carriers in itinerant ferromagnets with the non-magnetic periodic lattice and or impurities. An electron in a solid experiences a net electric field say E due to the ionic core in the lattice, other electrons or impurities. In the rest frame of the electron there is a magnetic field B as a result of relativistic transformation as given by

$$\vec{B} = -\vec{p} \times \vec{E} / mc \qquad (4\text{-}7)$$

where $\vec{p}$ is the momentum of the electron. This magnetic field interacts with the spin of the electron and favors anti-parallel orientation of orbital and spin angular momentum of the electron. This describes the intrinsic spin orbit interaction, and results in an additional term in the Hamiltonian given by[24]:

$$H_{SO} = \frac{1}{4m^2c^2}\vec{\sigma}\cdot(\nabla V \times \vec{p}) \tag{4-8}$$

where $\vec{\sigma} \equiv (\sigma_x, \sigma_y, \sigma_z)$ are the Pauli matrices and $\vec{E} = -\nabla V$, where V is the local potential that the electron experiences. At low temperatures when the dominant scattreing is due to impurities, V is the potential due to a single impurity. The Hamiltonian for such a disordered ferromagnetic metal including spin-orbit interaction as given by:

$$H = \int d^3r\psi^*(r)[-\frac{\nabla^2}{2m} + V(r)_{\cdot} - M\sigma_z - i\frac{\lambda_o^2}{4}\vec{\sigma}\cdot(\nabla V \times \nabla)]\psi(r) \tag{4-9}$$

where λ_o is effective of spin-orbit scattering strength and has the dimension of length, $V(\vec{r}) = \sum_j v(\vec{r} - \vec{R}_j)$ is a random potential due to impurities at positions $\vec{R}_j$, M is a strong exchange interaction in the z-direction and $\psi \equiv (\psi\uparrow,\ \psi\downarrow)$ are spinor fields corresponding to spin-up and spin-down electrons. The Hamiltonian in momentum representation can be written as[24]:

$$H = \sum_k \psi_k^*(\frac{k^2}{2m} - M\sigma_z)\psi_k + \sum_{k,k'}\psi_k^* V_{k-k'}[1 + \frac{i\lambda_0^2}{4}(\vec{k}\times\vec{k}').\vec{\sigma}]\psi_{k'} \tag{4-10}$$

Skew Scattering Mechanism

In 1955 Smit proposed a mechanism [25, 26] for AH effect in ferromagnets which is referred to as Skew Scattering. This mechanism is based on the fact that the scattering amplitude of an electron wave packet from an impurity due to spin-orbit coupling is

asymmetric in the sense that it depends on the relative directions of the scattered and incident waves and of the spin. Consider a Gaussian wave packet with average wave vector $\vec{k}_0$ incident on an impurity site at the origin at time *t*=0, resulting in a scattered wave given as the sum of normal and spin-orbit scattering,

$$\psi = \psi_v + \psi_{so} = \sum_k c_k \psi_k \tag{4-11}$$

For a short range impurity potential *V(r)* it can be shown that scattered wave function from the spin-orbit term far from the origin is given by

$$\psi_{so} = \sum_k c_k [-q_1 h_1(kr)(\vec{k} \times \vec{r}) \cdot \vec{\sigma}] / kr \tag{4-12}$$

where $h_1(kr) = -e^{ikr}[i/(kr)^2 + 1/kr]$ and the scattering wave from the normal potential scattering part is given by

$$\psi_v = \sum_k c_k [\exp(i\vec{k} \cdot \vec{r}) + b_o h_o(kr) + b_1 h_1(kr)(\vec{k} \cdot \vec{r}) / kr] \tag{4-13}$$

with $h_0 = -ie^{ikr} / kr$.

Thus for the normal case, the scattering amplitude depends on the angle between the incident and scattered direction and does not depend on the spin of the electron. To understand the "skewness" that arises from spin-orbit interaction, imagine a plane containing the incident direction $\vec{k}$ and the direction of the spin of the electron σ assumed to be polarized along a fixed z-direction. It follows from above, the scattered wavefunction for a given spin, the wave function has different sign on both sides of the plane. The signs are reversed when the spin of the electron is reversed. This results in a separation of scattered electrons depending on its spin as depicted in Fig. 4-2a. Thus for an itinerant ferromagnet with an unequal number of up and down spin electron, a

transverse potential develops as the up/down spins are scattered in opposite directions. Detail calculation for a simple parabolic band and short range random impurity potential shows that the AH conductivity is proportional to longitudinal conductivity.

$$\sigma_{xy}^{SS} = V_o N_o \lambda_o^2 (n_\uparrow - n_\downarrow)\sigma_{xx} \tag{4-14}$$

where M is the magnetization, impurity strength $v(\vec{k} - \vec{k}') = v_o$ independent of momentum for, and N_o is the spin averaged density of states at the Fermi energy. In general it can be shown that for skew scattering, the AH conductivity is directly proportional to conductivity. Using the inversion relation between conductivity and resistivity, it follows that the anomalous hall resistivity due to skew scattering is directly proportional to the longitudinal resistivity.

$$\rho_{xy}^{SS} \sim \rho_{xx} M \tag{4-15}$$

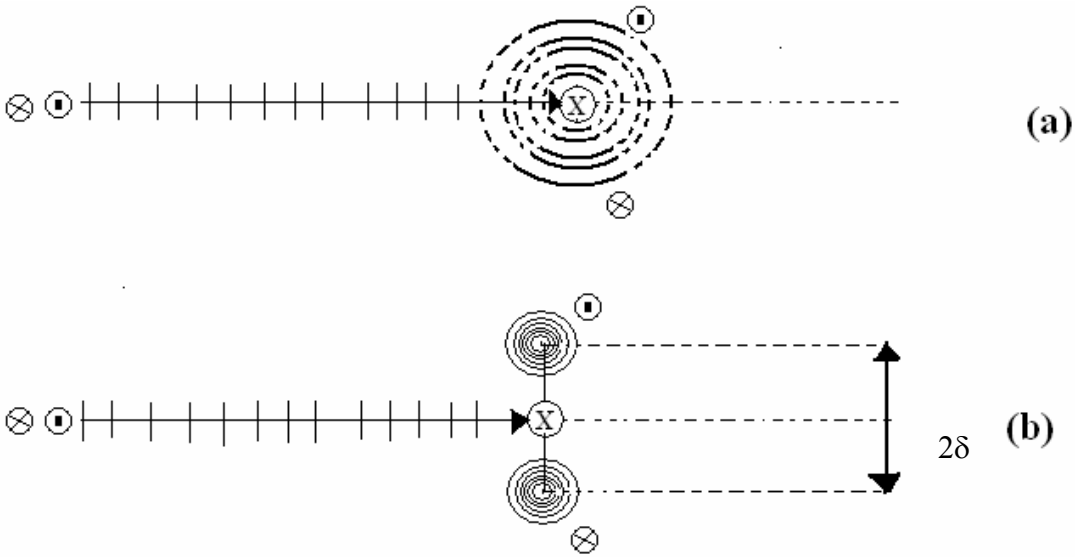

Figure 4-2:Schematic representation of (a) skew scattering and (b) side jump mechanism of AH effect. ⊙ and ⊗ represents spin up and spin down electron.

Side Jump Mechanism

In 1970, Berger proposed a new mechanism that can contribute to the AH effect called the Side Jump mechanism [27]. It is based on a quantum mechanical effect where the trajectory of the scattered electron is shifted sidewise due to spin orbit scattering from impurities. The quantum mechanical velocity operator for the Hamiltonian with spin-orbit interaction is given by,

$$\vec{v} = -i[\vec{r}, H] = \frac{\vec{p}}{m} + \lambda_o^2 \vec{\sigma} \times \nabla V \qquad (4\text{-}16)$$

Thus there is an additional term in the velocity operator, transverse to spin polarization which has a sign depending on the spin orientation. This corresponds to lateral displacement of the center of the scattered wavepacket with given spin as shown in Fig. 4-2b. The magnitude of the side-jump displacement δ is proportional to spin-orbit coupling and is expected to be small. We note that for a bare electron in vacuum, the spin-orbit scattering parameter is simply the normalized Compton wavelength i.e $\lambda_o = \hbar / mc$. However, Berger has shown that the spin orbit coupling is renormalized by the band structures by factors α~10^4 which results in side-jump displacements $\delta = \alpha \lambda_o k_F / 4 \approx 10^{-11} m$ and is independent of disorder. The characteristic length scale that replaces the mean free path is δ, hence this contribution is small compared to skew scattering, except in the case of short mean free path i.e. high resistivity. Detail calculation reveals that in this mechanism the AH conductivity is independent of impurity concentration and depends only on the side jump displacement.

$$\sigma_{xy}^{SJ} = \frac{e^2}{2\hbar} \lambda_o^2 (n_\uparrow - n_\downarrow) \qquad (4\text{-}17)$$

This implies that the AH resistance due to side jump scattering is proportional to the square of the longitudinal resistivity as given by

$$\rho_{xy}^{SJ} \sim \rho_{xx}^{2} M \tag{4-18}$$

Berry Phase Mechanism

We now discuss a mechanism for AH effect that has drawn considerable attention in the recent times. In a pioneering work in 1958, Karplus and Luttinger [28] pointed out the existence of an additional term in the velocity operator in ferromagnetic materials, that can give rise to AH effect. Later, this contribution was identified as the effect of Berry phase [29, 30] acquired by Bloch electrons moving in a periodic potential of a crystal with spin-orbit interaction with the lattice. The semi-classical dynamics of Bloch electrons including the Berry phase may be derived from the Bloch Hamiltonian

$$H_k = \varepsilon_{n\sigma}(\vec{k}) + V \tag{4-19}$$

where $\varepsilon_n(\vec{k})$ are energy bands including the effect of spin-orbit interaction and ferromagnetic polarization, and V is the applied external potential such that $\nabla V = -e\vec{E}$. The semi-classical equations of motion are

$$\begin{aligned} \dot{\vec{k}} &= e\vec{E} + e\dot{\vec{r}} \times \vec{B} \\ \dot{\vec{r}} &= \nabla_k \varepsilon_{n\vec{k}} - e\vec{E} \times \vec{\Omega} \end{aligned} \tag{4-20}$$

where $\vec{B}$ is the applied magnetic field and $\vec{\Omega}$ is an effective magnetic field in $\vec{k}$ space arising from the Berry phase.

$$\vec{\Omega}(\vec{k}) = \vec{\nabla}_k \times \vec{X}(\vec{k}) \tag{4-21}$$

where $\vec{X} = \int_{cell} d\vec{r} u^{*}_{n\vec{k}}(\vec{r}) \cdot i\nabla u_{n\vec{k}}(\vec{r})$ the Berry vector potential and $u_{n\vec{k}}$ are the Wannier functions for the unit cell of the crystal. The additional term in the velocity operator in equation (4-20) leads to a Hall current given by

$$\vec{j}_H = -e^2 n\left\langle \vec{\Omega} \right\rangle \times \vec{E} \tag{4-22}$$

implying an AH conductivity given by

$$\sigma_{xy}^{AH} = e^2 n\left\langle \Omega_z \right\rangle \tag{4-23}$$

where $\left\langle \vec{\Omega} \right\rangle = n^{-1} \sum_{\vec{k}\sigma} \vec{\Omega}_\sigma(\vec{k}) f(\varepsilon_{\vec{k}\sigma})$ is the average of Berry magnetic field over all occupied states in k-space. The average is zero unless time reversal symmetry is broken as it is in a ferromagnet where there is spin-orbit coupling between the spin-polarization and orbital motion. The important point is that the AH conductivity due to the Berry phase does not require any impurity scattering and is independent of mean free path and hence conductivity. Thus we have the Berry phase contribution to the AH resistivity proportional to square of the longitudinal resistivity.

$$\rho_{xy}^{B} \sim \rho_{xx}^{2} M \tag{4-24}$$

which is the same dependence found for side jump scattering (equation 4-18).

Anomalous Hall Effect in Ferromagnets with Localized Moments

For the sake of completeness we discuss models where the magnetic electrons (either *d* or *f* electrons) are not itinerant but rather localized at the ions and the charge carriers (*s* electrons) are equally distributed between states of opposite spins. The electron scattering is by thermal disorder in the localized spin system through direct spin–spin interaction also known as *s-d* interaction. Although the s-d interaction explains the resistivity of rare earth metals [31], it does not give rise to an AH effect. It was shown by

Kondo [32] that the s-d interaction is anisotropic, but it gives no skew scattering if the orbital ground state of the *d* or *f* magnetic electrons is degenerate. On the other hand, the anisotropy disappears when the ground state is non-degenerate. Thus a *s*-*d* interaction between the spin of a conduction electron and a spin angular momentum of an incomplete *d* or *f* shell cannot give rise to skew scattering and hence AH effect. To explain the AH effect in these systems, Kondo introduced an intrinsic spin-orbit interaction, which is a relativistic effect arising from a magnetic field appearing in the rest frame of the electron as the electron moves past the nucleus (equation 4-7). This kind of spin-orbit interaction favors anti-parallel alignment of orbital angular momentum and the spin. The intrinsic spin-orbit interaction allows odd powers of spin-spin interaction appropriate to a degenerate ground state to appear in transition probabilities and gives rise to skew scattering. Kondo [32] obtained an expression for Hall resistivity in this situation proportional to third moment of magnetization fluctuation as follows:

$$\rho_{xy} \sim \left\langle (M - \langle M \rangle)^3 \right\rangle \tag{4-25}$$

This fluctuation function can be evaluated only under special conditions. At T=0, the spin fluctuations are zero and hence AH resistivity will be zero. In the paramagnetic region (above Curie temperature), the correlation function can be evaluated exactly [32] and the Hall resistivity is given by:

$$\rho_{xy} \sim (2J^2 + 2J \pm 1)\chi H \tag{4-26}$$

where J is the orbital angular momentum and χ is the magnetic susceptibility. Thus the temperature dependence of Hall resistivity comes only from χ. In the ferromagnetic regime, the spin correlation function in the molecular field approximation was found to vary as the second derivative of the Brillouin function. Although this theory has had

some success especially for paramagnetic substances, it has some major drawbacks. For example gadolinium, a rare earth metal is known to be in an S state and hence zero orbital angular momentum. Thus in this case the intrinsic spin-orbit interaction will be zero, and hence skew scattering is not expected. However gadolinium is known to exhibit a particularly large AH effect.

Another spin-orbit interaction discussed in the context of AH effect is the interaction between the magnetic field produced by the localized moments and that due to the itinerant *s* electrons temporarily localized in the vicinity of the ions. Imagine a localized moment $\vec{M}$ at the origin of a rectangular coordinate. It sets up a vector potential at a position vector $\vec{r}$ given by $\vec{A} = (\vec{M} \times \vec{r}) / r^3$. The vector potential interacts with a charge carrier with momentum $\vec{p}$ as given by the term

$$H_{so} = -\frac{e}{2mc}(\vec{p}.\vec{A} + \vec{A}.\vec{p}) = -\frac{e}{mc}\vec{p}.\vec{A} \qquad (4\text{-}27)$$

using $\nabla.\vec{A} = 0$. Introducing the angular momentum of the charge carrier about the origin $\vec{L} = \vec{r} \times \vec{p}$, the spin-orbit term can be expressed as

$$H_{so} = -\frac{e}{mcr^3}\vec{M}.\vec{L} \qquad (4\text{-}28)$$

Clearly, the Hamiltonian changes sign when the position vector of the charge carrier is reflected in the plane defined by $\vec{M}$ and the primary current direction, thus giving rise to Skew Scattering.

Maranzana [33] has carried out calculation using mixed spin orbit interaction and scattering by thermal disorder and for the ferromagnetic case obtained the same expression found with intrinsic spin-orbit interaction by Kondo. For the mixed s-orbit/d-spin interaction,

while evaluating the three spin correlation function in molecular field approximation, the magnetization can be factored out to leave a two spin function giving the following expression for Hall resistivity,

$$\rho_{xy} \sim \rho_m M \tag{4-29}$$

where ρ_m is the magnetic spin disorder contribution to conductivity.

Superparamagnetism

We now consider a unique magnetic behavior, namely superparamagnetism, which is relevant for high resistance samples near percolation threshold. The following is a brief account based on a discussion due to Cullity [23]. Consider an assembly of uniaxial single domain ferromagnetic particles with an anisotropy energy $E = K_1 \sin^2(\theta)$, where K_1 is the anisotropy energy and θ is the angle between the easy axis and the saturation magnetization M_s. Thus if a single domain particle of volume V becomes small enough in size, the energy fluctuation due to finite temperature becomes comparable with $\Delta E = K_1 V$, the energy barrier associated with the reversal of magnetization. In this situation the magnetization of a particle given by $\mu = M_s V$ can be reversed spontaneously even in the absence of an applied magnetic field. Thus we have a situation similar to that of paramagnetic material where thermal energy tend to disalign the magnetic ordering and an applied field will tend to align them. However an important distinction is that each ferromagnetic particle can carry an enormous magnetic moment compared to the case of paramagnetism due to atoms or ions, and hence the name superparamagnetsim. This also leads to the saturation of magnetic moments in realistic magnetic fields even at room temperatures, which is impossible in ordinary paramagnetic materials.

If K_1=0, so that each particle in the assembly can point in any direction and the classical theory of paramagnetism will apply. The magnetization of a superparamagnetic system is thus given by

$$M = n\mu L(\mu B / k_B T) \tag{4-30}$$

where n is the number of particles per unit volume, and L is the Langevin function given by $L(x) = \coth(x) - 1/x$. Thus magnetization curves measured at different temperatures will superimpose when plotted as a fuction of B/T and there will be no hysterisis.

We note that superparamagnetism as described above, will disappear and hysterisis will appear when magnetic particles of certain sizes are cooled below a particular temperature or for a given temperature the particle sizes are increases beyond a particular diameter. These critical values of temperature and size are determined by rate at which thermal equilibrium is approached. For uniaxial particles, detailed analysis predicts the critical volume and temperature as given by

$$V_c = \frac{25 k_B T}{K_1} \tag{4-31}$$

$$T_B = \frac{K_1 V}{25 k_B} \tag{4-32}$$

T_B is known as the blocking temperature, below which magnetization will be stable.

CHAPTER 5
QUANTUM CORRECTIONS TO TRANSPORT PROPERTIES IN METALS

Transport properties of metals at low temperatures are drastically modified due to presence of disorder [34, 35], which leads to nontrivial quantum mechanical effects that cannot be described in terms of classical Boltzmann transport theory. To fully understand the nature of disordered conductors, two new concepts were introduced and have been studied extensively for the last five decades. The first concept is that of Anderson localization, which deals with the nature of a single electron wavefunction in the presence of a random potential. The second concept deals with the interaction among the electrons in the presence of a random potential. These quantum effects become manifest experimentally in the temperature dependence of conductivity, magnetoresistance and Hall effect measurements and are more pronounced in low dimensional systems like films and wires.

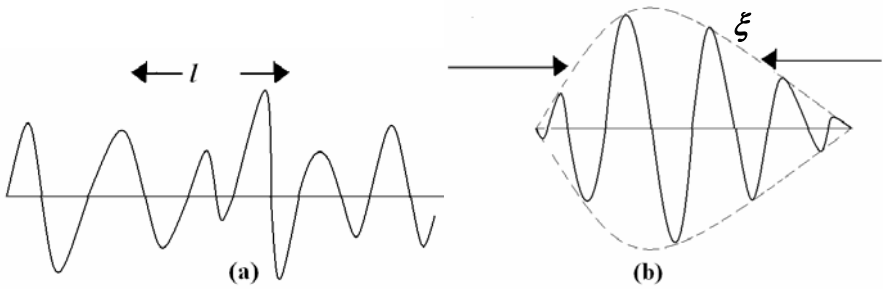

Figure 5-1: Typical wave functions of conduction electrons in presence of disorder;(a) extended state with mean free path l; (b) localized state with localization length ξ.

In the presence of a distribution of random impurity potentials, a conduction electron looses phase coherence at each elastic scattering event on the length scale of the

mean free path *l* but the wave function remains extended throughout the sample (Fig.5-1a). This is the definition of weak disorder. In 1958 Anderson pointed out that if the disorder is sufficiently strong, the wavefunction of the electron may be localized and can be described as a bound state arising because of deep fluctuations in the random potential. This is the strong disorder limit when the envelope of the electronic wavefunction decays exponentially from some point in space on a lengthscale ξ, (the localization length) (Fig.5-1b). An important point to note here is that a linear combinations of infinitely many localized orbitals will not produce an extended state as in the weakly disordered case. Thus entirely different quantum mechanical processes govern two limits of weak and strong disorder and the understanding of what happens in the intermediate region where the cross over occurs has lead to one of the most debated and extensively studied topic in condensed matter physics, namely the metal-insulator transition. We present below a brief account of how transport properties are modified due to quantum properties of conduction electrons in the presence of varying degree of disorder.

Weak Localization Effects

A conduction electron in a metal can be treated as a classical particle only in the limit $k_F l >> 1$, where k_F is the Fermi momentum and *l* is the elastic mean free path. At low temperatures when all inelastic processes like phonon scattering are quenched, the conductivity of a metal is dominated elastic scattering of electrons from impurities and is expressed by the Drude expression which in 2d is given by,

$$\sigma_{2d} = \frac{e^2}{h}(k_F l) \qquad (5\text{-}1)$$

where e^2/h is a universal number of the order of 25kΩ and $k_F l$ is a dimensionless quantity that determines the degree of disorder. Following is a simple and elegant reasoning [35] to obtain an order of magnitude estimate of the quantum corrections to the above classical Drude expression for the conductivity for non-interacting electrons and are known as weak localization corrections.

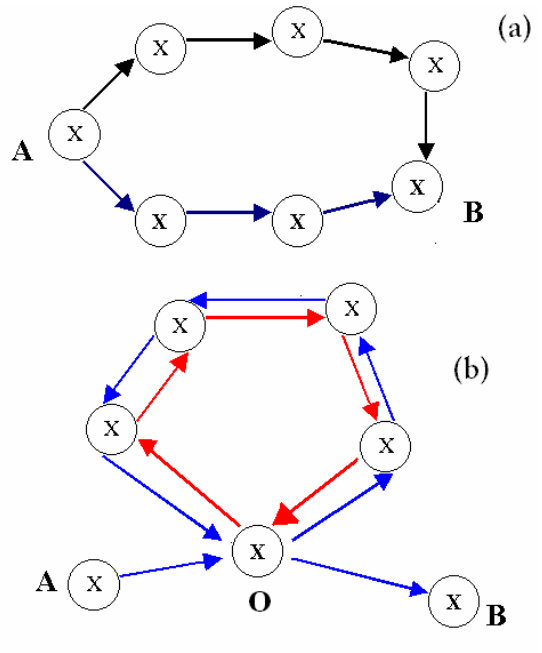

Figure 5-2: Motion of electrons in presence of impurities represented by X (a) Two different paths for an electron to move from point A to B (b) A self intersecting path with two possibilities of traversing the loop.

Consider an electron moving from point A to point B along various paths while being scattered from impurities (Fig. 5-2a). Quantum mechanically the total probability for the particle to reach from one point to another is the square of the modulus for the sum of the amplitudes A_i of individual paths:

$$W = \left|\sum_i A_i\right|^2 = \sum_i |A_i|^2 + \sum_{i \neq j} A_i A_j^* \qquad (5\text{-}2)$$

The first term describes the sum of probabilities of traveling each path, and the second term represents interference of various paths. Associated with each path of amplitude A_i there is a phase given by $\Delta\varphi = \hbar^{-1}\int_A^B \vec{k}\cdot\vec{dl}$, which depends on the length of each trajectory. Hence while calculating the total probability *W*, if we consider many distinct trajectories, the net interference term in *W* will be zero because of the wide distribution of the individual phases.

The above argument for neglecting the interference term does not hold for certain special trajectories that are self-intersecting trajectories that contain loops (Fig. 5-2b). For each loop there are two amplitudes A_1 and A_2 corresponding to opposite direction of traversal of the loop. However the phase does not depend of the direction of traversal of loop and remains same the same, hence for the two amplitudes A_1 and A_2 are coherent. Thus for a loop trajectory, the quantum mechanical probability to find the electron at the point O is given by,

$$\left|A_1 + A_2\right|^2 = \left|A_1\right|^2 + \left|A_2\right|^2 + A_1A_2^* + A_2A_1^* = 4\left|A_1\right|^2 \qquad (5\text{-}3)$$

which is twice as large if interference is neglected (classical situation). This simple example demonstrates that due to quantum mechanical nature of electron paths, interference effect for self-intersecting paths increases. Thus the probability of an electron leaving point A and reaching point B decreases, which leads to an increase in resistivity. The relative magnitude of this correction due to interference effect is determined by the probability of self-intersecting trajectories, which can be estimated as follows. The quantum mechanical path of an electron can be visualized as a tube of diameter of the order of its wavelength $\lambda \sim 1/k_F$. The mean distance traveled by an

electron diffusing through a configuration of impurities for a certain amount of time *t*, which is much larger than mean collision time τ from impurities, is given by $\sqrt{\bar{x}^2} = (Dt)^{1/2}$, where the diffusion constant $D \sim lv$. For a strictly two-dimensional metal film, the area accessible to an electron is Dt. In order for self-intersection to occur during a time d*t* it is required that the final point of the electron path enters the area element $v\mathrm{d}t\lambda$. The probability of this event is the ratio of the two volumes. The total probability of self-intersecting paths is found by integrating over the entire time *t*. The lower limit of the integration is τ, which is the shortest time for the concept of diffusion to apply. To put an upper limit to the integral one assumes that there are inelastic processes like electron-phonon and electron-electron interaction that lead to phase relaxation and hence break down the amplitude coherence. Lets denote this time scale as phase relaxation time τ_φ.. The relative change in conductivity for the 2d case is given by

$$\frac{\Delta\sigma_{2d}}{\sigma_{2d}} \sim -\int_{\tau}^{\tau_\varphi} \frac{v\lambda \mathrm{d}t}{Dt} \tag{5-4}$$

The negative sign illustrates that conductivity decreases due to interference. The change in conductivity due to quantum corrections for a thin film is given by [35],

$$\Delta\sigma_{2d} \sim -\frac{e^2}{\hbar}\ln(\frac{\tau_\varphi}{\tau}) \sim -\frac{e^2}{\hbar}\ln(\frac{L_\varphi}{l}) \tag{5-5}$$

where $L_\varphi \sim \sqrt{D\tau_\varphi}$. Equation (5-5), although derived for a strictly 2D case, is applicable for thin films of thickness $d < L_\varphi$.

The phase-relaxation time τ_φ has a strong temperature dependence of the form $\tau_\varphi \sim T^{-p}$, where *p* in an integer that depends on the exact phase relaxation mechanism.

For example p=1 for electron-electron interaction with small energy transfer [36], which is the dominant phase relaxation mechanism in low dimensions. Thus in general for a metallic film, the conductivity will have logarithmic temperature dependence due to interference corrections and is given by,

$$\sigma_{2d} \sim + \frac{e^2}{\hbar} p \ln(T) + const. \tag{5-6}$$

Magnetoresistance due to Weak Localization

The above correction is drastically modified if one places the sample in a magnetic field. For a vector potential $\vec{A}$ describing the magnetic field, one should replace the momentum $\vec{p}$ by the canonical momentum $\vec{p} - \frac{e}{c}\vec{A}$. This results in a phase difference in the amplitudes A_1 and A_2, for traversing loops (Figure 5-2b) in opposite directions as given by

$$\Delta\varphi_H = \frac{2e}{c\hbar}\oint \vec{A} \cdot d\vec{l} = 2\pi \frac{\Phi}{\Phi_0} \tag{5- 7}$$

where Φ is the magnetic flux enclosed by the loop and $\Phi_0 = hc/2e$ is the flux quantum. The appearance of a phase difference results in the destruction of the interference and hence a decrease in resistivity. To estimate this negative magneto-resistance due to an applied magnetic field, we introduce a new time scale τ_H. Since the average diffusion length is $(Dt)^{1/2}$ and using it as a characteristic size of loops, the magnetic flux through such loops is $\Phi \sim HDt$. We define τ_H so that $\Delta\varphi_H \sim 2\pi$ that gives

$$\tau_H \sim \frac{\Phi_0}{HD} \tag{5-8}$$

The characteristic magnetic fields are determined by the condition $\tau_H \sim \tau_\varphi$, so that

$$H \sim \frac{\Phi_0}{D\tau_\varphi} \tag{5- 9}$$

Substituting $D \sim lv \sim E_F \tau / m$, and using $\omega_B = eH / mc$, we find that $\omega_B \tau << 1$. This means that one needs small magnetic fields.

The asymptotic formula for quantum corrections in presence of magnetic field $\Delta\sigma_{2d}(H)$, for H is much larger than characteristic field given in equation (5-9), is obtained by replacing τ_φ by τ_H in equation (5-5). Thus for the 2d case the magneto-conductance is given by [35],

$$\sigma(H) - \sigma(0) = \Delta\sigma_{2d}(H) - \Delta\sigma_{2d}(H = 0) \approx \frac{e^2}{\hbar} \ln(\frac{eHD\tau_\varphi}{\hbar c}) \tag{5-10}$$

In the above formula H refers to the component perpendicular to the film. The component of applied field parallel to the film does not affect the weak localization correction in a 2d sample as the magnetic flux does not penetrate through any closed electron paths.

Weak Localization in Presence of Spin-Orbit Interaction

Quantum interference depends significantly on electron spin if there exists a scattering mechanism leading to a flip of electron spin. The following is a brief description of an estimate of the interference correction in the presence of spin-orbit scattering. Since the spin is not conserved and can flip while the electron moves from one point to another, one needs to consider all possibilities of initial and final spin while calculating the interference term of the self-intersecting loops (Figure 5-2b). If the initial and final states are given by the wave functions φ_α and φ_β respectively, the interference term is given by

$$C = A_1 A_2^* = \frac{1}{2} \sum_{\sigma\sigma'} \varphi_\alpha^{(1)} \varphi_\beta^{(2)} \varphi_\beta^{*(1)} \varphi_\alpha^{*(2)} \tag{5-11}$$

where the sum is taken over the final spin β and the average is taken over the initial spin state α. To simplify the expression, instead of assuming two possible trajectories along the loop (Figure 5-2b) for a single particle, we assume two particles moving simultaneously in opposite directions. The interference term can be written in terms of eigenfunctions of total spin denoted by ψ_0 for total spin zero and $\psi_{1,m}$ for spin1 and projections *m*=1,2,3 as given by

$$\begin{aligned}
\psi_0 &= \frac{1}{\sqrt{2}}(\varphi_+^{(1)}\varphi_-^{(2)} - \varphi_-^{(1)}\varphi_+^{(2)}) \\
\psi_{1,1} &= \varphi_+^{(1)}\varphi_+^{(2)} \\
\psi_{1,-1} &= \varphi_-^{(1)}\varphi_-^{(2)} \\
\psi_{1,0} &= \frac{1}{\sqrt{2}}(\varphi_+^{(1)}\varphi_-^{(2)} + \varphi_-^{(1)}\varphi_+^{(2)})
\end{aligned} \tag{5-12}$$

Thus the interference term in equation 5-11 can be expressed as follows,

$$C = \frac{1}{2}(\sum_m |\psi_{1,m}|^2 - |\psi_0|^2) \tag{5-13}$$

In the presence of spin-orbit scattering with characteristic times $\tau_{so} << \tau_\varphi$, the states $\psi_{1,m}$ that carry spin information are damped with a characteristic time τ_{so}, while ψ_0 is damped with time τ_φ. Therefore for the 2d case it was shown [37],

$$\frac{\Delta\sigma_{2d}}{\sigma_{2d}} \sim -\int_\tau^{\tau_\varphi} \frac{\lambda v dt}{Dt}(\frac{3}{2}e^{-t/\tau^{so}} - \frac{1}{2}) \tag{5-14}$$

Thus depending on the spin-orbit scattering time τ_{so} relative to τ_φ we have the following two cases for 2d samples [37],

$$\Delta\sigma_{2d} \sim -\frac{e^2}{\hbar}\ln(\frac{\tau_\varphi}{\tau}) \qquad \text{for } \tau_{so} >> \tau_\varphi \tag{5-15}$$

$$\Delta\sigma_{2d} \sim \frac{e^2}{\hbar}(-\frac{3}{2}\ln(\frac{\tau_{so}}{\tau})+\frac{1}{2}\ln(\frac{\tau_{\varphi}}{\tau})) \quad \text{for } \tau_{so} << \tau_{\varphi} \qquad (5\text{-}16)$$

thus it follows from equation (5-16) that the spin-orbit correction reverses the sign of the temperature dependence of conductivity due to τ_{φ}. In weak magnetic fields and under strong spin-orbit, the magnetoresistance becomes positive. For sufficiently strong magnetic field such that $\tau_H < \tau_{so}$, the magneto-resistance changes sign and becomes negative. The combined effect of positive quantum correction to conductivity and positive magnetoresistance is known as 'weak anti-localization'. If however, scattering occurs from paramagnetic impurities, then both the singlet and the triplet wavefunctions in equation (5-13) decay with time of the order of τ_s, so that for $\tau_s << \tau_{\varphi}$ the corrections to conductivity are no longer temperature dependent.

Weak Localization in Ferromagnetic Films

We now review the weak localization corrections in ferromagnetic materials with strong spin-orbit scattering based on a theoretical treatment by Dugaev *et.*al [38]. The relevant Hamiltonian considered in this case is given by

$$H = \int d^3\vec{r}\,\psi^*[-\frac{\nabla^2}{2m} - M\sigma_z + V(\vec{r}) - \frac{i\lambda_0^2}{4}(\vec{\sigma}\times\nabla V(\vec{r}))\cdot\nabla]\psi(\vec{r}) \qquad (5\text{-}17)$$

where $\psi \equiv (\psi_\uparrow, \psi_\uparrow)$ is a spinor field , $\vec{\sigma} = (\sigma_x, \sigma_y, \sigma_z)$ are the Pauli matrices, M is the magnetization assumed to be along z-direction and V is the random impurity potential, and λ_0 is the spin-orbit scattering strength. The exchange term $M\sigma_z$ acts only on the spins and has no direct effect on the orbital motion.

In the language of many-body theory, weak localization corrections arise from the particle-particle channel with two propagators describing electrons with vanishing total

momentum and with very close energy (Cooper channel). Physically, the so-called "Cooperon" propagator represents two electrons traversing a self intersecting loop (Figure 5-2b) in opposite directions. There are two possible situations depending on the relative spin orientation of the two electrons. In a ferromagnet the exchange energy is strong so that $M >> \tau_{\uparrow}^{-1}, \tau_{\downarrow}^{-1}$, where $\tau_{\uparrow}$ and $\tau_{\uparrow}$ are momentum relaxation times for spin up and spin down conduction electrons. Physically, this condition implies that spin-flip processes are suppressed due to the exchange field *M*, and it was shown that for a bulk 3d ferromagnetic sample, the contribution to the "Cooperon" from the singlet pairs i.e. electrons with opposite spins is small compared to that of triplet pairs of electrons with parallel spins by the factor $1/M\tau_{\uparrow(\downarrow)}$. The exclusion of the singlet channel is crucial and leads to the absence of weak antilocalization in ferromagnets and the weak localization correction to the conductivity is found to be a direct generalization of the non magnetic case with two bands of electrons of opposite spin polarization. We are interested in the two dimensional ferromagnetic samples and quote the final result in two dimensions [38] as follows,

$$\Delta\sigma_{2d} = \frac{e^2}{4\pi^2\hbar}\{\ln[\tau_{\uparrow}(\frac{1}{\tau_{\varphi_{\uparrow}}} + \frac{1}{\widetilde{\tau}_{SO_{\uparrow}}})] + \ln[\tau_{\downarrow}(\frac{1}{\tau_{\varphi_{\uparrow}}} + \frac{1}{\widetilde{\tau}_{SO_{\uparrow}}})]\} \qquad (5\text{-}18)$$

where $\tau_{\varphi\uparrow(\downarrow)}$ is the temperature dependent phase breaking time. $\tau_{\uparrow(\downarrow)}$ is the momentum relaxation time and $\widetilde{\tau}_{SO\uparrow(\downarrow)}$ is the effective spin-orbit scattering time for spin up (down) electrons and depends on the relative orientation of the magnetization *M* with respect to the plane of the film. The important point is that for $\tau << \widetilde{\tau}_{SO}, \tau_{\varphi}$, the above correction to conductivity is negative just like the nonmagnetic case.

Electron Interaction Effects

In this section we discuss the corrections to conductivity due to interactions between conduction electrons. We note that within the Boltzmann transport equation, electron-electron collisions cannot affect the conductivity in the case of a single band structure and in the absence of Umklapp processes. This is because electron-electron collisions conserve the total momentum. Inclusion of the Fermi liquid corrections that takes into account a finite inter electron interaction potential, renormalizes the residual conductivity but does not introduce any essential temperature dependence. However, taking into account the interference of elastic scattering by impurities with electron-electron interaction produces nontrivial temperature dependence of the conductivity and the one particle density of states. The following is brief account of some simple physical ideas that illustrates the origin of quantum corrections to transport properties due to electron-electron interaction.

Scattering by Friedel Oscillations

We now discuss a very important concept of the Friedel oscillations that arise due to standing waves formed as a result of interference between incoming and backscattered electron waves. To illustrate this we consider a simple situation in 1D with an infinitely high barrier at x=0. For each wave vector k, the wavefunction is a superposition of the incoming plane wave $\exp(ikx)/\sqrt{L}$ and a reflected wave $\exp(-ikx)/\sqrt{L}$ and is given by $\psi = 2i\sin(kx)/\sqrt{L}$. Accordingly, the probability density is given by $|\psi|^2 = 4\sin^2(kx)/L$ and oscillates in space. The probability that a state with momentum k is occupied is given by the Fermi function f_k. The electron density is described by

$$n(x) = 2\sum_k \frac{dk}{2\pi} f_k |\psi|^2 = 8\int_0^{k_F} \frac{dk}{2\pi} \sin^2(kx) = n_o - \frac{\sin(2k_F x)}{\pi x} \qquad (5\text{-}19)$$

where $n_o = 2k_F / \pi$ is the density of the homogeneous electron gas, is oscillatory and damps from the origin as x^{-1}.

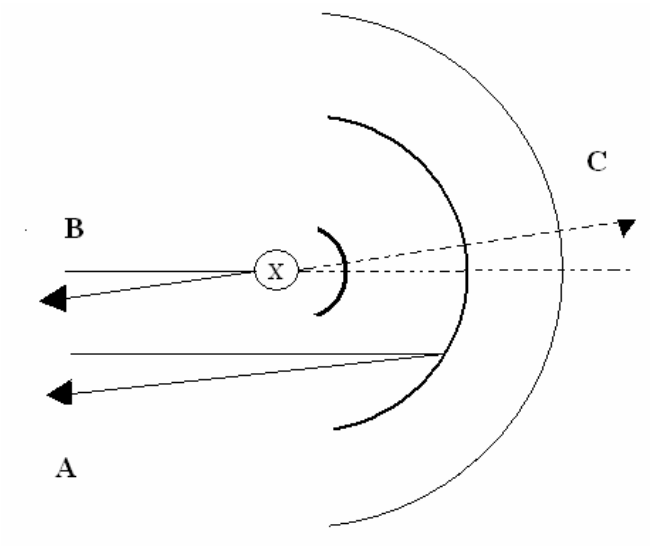

Figure 5-3: Schematic diagram of Friedel oscillation due to a single impurity due to backscattering described by path C. Interference between two paths A and B contributes mostly to backscattering.

A single impurity at the origin with a general potential $U(\vec{r})$ also induces a modulation of electron density close to the impurity. The oscillating part of the modulation in 2D(shown schematically in Fig. 5-3) is given by [39],

$$\delta\rho(\vec{r}) = -\frac{\nu\lambda}{2\pi \cdot r^2} \sin(2k_F r) \qquad (5\text{-}20)$$

where *r* is the distance from the impurity, which has a potential treated in the Born approximation $\lambda = \int U(\vec{r}) d\vec{r}$, and $\nu = m/\pi\hbar^2$ is the density of states in 2D. Taking into account the electron-electron interaction $V_o(\vec{r}_1 - \vec{r}_2)$ one finds additional scattering due to

the Friedel oscillation. This potential can be presentation as a sum of the direct (Hartree) and exchange (Fock) terms [39]:

$$\begin{aligned} &\delta V(\vec{r}_1,\vec{r}_2) = V_H(\vec{r}_1)\delta(\vec{r}_1-\vec{r}_2) - V_F(\vec{r}_1,\vec{r}_2) \\ &V_H(\vec{r}_1) = \int d\vec{r}_3 V_o(\vec{r}_1-\vec{r}_3)\delta\rho(\vec{r}_3) \\ &V_F(\vec{r}_1-\vec{r}_2) = \frac{1}{2}V_o(\vec{r}_1-\vec{r}_2)\delta n(\vec{r}_1,\vec{r}_2) \end{aligned} \tag{5-21}$$

where $\rho(\vec{r})$ is the diagonal element of the one electron density matrix *n* given by,

$$n(\vec{r}_1,\vec{r}_2) = \sum_k \Psi_k^*(\vec{r}_1)\Psi_k(\vec{r}_2) \tag{5-22}$$

The factor ½ indicates that only electrons with the same spin participate in exchange interaction. As a function of the distance from the impurity, the Hartree-Fock energy oscillates similarly to the Friedel oscillation.

The leading correction to conductivity is a result of interference between two semiclassical paths as shown in Fig.5-3. If an electron follows path A, it scatters off the Friedel oscillation created by the impurity and path B corresponds to scattering by the impurity itself. Interference is most important for scattering angles close to π (backscattering), since the extra phase factor on path A is cancelled by the phase of Friedel oscillation $\exp(-i2k_F R)$, so that the amplitudes corresponding to the two paths are coherent and interfere constructively. This interference persists to large distances *R* and is limited only by temperature, $R \approx 1/|k-k_F| \le \hbar v_F / k_B T$. At finite temperature the amplitude of the Friedel oscillation assumes temperature dependence. Explicit calculations for the scattering amplitude as function of scattering angle exhibit a sharp peak for back scattering with a width and height proportional to $\sqrt{T}$. The correction to conductivity with respect to the classical Drude conductivity is given by [39],

$$\frac{\Delta\sigma}{\sigma} = \nu[V_o(0) - 2V_o(2k_F)]\frac{T}{\varepsilon_F} \qquad (5\text{-}23)$$

where the first term is the exchange correction and the second term is the Hartree correction. The above is the conductivity correction in the ballistic limit defined by $T\tau << 1$. We note some important points in the above expression. Firstly, the sign of the Hartree and exchange corrections are opposite. Secondly, the leading temperature correction comes from the Fourier component at $q=0$ and $q=2k_F$ for the exchange and Hartree term respectively. The sign of the total correction is not universal and depends on the details of the electron-electron scattering.

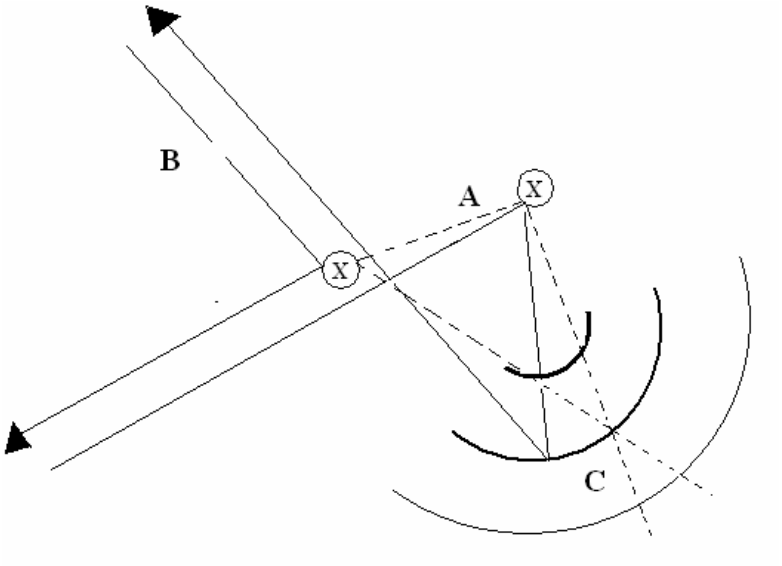

Figure 5-4: Friedel oscillation due to two impurities created by the self-intersecting path C. Scattering at all angles are affected by interference.

So far we have considered the effect of single impurity. For the case of multiple impurities, the Friedel oscillations can occur from self-intersecting paths of electrons. In Fig. 5-4 we show scattering process that involves two impurities and the resulting Friedel oscillation due to path C shown in dashed lines. In this case the scattering amplitude at all angles and not just the back scattering are affected. Scattering by multiple Friedel

oscillations have been calculated in the framework of many body theory and is known as the Altshuler-Aronov [35] correction. Although interaction between two electrons is independent of spin, summation of terms in the perturbation theory depends on the spin state of the two electrons involved. The total number of channels is 4. These channels are classified by the total spin of the two electrons; one state with total spin zero (singlet channel) and three states with total spin 1(triplet channel) differing by the projection of the spin. For long range interaction the perturbation theory for the Hartree corrections singlet and triplet channels is different.

The singlet channel contribution combined with exchange corrections as a renormalization of coupling constant and the final result is still universal. The triplet channel contribution depends on the Fermi-liquid constant F_0^σ. The total conductivity correction in 2D is given by [35, 39]:

$$\delta\sigma = -\frac{e^2}{2\pi^2\hbar}\ln(\frac{\hbar}{T\tau})[1+3(1-\frac{\ln(1+F_0^\sigma)}{F_0^\sigma})] \qquad (5\text{-}24)$$

The above equation was derived for the so-called "Diffusive regime" characterized by $T\tau << 1$. The sign and magnitude of the correction is non-universal and depends on the competition between the universal and positive exchange term and the coupling dependent and negative Hartree contribution. For short-range electron-electron interactions due to screened Coulomb interactions in good metals, the Hartree term is neglected and one has a universal correction to conductivity due to the exchange term.

The above result is obtained by treating interaction in lowest order perturbation theory and in weak impurity scattering regime. Now we quote some results of scaling theory of interaction problem that goes beyond the perturbation theory. For a two

dimensional conductor with spin-split bands like in ferromagnet and long range Coulomb interaction, the scaling theory predicts a universal correction [40] given by

$$\Delta\sigma = \frac{e^2}{2\pi^2\hbar}(2-2\ln 2)\ln(T\tau) \qquad (5\text{-}25)$$

The above results were obtained for the case when weak localization corrections are completely suppressed. For short range electron interaction the logarithmic coefficient is found to be non-universal [40].

Moreover, for 2d conductors with strong spin-orbit or spin-flip scattering, with long range Coulomb interaction, it was argued [41] that the triplet channel is suppressed and only the exchange term survives, predicting a universal correction given by,

$$\Delta\sigma = \frac{e^2}{2\pi^2\hbar}\ln(T\tau) \qquad (5\text{-}26)$$

Magnetoresistance due to Electron Interaction

We have discussed earlier how even a weak magnetic field can suppress the localization effects resulting in a negative magnetoresistance. In the language of many-body theory, weak localization effects arise from the particle-particle channel and are supposed to be sensitive to magnetic flux. The electron interaction effects arise from the particle-hole diffusion channel and do not have similar sensitivity to magnetic field. The dominant effect of magnetic field in this case is the splitting of the spin up and spin down bands [34]. This physical idea is most simply illustrated for the self-energy correction, where the singular correction is due to the correlation between the wavefunction of the added electron and the wavefunctions of the occupied electrons that are nearby in energy. In the presence of a magnetic field, the triplet term is divided into an S_z=0 and two $|S_z| = 1$ terms. The exchange (singlet) and the S_z=0 triplet terms involve correlation with

electrons with the same spin and are unaffected by the spin splitting. For the $S_z = \pm 1$ terms, the spin splitting produces a gap $g\mu_B H$ between the lowest unoccupied spin-up and the highest occupied spin-down electron. The singularity of that term is cut off for $g\mu_B H$ greater than $k_B T$. In a magnetic field, the correction to the conductivity can be written as a sum of two terms,

$$\delta\sigma(H,T) = \delta\sigma^C(T) + \delta\sigma^S(H,T) \tag{5-27}$$

The first term is the field independent "charge channel" contribution which is the sum of exchange and S_z=0 Hartree contribution, is same as equation (5-21). The second term is the $|S_z| = 1$ triplet contribution or the "spin channel", with a field dependence for the 2d case given by [34],

$$\delta\sigma^S(H,T) - \delta\sigma^S(0,T) = \frac{e^2}{2\pi^2\hbar}\left(1 - \frac{\ln(1+F_0^\sigma)}{F_0^\sigma}\right)\begin{cases} \ln h & h >> 1 \\ h^2 & h << 1 \end{cases} \tag{5-28}$$

where $h = g\mu_B H / k_B T$. The quantity in the parenthesis is the Hartree contribution to conductivity and is non-universal in both sign and magnitude and depends on the details of the potential describing electron-electron interaction.

Transport Properties of Granular Metals

So far we have discussed quantum transport properties of homogeneous systems with a uniform distribution of impurities that determine the mean free path. In this section we discuss the transport properties of granular metals with Coulomb interaction between electrons. The motion of electrons inside each grain is diffusive and they can tunnel from one grain to another. In principle the grains can be clean so that electron scattering is mainly from surfaces. In this limit the tunnel conductance is smaller than the grain

conductance and inter-granular transport can be distinguished from intra-granular transport. The process of electron tunneling from grain to grain that governs the transport properties are accompanied by charging of grains. This may lead to Coulomb blockade especially in the limit of weak coupling between grains. A step towards formulating a theory on transport in granular medium was due to Beloborodov *et. al*.[42]. It was shown that depending on the dimensionless tunneling conductance g_T one observes exponential (at $g_T<<1$) or logarithmic (at $g_T>>1$) temperature dependence of conductivity. This theoretical approach was based on an earlier paper by Ambegaokar [43], which however was applicable only at temperatures $T > g_T\delta$, where δ is the mean energy level spacing in a single grain. In this regime the electron coherence does not extend beyond the grain size. The low temperature regime $T \le g_T\delta$, where the electron moves coherently over distances exceeding the single grain size, was discussed in a later paper by Beloborodov *et.al* [42] for large tunneling conductance g_T. The following Hamiltonian describes a system of weakly coupled metallic grains,

$$H = H_o + H_C + \sum_{ij} t_{ij}[\Psi^*(r_i)\Psi(r_j) + \Psi^*(r_j)\Psi(r_i)] \qquad (5\text{-}29)$$

where t_{ij} is the tunneling matrix element between *i*-th and *j*-th grain, H_o is the Hamiltonian for non-interacting isolated grains, and H_c describes the Coulomb interaction inside (i=j) and between grains (i≠j) as described by

$$H_c = \frac{e^2}{2}\sum_{ij} \hat{n}_i C_{ij}^{-1} \hat{n}_j \qquad (5\text{-}30)$$

where C_{ij} is the capacitance matrix and $\hat{n}_i$ is the operator of electron number in the i-th grain.

Beloborodov *et. al.* [42] show that in the low temperature regime, properties of the granular metal depend on dimensionality and corrections to conductivity and density of states due to Coulomb interaction are similar to those obtained for homogeneous metals. The critical grain size in 3D where a metal to insulator transition occurs is estimated to be,

$$g_T^c = \frac{1}{6\pi}\ln(\frac{E_C}{\delta}) \tag{5-31}$$

where E_C is the charging energy of an isolated grain. The conductivity of a granular metal is given by

$$\sigma = \sigma_o + \delta\sigma_1 + \delta\sigma_2 \tag{5-32}$$

The classical Drude conductivity for a granular metal in a general dimension *d*, with grain size *a* is given by

$$\sigma_o = 2\frac{e^2}{\hbar} g_T a^{2-d} \tag{5-33}$$

The correction to conductivity due to large energy scales $\varepsilon > g_T\delta$ is given by

$$\frac{\delta\sigma_1}{\sigma_o} = -\frac{1}{2\pi g_T d}\ln[\frac{g_T E_C}{\max(T, g_T\delta)}] \tag{5-34}$$

We note that the dimensionality in this case appears only as a coefficient but the logarithmic temperature dependence remains same for all dimensions. This means tunneling of electrons with energies $\varepsilon > g_T\delta$ can be considered as incoherent.

On the other hand corrections from low energy scale $\varepsilon \le g_T\delta$ arises from coherent electron motion on the scales larger than grain size, and is given by

$$\frac{\delta\sigma_2}{\sigma_o}=\begin{cases}\dfrac{\alpha}{12\pi^2 g_T}\sqrt{\dfrac{T}{g_T\delta}} & d=3\\ -\dfrac{1}{4\pi^2 g_T}\ln(\dfrac{g_T\delta}{T}) & d=2\\ -\dfrac{\beta}{4\pi}\sqrt{\dfrac{\delta}{Tg_T}} & d=1\end{cases} \tag{5-35}$$

where α and β are numerical constants. We summarize the results for a 2D granular system for $T < g_T\delta$ as follows,

$$\sigma=\frac{e^2}{2\pi^2\hbar}[4\pi^2 g_T+\pi\ln(\frac{\delta}{E_C})+\ln(\frac{T}{g_T\delta})] \tag{5-36}$$

and for $T > g_T\delta$

$$\sigma=\frac{e^2}{2\pi^2\hbar}[4\pi^2 g_T+\pi\ln(\frac{T}{g_T E_C})] \tag{5-37}$$

For samples with weak inter grain coupling $g_T << 1$ at low temperatures $T << E_C$, the conductivity was shown to be [42],

$$\sigma=2\sigma_o\exp(-E_C/T) \tag{5-38}$$

where E_C is the charging energy. However this behavior is usually not observed experimentally because of the distribution of grain sizes in real samples, as discussed in the next section.

Transport in Weakly Coupled Granular Metals

A theory of transport in granular metallic films was developed by Sheng *et.al* [44] in the limit of weak coupling between grains. They proposed a picture of granular metal represented by a conductance network in which the metal grains are interconnected by conductances of the form:

$$\sigma_s \sim \exp(-2\chi s - E_c^o / 2k_B T) \tag{5-39}$$

where s is the tunnel-barrier thickness and $\chi = (2m\varphi/\hbar^2)^{1/2}$ for a barrier height of φ. The calculations are simplified by assuming the grains to be spherical with a distribution of grain diameters d and the charging energy $E_C \sim 1/d$, such that the product sE_c is constant for a given film: $sE_C\chi = C$, where C and χ are constants that depend only on the volume fraction of the metal. The second assumption was to include only tunneling between nearest neighbors, which are nearly equal in size. This implies that for a given temperature there is an optimum tunnel-barrier thickness given by $s_m = (C/k_B T)^{1/2}/2\chi$ for which the inter grain conductivity is maximum. The final assumption is that the temperature dependence of the conductivity network is given by that of the maximum inter-grain conductivity so that,

$$\sigma(T) \sim \exp[-2(C/k_B T)^{1/2}] \tag{5-40}$$

The constant C is proportional to the charging energy E_C, which is inversely related to the mean grain diameter $\langle d \rangle$. Thus, the dominant contribution to conductivity at high temperatures is due to tunneling between small grains (large E_c) separated by thin tunnel barriers, while at low temperatures the dominant contribution is due to large grains separated by thick tunnel barriers.

Now we consider the case for ferromagnetic metallic grains so that in addition to the charging energy E_C there is a magnetic exchange energy E_M associated with a tunneling event. The exchange energy arises when the magnetic moments of the participating grains are not parallel and electron energy is conserved during tunneling. The intergrain conductance in this case is given by [45],

$$\sigma_s \sim \exp(-2\chi s)\{\frac{1}{2}(1+P)\exp[-(E_c^o + E_M)/2k_BT] + \frac{1}{2}(1-P)\exp[-(E_c^o - E_M)/2k_BT]\} \quad (5\text{-}41)$$

Here *P* is the polarization of tunneling electrons, so that the coefficients *(1+P)/2* and *(1-P)/2* are the probabilities that an electron tunneling from one grain to another has its spin parallel and anti-parallel, respectively, to that of the initial grain. Using the same assumptions for the non-magnetic grains discussed earlier, the magneto-conductivity is given by [45],

$$\sigma(H,T) = \sigma(0,T)[\cosh(E_M / k_BT) - P\sinh(E_M / k_BT)] \quad (5\text{-}42)$$

The magnetic exchange energy can be expressed in terms of spin correlations of two neighboring grains and is given by [45],

$$E_M = \frac{1}{2}J[1 - \langle \vec{S}_1 \cdot \vec{S}_2 \rangle / S^2] \quad (5\text{-}43)$$

An important point to note is that by applying a magnetic field strong enough to align all the moments, the exchange energy is zero, and the temperature dependence of conductivity reduces to that of the non-magnetic case shown in equation (5-40).

Quantum Corrections to Hall Conductivity

The normal Hall coefficient defined as $R_n = E_y / J_x H$, is another quantity in addition to magnetoresistance that behaves differently for weak localization and electron interaction effects. The quantum correction to the Hall conductivity due to weak localization effects was first calculated by Fukuyama [46] and it was shown that the Hall resistance given by $R_{xy}^n = R_n B$ remains unchanged so that

$$\delta R_{xy}^n / R_{xy}^n = 0 \quad (5\text{-}44)$$

Thus in a disordered conductor subject solely to weak localization effects, the normal Hall resistance at given magnetic field will remain constant as temperature is varied. The longitudinal resistance R_{xx} will have the usual logarithmic temperature dependence due to interference effects. The normal Hall conductivity has logarithmic temperature dependence and has a slope twice that of longitudinal conductivity. This is easily deduced using the fact that $\sigma_{xy}^{n} \approx R_{xy}^{n} / R_{xx}^{2}$ and taking logarithmic derivative we have

$$\frac{\delta\sigma_{xy}^{n}}{\sigma_{xy}^{n}} = \frac{\delta R_{xy}^{n}}{R_{xy}^{n}} - 2\frac{\delta R_{xx}}{R_{xx}} \tag{5-45}$$

Thus it follows from equation (5-44) that the normal Hall conductivity has logarithmic temperature dependence with a slope twice that of longitudinal conductivity as shown by the relation,

$$\frac{\delta\sigma_{xy}^{n}}{\sigma_{xy}^{n}} = -2\frac{\delta R_{xx}}{R_{xx}} = 2\frac{\delta\sigma_{xx}}{\sigma_{xx}} \tag{5-46}$$

For the case of only electron interaction effect (no weak localization) in the diffusion channel it was shown by Altshuler *et. al*.[35] that the normal Hall conductivity has zero quantum correction and hence remains independent of temperature so that,

$$\delta\sigma_{xy}^{n} / \sigma_{xy}^{n} = 0 \tag{5-47}$$

Thus it follows from equation (5-45) the effect of only electron interaction implies that

$$\frac{\delta R_{xy}^{n}}{R_{xy}^{n}} = 2\frac{\delta R_{xx}}{R_{xx}} \ . \tag{5-48}$$

This means that both R_{xx} and R_{xy}^{n} will exhibit logarithmic temperature dependence due to electron interaction, and the slope of R_{xy}^{n} will be twice that of R_{xx}.

Quantum corrections to the anomalous Hall conductivity have not been studied as extensively as the normal Hall conductivity. The effect of short-range electron interactions to the AH conductivity within the framework of the skew scattering mechanism were first studied by Langenfeld *et. al.* [47] who showed that there is no finite correction due to the exchange(Fock) part of interaction, so that

$$\sigma_{xy}^{AH} = 0 \Rightarrow \frac{\delta R_{xy}^{AH}}{R_{xy}^{AH}} = 2\frac{R_{xx}}{R_{xx}} \tag{5-49}$$

Thus the AH effect was found to have a behavior similar to that of the normal Hall effect. We note that the above calculation does not include the contributions from the Hartree terms to the interactions and also assumes the absence of weak localization corrections. The above theoretical prediction (equation 5-49) was found to be in good agreement with experimental results of Bergmann and Ye [48] where the AH conductivity in thin amorphous films of iron was found to independent of temperature.

Weak localization contributions to the AH conductivity were studied by Dugaev *et. al*. [24] for the Hamiltonian given by equation (5-17). For the case of side jump (SJ) mechanism in a 2d ferromagnetic sample it was predicted [24] that

$$\frac{\delta\sigma_{xy}^{AH(SJ)}}{\sigma_{xy}^{AH(SJ)}} \sim \frac{1}{(k_F l)^3}. \tag{5-50}$$

The corresponding weak localization correction to longitudinal conductivity is given by $\delta\sigma_{xx}/\sigma_{xx} \sim (k_F l)^{-1}$. We note that the weak localization calculations are valid in the metallic regime that corresponds to $k_F l >> 1$. Thus it was concluded that the weak localization correction to AH conductivity due to side jump mechanism is negligible [24],

$$\frac{\delta\sigma_{xy}^{AH(SJ)}}{\sigma_{xy}^{AH(SJ)}} << \frac{\delta\sigma_{xx}}{\sigma_{xx}} \tag{5-51}$$

The above theoretical prediction provided an alternative explanation[24] to the experimental results of Bergmann and Ye [48].

For the case of skew scattering(SS) mechanism, the weak localization corrections were shown [24] to give rise a finite correction as given by

$$\delta\sigma_{xy}^{AH(SS)} = -\frac{e^2}{36\pi\hbar}\lambda_0^2 v_0 \{k_{F\uparrow}^2 \nu_\uparrow \ln[\tau_\uparrow(\frac{1}{\tau_{\varphi\uparrow}} + \frac{1}{\widetilde{\tau}_{SO\uparrow}})] - k_{F\downarrow}^2 \nu_\downarrow \ln[\tau_\downarrow(\frac{1}{\tau_{\varphi\uparrow}} + \frac{1}{\widetilde{\tau}_{SO\uparrow}})]\} \tag{5-52}$$

The above expression was derived for the case of a random short-range impurity potential of the form $V(\vec{r}) = v_o \sum_i \delta(\vec{r} - \vec{R}_i)$ is assumed. Within this model, the contribution to the AH conductivity solely due to impurity scattering, in the absence of weak localization or electron interactions was shown [24] to be,

$$\sigma_{xy}^{AH(SS)} = -\frac{\pi e^2}{18}\lambda_0^2 v_0 \{k_{F\uparrow}^2 \nu_\uparrow^2 v_{F\uparrow}^2 \tau_\uparrow - k_{F\downarrow}^2 \nu_\downarrow^2 v_{F\downarrow}^2 \tau_\downarrow\} \tag{5-53}$$

Using the fact that the residual longitudinal conductivity is given by

$$\sigma_{xx} = \frac{n_\uparrow e^2 \tau_\uparrow}{m} + \frac{n_\downarrow e^2 \tau_\downarrow}{m} \tag{5-54}$$

and assuming a parabolic band, one can simplify the expression for weak localization correction to the AH conductivity for each of the two bands with opposite spin polarization and is given by the following expression,

$$\frac{\delta\sigma_{xy\uparrow(\downarrow)}^{AH(SS)}}{\sigma_{xy\uparrow(\downarrow)}^{AH(SS)}} = \frac{1}{2}\frac{e^2}{2\pi^2\hbar}\frac{1}{\sigma_{xx\uparrow(\downarrow)}}\ln[\tau_{\uparrow(\downarrow)}(\frac{1}{\tau_{\varphi\uparrow(\downarrow)}} + \frac{1}{\widetilde{\tau}_{SO\uparrow(\downarrow)}})] \tag{5-55}$$

Comparing the above equation with equation (5-18) it follows that both the longitudinal and the AH conductivity have finite logarithmic corrections due to weak localization.

CHAPTER 6
EXPERIMENTAL RESULTS AND DISCUSSION

Experimental study of magnetism in ultrathin films of ferromagnetic transition elements like iron, cobalt and nickel pose a serious challenge because of their air sensitive nature. Previously, Bergmann and Ye [48] have reported , *in situ* transport measurements on pure amorphous iron films few monolayers thick, which were quench-condensed on antimony substrates at liquid helium temperature. These experiments revealed an important finding that the Anomalous Hall effect behaves similar to that of normal Hall effect in non-magnetic materials and has no quantum correction at low temperatures due to electron-electron interactions or weak localizations effects. However, one might argue that the presence of a "polarizable" substrate, namely antimony, might dope the few atomic layers of iron on top and these might affect its properties. We undertook a study of magnetic properties of thin films of iron and cobalt grown on inert glass substrates, ordinarily used as microscope slides. Using the SHIVA apparatus described in chapter 2, we were able to investigate the magnetic properties of iron and cobalt films with polycrystalline morphology, while protecting them from oxidation, using the Anomalous Hall ^{2} measurement. The following is a detailed account of our experimental findings.

Experimental Details

Sample Fabrication

Iron and cobalt samples were grown by r.f. magnetron sputtering techniques under identical growth conditions. We used r.f. power of 35W with an argon flow of 10

sccm, which developed a DC bias of around -145V with respect to target. The pressure in the chamber is of the order of 10^{-4} Torr. The samples were grown in the Hall bar geometry through a shadow mask onto glass substrates at room temperatures. Under the conditions described above, films are known to grow through various stages of different morphology [49] rather than gradual layer by layer growth. Initially, film growth proceeds via nucleation of isolated grains of metals. With more arriving adatoms the grains continue to grow in size and at some critical thickness, the grains coalesce into several discrete and continuous percolating channels. As the substrates are exposed further the film eventually becomes homogeneous with well-connected microscopic grains, such that the film resistivity scales with thickness [17, 18]. Such a film behaves like a good metal with a low temperature residual conductivity determined by impurities and imperfections. Even in the case of metallic grains not physically touching each other, there could be electrical conduction due to tunneling of electrons between grains. The polycrystalline films in our experiments were thicker than the quench-condensed films in the previous investigation [48] by Bergmann and Ye, but are outside the homogeneous regime where film resistance scales with thickness. Thus resistivity is not a well-defined quantity, and we use sheet resistance, to characterize our films. The sheet resistance is defined as the resistance of a square film and is independent of the lateral dimensions of a film and depends only on thickness and morphology. In the Hall-bar geometry, where the sample is rectangular shaped, where the current I is uniformly distributed along the width W and where voltage V is measured between leads separated by L. The number of squares involved in such a measurement is L/W. The sheet resistance is given by dividing the measured resistance $R=V/I$ by the total number of squares so that $R_{sq} = R/(L/W)$.

Measurement Setup

We have investigated films over a wide range of sheet resistances from 50Ω to 1000000Ω. All our samples are in the Hall bar geometry with six terminals as shown in Figs. 6-1and 6-2. We performed standard four terminal techniques using separate pair of leads for sourcing current in the sample and measuring transverse and longitudinal voltages, to eliminate the effect of contact resistances. We have used two different experimental setups to measure longitudinal and transverse resistances simultaneously, depending on the magnitude of the two terminal resistances of the leads.

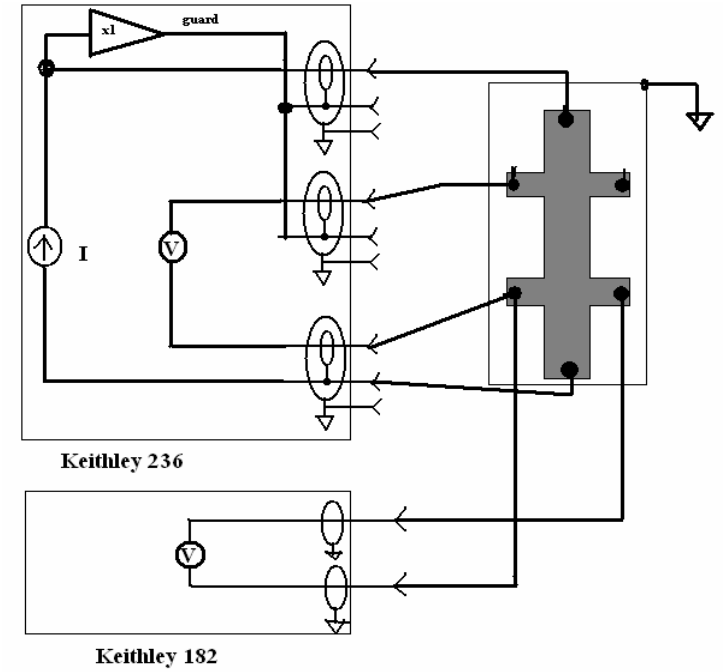

Figure 6-1: A d.c. transport measurement setup using Keithly 236 for sourcing a constant current and measure longitudinal voltage and Keithly 182 nano-voltmeter to measure transverse voltage. The sample in Hall-bar shape is shown as a shaded.

Figure 6-1 shows the circuit diagram for d.c. measurement using a Keithley 236 Source-Measure Unit and a Keithley 182 Nanovoltmeter. We programmed the 236 unit to

source a constant current through the sample and measure the voltage developed across the longitudinal leads. Simultaneously the Keithley182 is used to measure the voltage developed across the Hall leads. This setup is particularly useful for measuring high resistance samples as the Keithley 236 is equipped with guarding buffers which increase the input resistances of source/sense leads to greater than$10^{14}\Omega$ and also reduce cable capacitance, thus leading to more accurate high resistance measurements with faster settling times. However, since the sensitivity of the Keithley 236 is only 1μV, it is not suitable for measuring small changes in resistance.

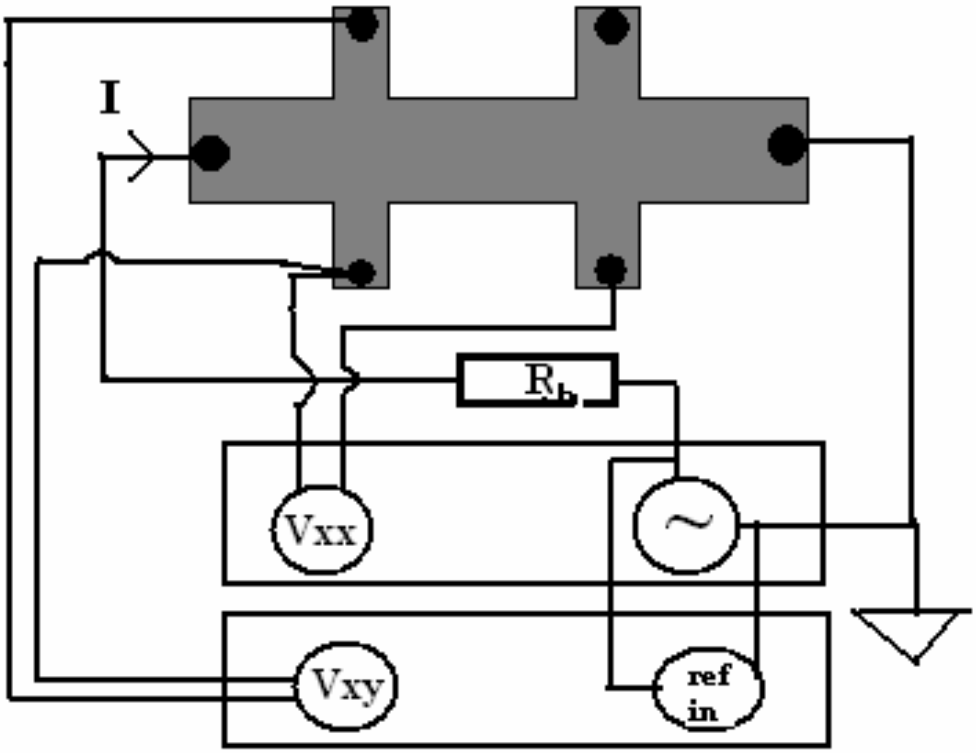

Figure 6-2:An a.c. transport measurement setup using two SR830 lock-in amplifiers operating at same frequency to measure longitudinal and transverse resistance, used in samples with low contact resistances. A constant current is generated from the voltage source of the upper SR830 and by placing a ballast resistor R_b of 1MΩ in series with the sample. The sample in Hall-bar geometry is shown as shaded

Figure 6-2 shows the circuit diagram for an a.c. measurement setup using two Stanford Research SR830 lockin amplifiers. Lockin amplifiers use phase sensitive detectors to make low noise measurement of a.c. signals of a given reference frequency with sensitivity of 1nV. The SR830 also has a voltage output that can be used to source constant current through a ballast resistor in series with the sample. Both SR830's are programmed to measure signals at the same frequency and phase as the current through the sample, and make it possible to measure longitudinal and transverse voltages simultaneously. The input resistance for the SR830 is only 1MΩ, hence only samples with two terminal contact resistances less than 10kΩ are measured using this setup.

Weak Disorder: Iron Films

Transport Properties at B=0

We monitor the resistances of all samples during growth, which allowed us to grow samples with specific sheet resistances and transfer them to the cryostat for magneto-transport measurements. As a measure of the disorder characteristic of each film, we use the sheet resistance at T=5K, which we denote by R_o. We note that in our polycrystalline films, the resistance of individual grains is much smaller than the inter-grain tunneling resistance and hence the later determines the low temperature residual resistance R_o. We grew a series of iron films on glass substrates with R_o varying over a range of 50Ω to 50000Ω. We observed a crossover in the temperature dependence of sheet resistance $R_{xx}(T)$ as R_o is systematically increased . Figure 6-3a shows $R_{xx}(T)$ for an iron film of thickness d=100Å and R_o=70Ω. This represents typical behavior for all films with R_o<1000Ω, with resistance decreasing linearly with temperature and reaching a

minimum at some temperature T_{min} that shifts towards higher temperature as R_o increases. This linear decrease of resistance is typical of homogeneous metallic samples and is due to decreased phonon scattering at low temperatures. For films with R_o<1000Ω, the grains are well connected and R_o is determined by impurities and lattice imperfections in the grains. For $T<T_{min}$ the resistance curves show a weak logarithmic increase as shown in the inset of Fig. 6-3a, which is a manifestation of low temperature quantum corrections discussed in chapter 5.

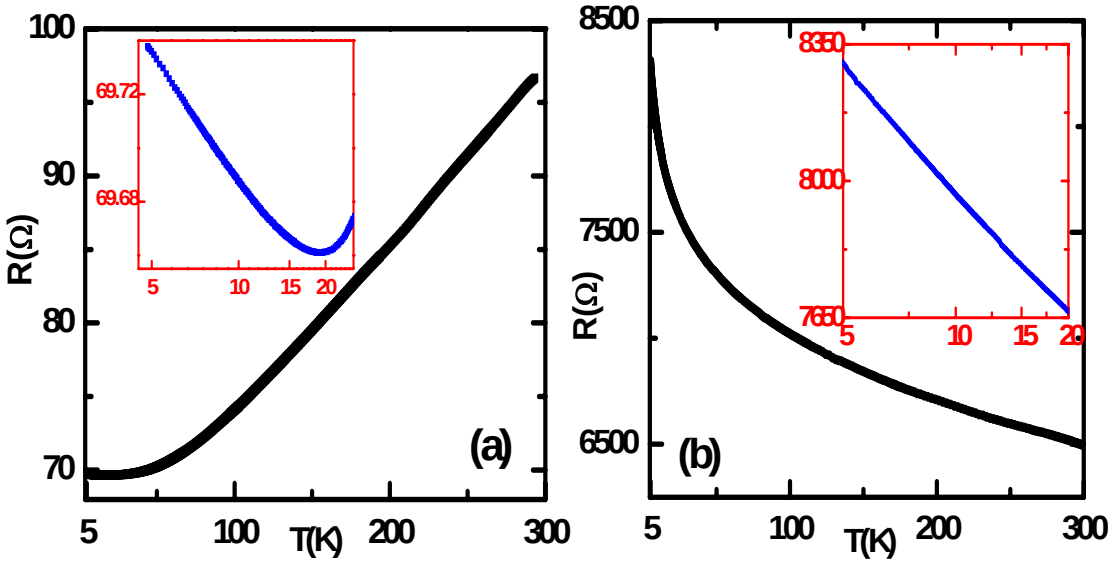

Figure 6-3:Typical behaviors for temperature dependence of resistance for iron films in the absence of magnetic field for (a) R_o=70Ω showing a good metallic behavior with decreasing resistance with temperature and (b) R_o=8400Ω showing a monotonic increase in resistance with decreasing temperature. Inset of both graphs is a blow up of low temperature behavior showing logarithmic divergence of resistance in both cases.

For samples with higher sheet resistances, R_o>1000Ω, the resistance increases monotonically with decreasing temperature and with no minimum. Figure 6-3b shows $R_{xx}(T)$ for an iron film with d=20Å and R_o=8400Ω. At high temperatures, the increase in resistance with decreasing temperature is due to decreased phonon assisted "hopping" processes of conduction electrons over the tunnel barriers between grains. At low

temperatures the residual resistance should be due to temperature independent inter-grain tunneling processes. However at low temperatures (T<15K), the resistance is found to increase logarithmically as shown in the inset of Fig. 6-3b, which is a manifestation of quantum corrections in the presence of tunneling processes. The crossover in the sign of temperature coefficient of resistance *dR/dT* in the high temperature regime, is consistent with the usual observation for thin metallic films described by the so called Mooij limit [50, 51] for film resistivity around 100μΩcm.

Thus the iron films used in our experiment with R_o in the range 50Ω to 50000Ω, exhibit a logarithmic increase at low temperatures and are considered to be weakly disordered in the context of quantum theory of transport. To compare the experimental data with existing theories on quantum corrections to conductivity in 2D metals, we use the following functional form to fit the data at low temperature (T=4.5– 15K):

$$L_{xx} = \frac{1}{R_{xx}} = A_R L_{oo} \ln(T) + const. \qquad (6\text{-}1)$$

where $L_{oo} = e^2 / 2\pi^2\hbar = (81k\Omega)^{-1}$,the quantum of conductance and A_R is a numerical prefactor that depends on the microscopic scattering parameters that determine the quantum corrections.

Figure 6-4 shows a plot of A_R as a function of R_o. We note that there is a distinct crossover in the value of A_R as R_o is systematically increased beyond 3000Ω. For low resistance samples, the prefactor is constant with A_R =0.95±0.03 and did not show any pronounced dependence on R_o. However, for samples with higher sheet resistances, A_R systematically decreases as R_o increases. For example, for a sample with R_o=49000Ω, the prefactor A_R=0.326±0.001. We note that the red square data points refer to films that had

been exposed to an Ar ion beam prior to the transport measurement, a process that smoothens the film surfaces [16] and results in a pronounced reduction in the resistance, as discussed in detail in chapter 3. However as seen from our data, the ion-milled films follow similar trends to those of the pristine films as far as low temperature transport property as measured by the value of A_R is concerned. These data further justify the use of sheet resistance is a measure of disorder.

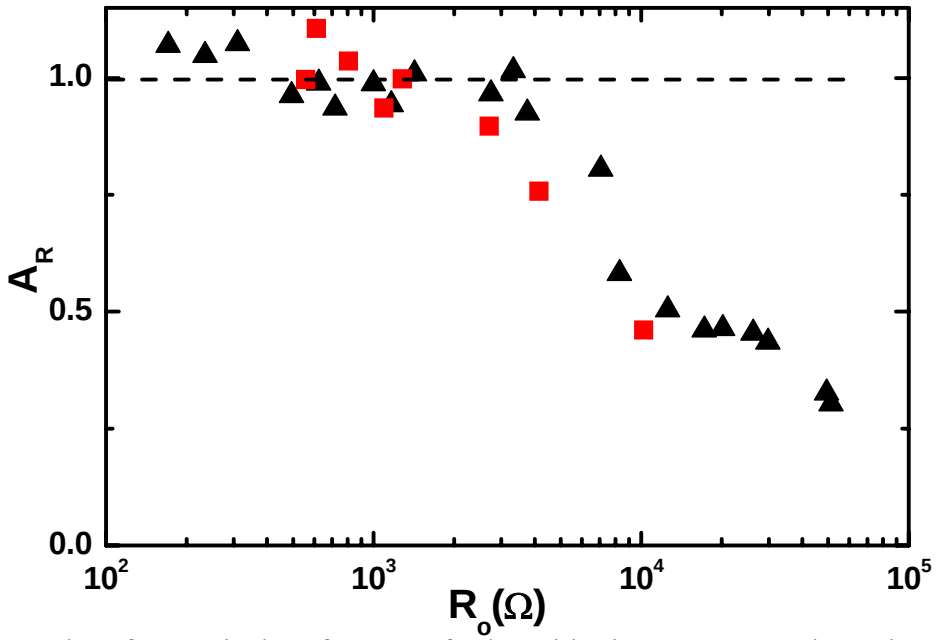

Figure 6-4:Plot of numerical prefactor A_R for logarithmic temperature dependence of longitudinal conductance (equation 6-1) for different iron films, as a function of R_o, sheet resistance at T=5K. Red square points corresponds to ion-milled films.

Anomalous Hall Effect in Iron

In this section we present anomalous Hall (AH) measurements on our films at T=5K, and discuss their dependence on R_o which is a measure of effective disorder in the film. In principle, ferromagnetic samples with uniform magnetization should exhibit a transverse Hall potential due to an applied electric field, even in the absence of an

external magnetic field. However, an external magnetic field is required to align the magnetic domains thereby maximizing the magnitude of magnetization and hence the AH resistance. In most samples, there may be a small unavoidable misalignment of the Hall leads, as a result of which a fraction of the measured potential between the Hall leads (V_{xy}) will be due to the longitudinal potential drop along the sample. Hence, to properly calculate the Hall potential, we scan the magnetic field in both positive and negative directions to measure the transverse potential $V_{xy}(B)$, keeping the sample at a fixed temperature. The Hall potential is extracted from the raw data as the antisymmetric part given by $V_H = (V_{xy}(B) - V_{xy}(-B))/2$.

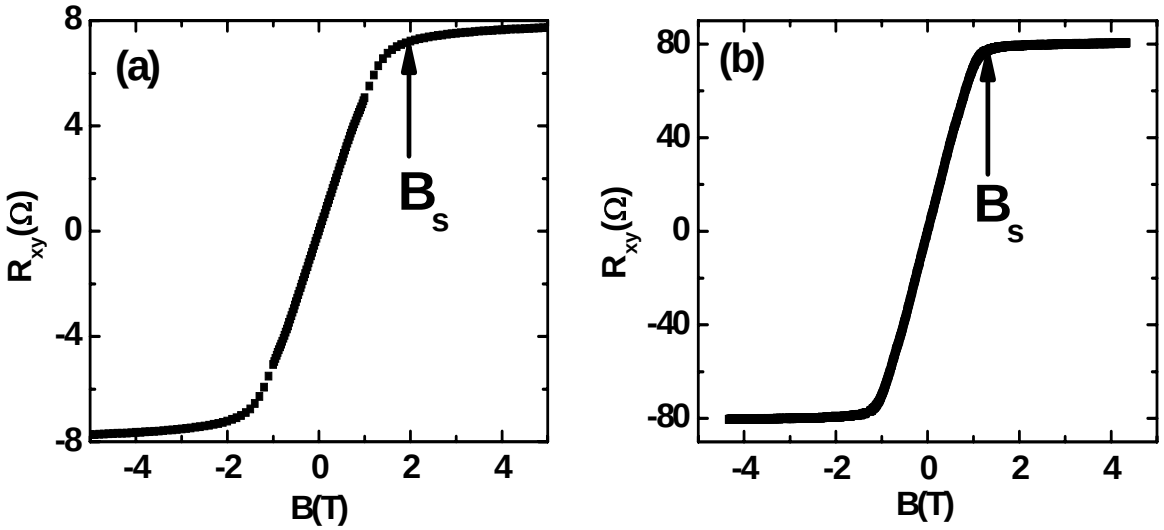

Figure 6-5: The anomalous Hall curves for iron films with (a) R_o=300Ω and (b) R_o=2700Ω. Note decrease in B_s and simultaneous increase of R_{xy} as R_o increases.

Typical AH curves for two different iron films are shown in Figs 6-5(a) and 6-5(b) corresponding to R_o=300Ω and R_o=2700Ω respectively. Both Hall curves exhibit anomalous behavior with a steep rise in Hall resistance with increasing magnetic field *B,* due to moments lining up along the field until the saturation value at $B=B_s$ (shown by the vertical arrow), followed by a much slower increase due to the normal Hall effect. An

important point to note is that for R_o=300Ω, the AH curve saturates at an applied field of B_s~1.7T to a value R_{xy}~8Ω, while for the sample with R_o=2700Ω, the saturation field B_s~1.2T and high field value R_{xy}~80Ω. This points out an important trend seen in our samples: as R_o increases, B_s decreases while the high field saturation value of Hall resistance increases as R_o increases. However, as we will show subsequently, this monotonic dependence on sheet resistance breaks down above R_o~2000Ω. We also note that the sign of the slopes of both anomalous and normal part of the Hall curve are positive, which is in agreement with experiments on bulk iron samples [22].

We have undertaken a study of the dependence of the high field saturation value of AH resistance R_{xy}^{AH} on R_o, into the very high resistance regime ~1MΩ, which to the best of our knowledge has not been studied experimentally. We use the following scheme to analyze our data and extract the saturation value of AH resistance, which allows us to systematically compare R_{xy}^{AH} for different R_o at T=5K. As discussed earlier, the Hall resistance in a ferromagnet is the sum of the anomalous contribution proportional to M and the normal Hall effect. When the applied magnetic field exceeds B_s, the net magnetization along the field remains constant at M_s and the observed slow increase in R_{xy} with increasing field is due to the normal Hall effect plus any background susceptibility effects. So the high field part of the AH curve can be fit to the following phenomenological expression [2] linear in magnetic field B:

$$R_{xy} = \mu_o R_s M_s + R_n B \qquad (6\text{-}2)$$

where R_s and R_n are the anomalous and normal Hall coefficients respectively in two dimensions. Thus the intercept of such a fitted straight line is the contribution to Hall

resistance at zero applied field B and arises only from the spontaneous magnetization in the material. We identify the intercept as the AH resistance $R_{xy}^{AH} = \mu_0 R_s M_s$, which is the contribution at zero applied field and solely due to magnetization of the film.

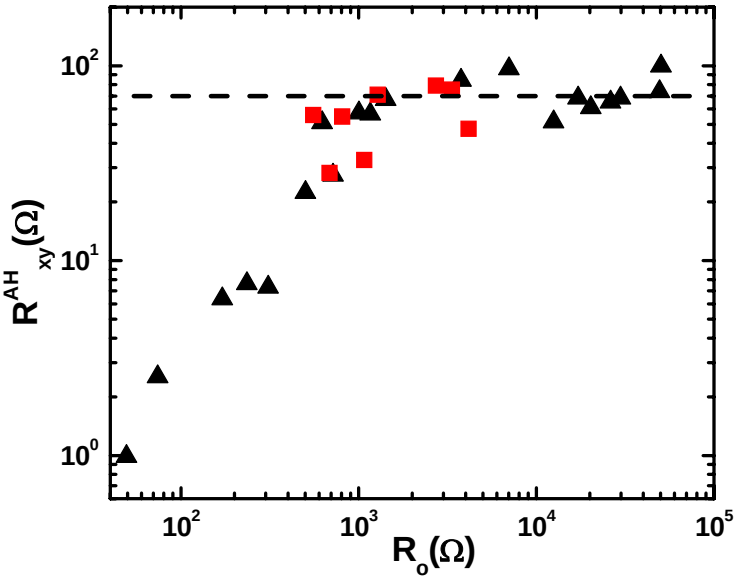

Figure 6-6:The anomalous Hall resistance at T=5K for different iron films as a function of R_o on a log-log scale. Red square points are ion-milled films. The dashed line represents the average value of the AH resistance at 80Ω.

Figure 6-6 shows the dependence of R_{xy}^{AH} on iron samples with different R_o using a log-log scale. For iron samples with sheet resistances as high as R_o=49000Ω, we observe the anomalous behavior in Hall resistance indicating the presence of a local finite magnetic moment in the films. However we observe a distinct crossover in the dependence of R_{xy}^{AH} with increasing R_o. For R_o>2000Ω, the monotonic increase in R_{xy}^{AH} seen at lower resistances, ceases to hold. Instead the AH resistance attains a constant value $R_{xy}^{AH} = 80 \pm 10\Omega$, independent of R_o. We point out that the crossover is observed around values of R_o where the zero field coefficient of logarithmic temperature dependence A_R, starts to deviate from unity.

Temperature Dependence of Anomalous Hall Conductivity

We have shown in the previous section that at low temperatures (4.5 to 15K), for all iron samples, $R_{xx}(T)$ exhibits a logarithmic dependence at B=0. To find the quantum corrections to the AH conductivity a magnetic field of 4T, which is well above the saturation field B_s, is applied to each sample and $R_{xx}(T)$ and $R_{xy}^{AH}(T)$ are simultaneously measured while temperature is slowly increased. We will show that R_{xy}^{AH} also has logarithmic temperature dependence for T<20K for all the iron samples, and discuss the relative resistance (RR) scaling of $R_{xx}(T)$ and R_{xy}^{AH} for each sample with different R_o.

In most samples there is always a misalignment in the Hall leads as result of which a fraction of the transverse potential has contribution from the longitudinal potential drop along the sample. Similarly, there may be a contribution of transverse Hall voltage between misaligned longitudinal leads. Thus, for each sample we perform two sets of experiments, at B=+4T and B=-4T, and measure simultaneously the longitudinal potential $V_{xx}(T)$ and transverse potential $V_{xy}(T)$ for each field. Then we extract the symmetric response as longitudinal resistance $R_{xx}(T,B) = (V_{xx}(T,B) + V_{xx}(T,B))/2I$ and antisymmetric response as the AH resistance $R_{xy}^{AH}(T,B) = (V_{xx}(T,B) - V_{xx}(T,B))/2I$, with B=4T. The contribution from the normal Hall effect is found to be negligible.

To quantify our experimental results and facilitate comparison between different samples, we define a function $\Delta^N(K)$ that we call the "normalized relative change" in a transport quantity, say K, with respect to some reference temperature T_0 evaluated for temperatures $T > T_o$:

$$\Delta^N(K) = \frac{K(T) - K(T_o)}{K(T_0)} \frac{1}{L_{00} R_{xx}(T_0)} \tag{6-3}$$

where $L_{00} = (81\text{k}\Omega)^{-1}$ is the quantum of conductance and $R_{xx}(T_0)$ is the sheet resistance at T_0. We note that the "relative change" is defined as:

$$\frac{\delta K}{K} = \frac{K(T) - K(T_0)}{K(T_0)} \tag{6- 4}$$

Thus the normalized relative change $\Delta^N(K)$ is the relative change in the quantity $\delta K / K$, divided by the factor $L_{00}R_{xx}(T_0)$, a dimensionless quantity that is a measure of the effective disorder in a two dimensional system. Using the above notation and keeping in mind the fact that the low temperature behavior of both R_{xx} and R_{xy}^{AH} is logarithmic, we employ the following equations to fit our data:

$$\Delta^N(R_{xx}) = \frac{R_{xx}(T) - R_{xx}(T_o)}{L_{00} R_{xx}^2(T_o)} = -A_R \ln(\frac{T}{T_o}) \tag{6-5}$$

$$\Delta^N(R_{xy}^{AH}) = \frac{R_{xy}^{AH}(T) - R_{xy}^{AH}(T_o)}{L_{00} R_{xy}^{AH}(T_o) R_{xx}(T_o)} = -A_{AH} \ln(\frac{T}{T_o}) \tag{6-6}$$

where A_R and A_{AH} are coefficients of the logarithmic temperature dependence of R_{xx} and R_{xy}^{AH} respectively. The coefficients depend on the parameters describing the quantum corrections to longitudinal and AH resistance respectively. Using the approximation that $\left|R_{xx}(T) - R_{xx}(T_o)\right| << R_{xx}(T)$, the longitudinal conductivity is calculated from the raw data as $L_{xx} = 1/R_{xx}$ so that $\delta L_{xx} / L_{xx} = -(\delta R_{xx} / R_{xx})$. Thus it follows from equations (6-5) that

$$\Delta^N(L_{xx}) = \frac{\delta L_{xx}}{L_{xx}(T_0)} \frac{1}{R_{xx}(T_o) L_{00}} = -\frac{R_{xx}(T) - R_{xx}(T_o)}{L_{oo} R_{xx}^2(T_o)} = A_R \ln(\frac{T}{T_o}) \tag{6-7}$$

The AH conductivity has contributions from both R_{xx} and R_{xy}^{AH}, and is calculated from raw data as $L_{xy}^{AH} = R_{xy}^{AH} / ((R_{xy}^{AH})^2 + R_{xx}^2)$. Using the approximation $R_{xy}^{AH}(T) << R_{xx}(T)$, which is true for most materials, we have $L_{xy}^{AH} \approx R_{xy}^{AH} / R_{xx}^2$. It follows from equations (6-5) and (6-6),

$$\Delta^N(L_{xy}^{AH}) = \frac{\delta L_{xy}^{AH}}{L_{xy}^{AH}} \frac{1}{R_{xx}(T_0)L_{00}} \approx (\frac{\delta R_{xy}^{AH}}{R_{xy}^{AH}} - 2\frac{\delta R_{xx}}{R_{xx}}) \frac{1}{R_{xx}(T_o)L_{00}} = (2A_R - A_{AH}) \ln(\frac{T}{T_o}) \tag{6-8}$$

Moreover, it follows directly from equations (6-5) and (6-6),

$$\frac{\Delta^N(R_{xy}^{AH})}{\Delta^N(R_{xx})} = \frac{A_{AH}}{A_R} \tag{6-9}$$

Thus the coefficient of logarithmic temperature dependence of conductivity is A_R and that of the AH conductivity is $2A_R$-A_{AH}. Also it follows from equations (6-8) and (6-9) that $A_{AH}/A_R = 2$ implies that $\Delta^N(L_{xy}^{AH}) = 0$. Any deviation of this ratio from 2 implies a non-zero logarithmic temperature dependence of L_{xy}^{AH}.

We note that the logarithmic prefactor A_R, as defined in equation (6-1) and equation (6-5), are self consistent and always give the same value for a given data set as they refer to the slope of the temperature dependence of L_{xx}. We have already discussed how A_R varies with changing R_o when B=0(Figure 6-4). We found that, even in the presence of B=4T, the magnitude of A_R did not show any significant change. The reason is that the iron films under consideration have very small magnetoresistance(MR). In Fig. 6-7 we show the MR for a film with R_o=300Ω is of the order of 0.15%. The magnetoresistance curves for all the iron samples are found to be predominantly negative with small hysteresis and showed a pronounced saturation at applied fields that also

corresponds to saturation of AH resistance (compare Figs. 6-5(a) and 6-7). The hysteretic behavior progressively decreases with increasing R_o, which we will argue later, is due to weakening of ferromagnetic coupling between grains, and for very high resistance samples the hysteresis disappears, as it should for a paramagnetic response.

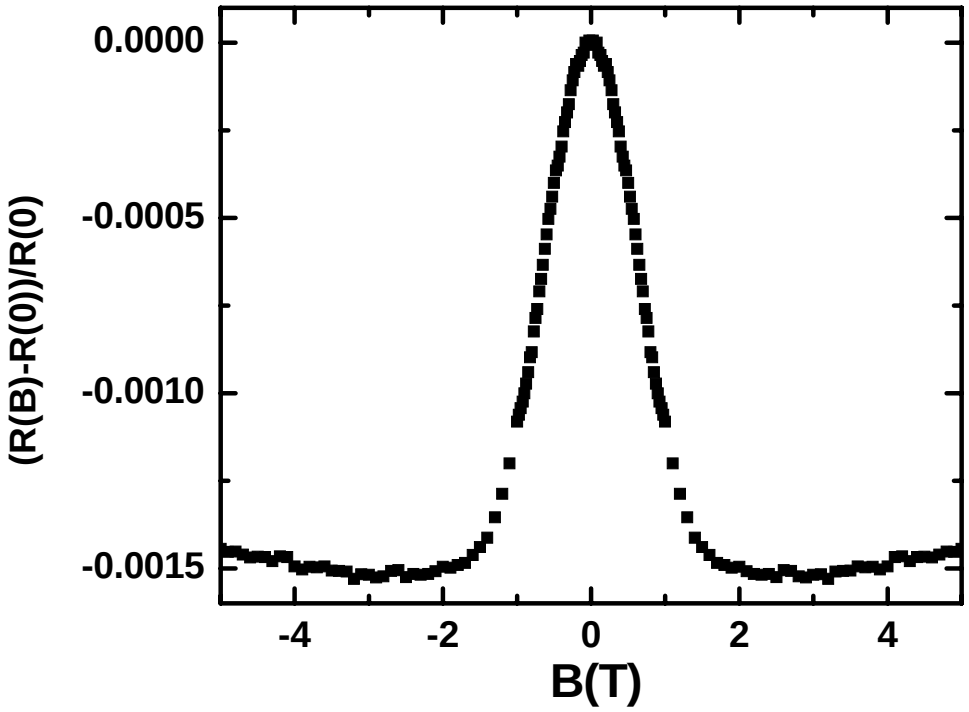

Figure 6-7: Magnetoresistance as a function of field for an iron film with R_o=300Ω.

To show the relative scaling behavior of resistance and AH resistance, we have plotted in Fig. 6-8 on a logarithmic temperature scale the normalized relative changes $\Delta^N R_{xx}(T)$, $\Delta^N R_{xy}^{AH}(T)$ and $\Delta^N L_{xy}^{AH}(T)$, with T_0=5K as reference temperature and at an applied magnetic field of 4T, for a film with R_0=2733Ω. We observe a distinct feature that the curves for $\Delta^N(R_{xy}^{AH})$ and $\Delta^N R_{xx}(T)$ exactly overlap each other while obeying logarithmic temperature dependence at low temperatures up to T~20K. At higher temperatures, we observe that $\Delta^N(R_{xy}^{AH})$ deviates from logarithmic behavior and decreases at a faster rate than $\Delta^N R_{xx}(T)$. The importance of this behavior becomes

apparent by comparing with the results of a previous similar experiment by Bergmann and Ye on ultrathin amorphous iron [48], where the logarithmic slope of R_{xy}^{AH} was found to be a factor of two higher than that of R_{xx}.The deviation of $\Delta^N(R_{xy}^{AH})$ from $\Delta^N(R_{xx})$ at high temperatures(Figure 6-8) is also interesting and is a possible indication that the dominant quantum corrections to R_{xx} and R_{xy}^{AH} are due to different mechanisms. We note that the quench-condensed amorphous films [48] in Bergmann's experiments could not be heated above 20K without incurring irreversible morphological changes, hence we could not compare our high temperature data.

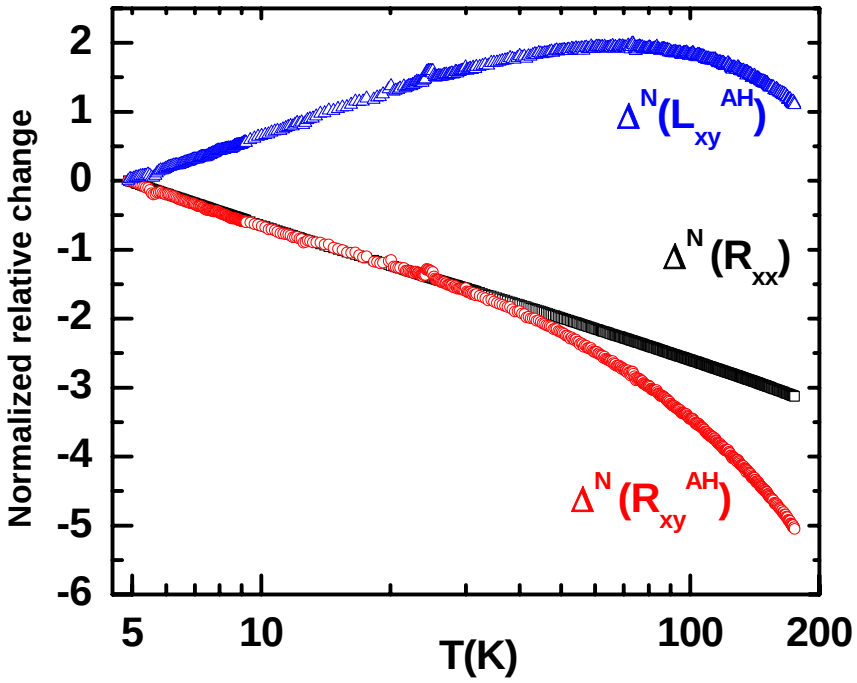

Figure 6-8: Relative resistance (RR) scaling behavior at T<20K for an iron film with R_o=2700Ω. The uppermost (blue) curve exhibits finite logarithmic temperature dependence of $\Delta^N(L_{xy}^{AH})$.

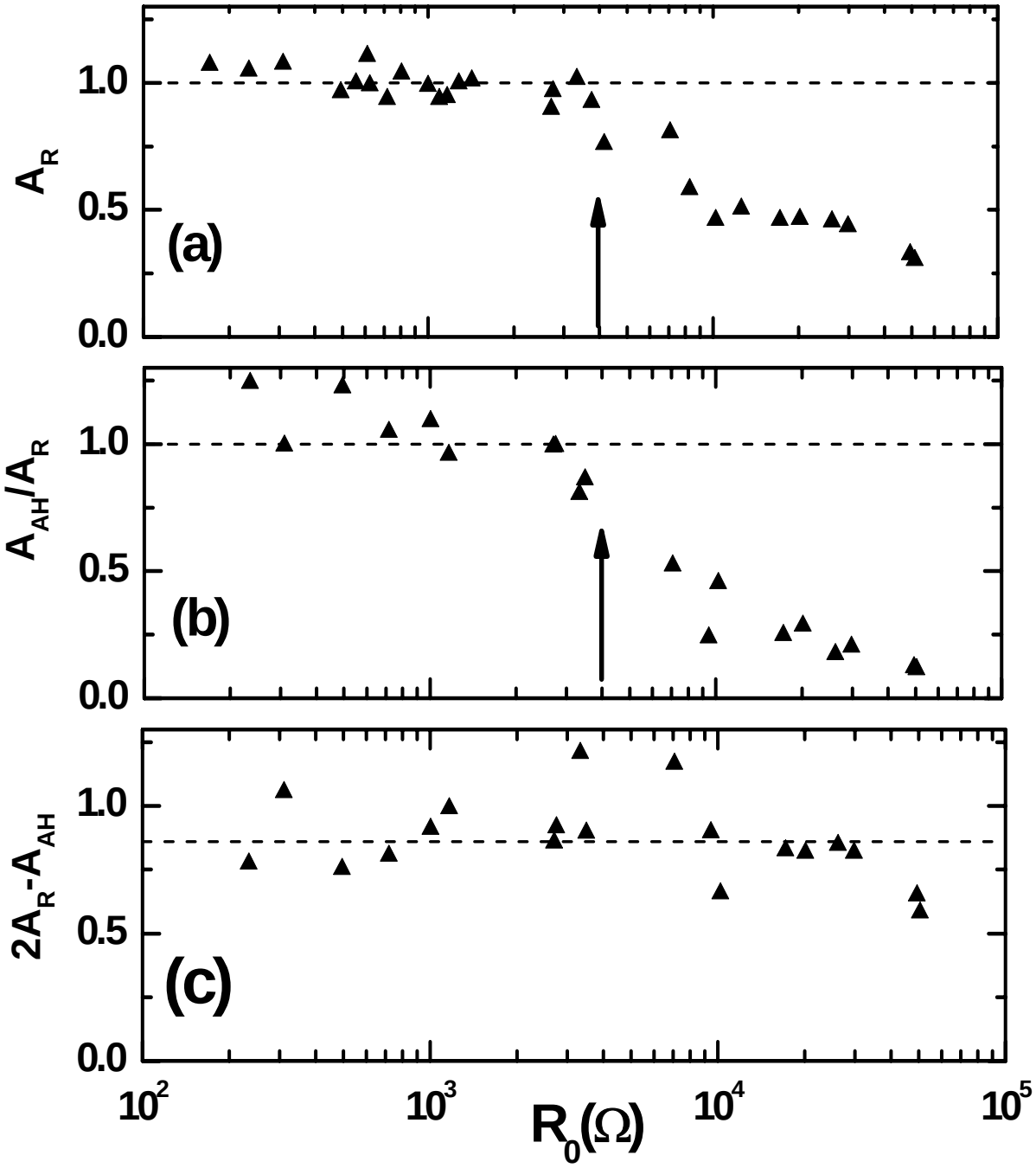

Figure 6-9: Plots showing dependence on R_o of the extracted transport coefficients (a) A_R and (b) A_{AH}/A_R showing a crossover in value (shown by arrow) near $R_o \sim \hbar/e^2 = 4100\Omega$. Values close to unity in both cases correspond to RR scaling. (c) $2A_R$-A_{AH} is the numerical prefactor for AH conductivity showing no pronounced dependence on R_o. The average value of 0.8 is shown by the dotted line.

Fitting the data in Fig. 6-8 for low temperature (T=5-20K) part to equations (6-5) and (6-6), we find for this particular film that A_R=0.897±0.001, and A_{AH}=0.908±0.005. The AH conductivity L_{xy}^{AH} calculated from the raw data also exhibits a logarithmic temperature dependence below 20K with a positive slope as shown by the blue data points in Figure 6-8 and the prefactor for $\Delta^N(L_{xx})$ is found to be 0.908±0.005 close to the value of $2A_R$-A_{AH} =0.89±0.01 in accordance with equation (6-7). For simplicity and future reference we call the low temperature scaling behavior for samples where the A_{AH}/A_R=1 (Figure 6-8) so that the relative changes in $R_{xx}(T)$ and $R_{xy}^{AH}(T)$ are equal, the relative resistance (RR) scaling. The RR scaling behavior is observed in all of our samples with R_o<3000Ω, and implies a finite temperature dependence of anomalous Hall conductivity. This behavior is significantly different from that reported in previous experiments by Bergmann and Ye on amorphous iron films [48] where A_{AH}/A_R=2 implying that there are no temperature dependent quantum corrections to L_{xy}^{AH} .

In Fig. 6-9(a) we have re-plotted for reference the coefficient A_R as a function of R_o. The plot is essentially the same as Fig. 6-4 and shows a deviation from A_R~1 for R_o>3000Ω. There is also a crossover in the relative scaling behavior of AH resistance and resistance, which is measured quantitatively by the ratio of coefficients A_{AH}/A_R as shown in Fig.6-9(b). All samples with R_o in the range 300-3000Ω were found to exhibit RR scaling behavior (Figure 6-8) with the average value for the ratio A_{AH}/A_R=1.07±0.1. However as R_o increases beyond 3000Ω, the ratio A_{AH}/A_R systematically decreases from unity, which according to equation (6-9) implies that the relative change in R_{xx} is larger than the relative change in R_{xy}^{AH} . For a sample with R_0=50000Ω for example, which is

the last data point in Figure 6-9b, we found that A_{AH}/A_R=0.122±0.002. In Fig. 6-10 we have plotted $\Delta^N(R_{xx})$ and $\Delta^N(R_{xy}^{AH})$ for this sample, which clearly shows that the logarithmic slope for $\Delta^N(R_{xx})$ is much greater than $\Delta^N(R_{xy}^{AH})$. We emphasize that even if the ratio A_{AH}/A_R decreases from unity in the high resistance regime, there remains a finite and positive quantum correction to the AH conductivity as shown by the finite value of $2A_R$-A_{AH} =0.6 (Figure 6-9c).

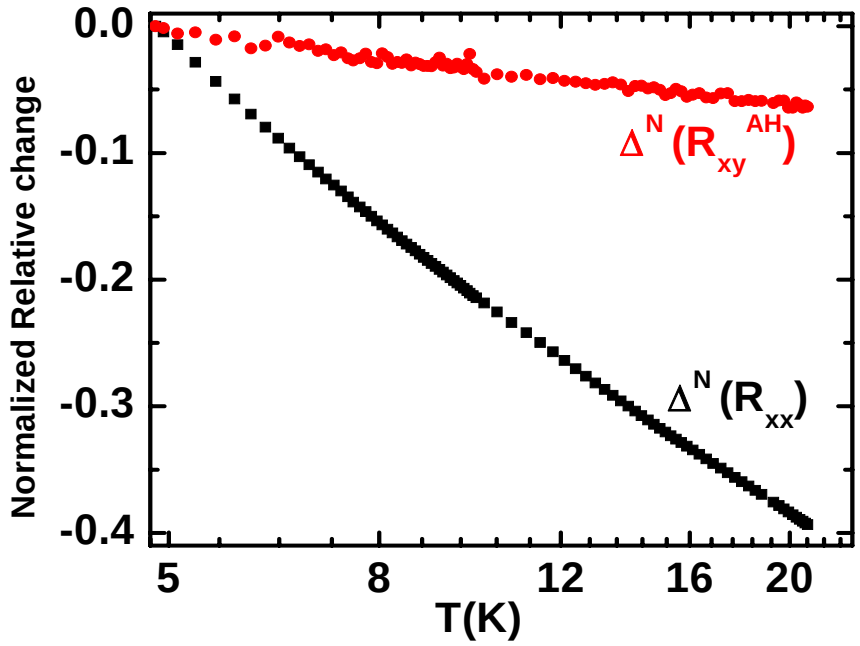

Figure 6-10:An iron film with R_o=49000Ω showing deviation from RR scaling. The ratio A_{AH}/A_R =0.12 as shown in the final point in Fig. 6-9c.

An important observation related to the high resistance regime is shown inFig. 6-11, where we have plotted the relative changes in the AH resistances $\delta R_{xy}^{AH} / R_{xy}^{AH}$ as defined in equation (6-4), for three samples with R_o varying over a wide range from 2400Ω to 49000Ω. In the low temperature range of T=5-20K, the curves for all three samples are shown to overlap each other, indicating that the AH resistance in these polycrystalline films is not affected by the increasing longitudinal resistance. Thus for

R_o>3000Ω, in addition to the fact that the magnitude of R_{xy}^{AH} at T=5K attains a constant value ~80Ω as shown in Fig. 6-6, the relative change in R_{xy}^{AH} over the temperature range of 5-20K also remains constant.

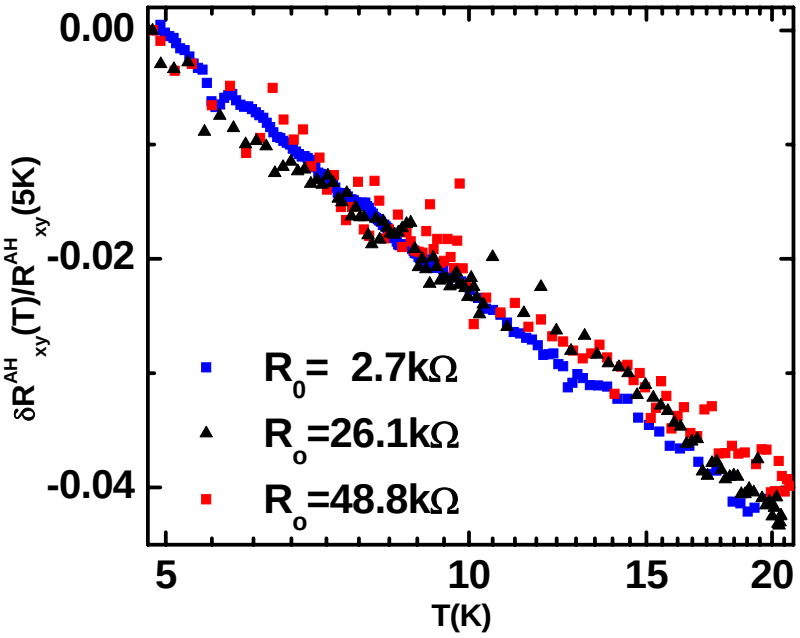

Figure 6-11:The relative changes in AH resistances for three different iron films. The curves overlap each other even though the corresponding R_o as shown in the legend varies over a wide range.

Thus for all iron films a finite positive logarithmic correction to L_{xy}^{AH} is observed. Interestingly, the coefficient of AH conductivity $2A_R$-A_{AH} as defined in equation (6-8), does not show any pronounced dependence on R_o and is scattered around an average value of 0.86±0.2(Figure 6-9c). Thus, there is a "universal" behavior in the low temperature logarithmic dependence of AH conductivity over the whole range of R_o, in comparison with the magnitude of variation of longitudinal conductivity that showed a crossover behavior around $R_o \sim \hbar / e^2$. This is a strong indication that the dominant

mechanisms that are responsible for the temperature dependence of the longitudinal (L_{xx}) and AH (L_{xy}^{AH}) conductivity are different.

Strong Disorder: Iron/C_{60} Bilayers

So far we have presented data on iron films directly grown on glass substrates with R_o varying from 50-50000Ω. The transport properties of all the films showed logarithmic temperature dependence, which in the context of quantum theory of transport should be considered as 'weakly disordered' metals. This means that despite the granular morphology of the films, at low temperatures the phase coherence length extends over several grains [42], and the motion of the carriers can be considered as diffusive. To make the samples insulating where the dominant conduction process is hopping from one localized state to another, one needs to grow even higher sheet resistance samples where the inter-grain barrier separation and/or barrier height is larger compared to iron films. However, it is an experimental challenge to grow a sample with arbitrarily high sheet resistance, mainly because of resistance drifts up at room temperature even at very high vacuum. These drifts, which result from slow oxidation and/or thermally activated annealing, decrease as temperature is lowered.

To grow films with even higher sheet resistances we used a novel technique where a monolayer of C_{60} is grown first on the glass substrate and then iron films were grown top. C_{60} in solid form is known to be an insulator with completely filled bands. However, C_{60} molecules have a high electron affinity; hence when in contact with a metal, electrons are transferred from the metal to the C_{60} and can move freely within the monolayer [21]. Thus, the underlying C_{60} monolayer provides an extra shunting path for conduction electrons between otherwise isolated grains, as shown schematically in Fig. 6-

12. The critical thickness at which a metal film starts to conduct is much less when grown on C_{60} than when grown directly on glass. Using these techniques, we were able to grow high resistance stable ferromagnetic films.

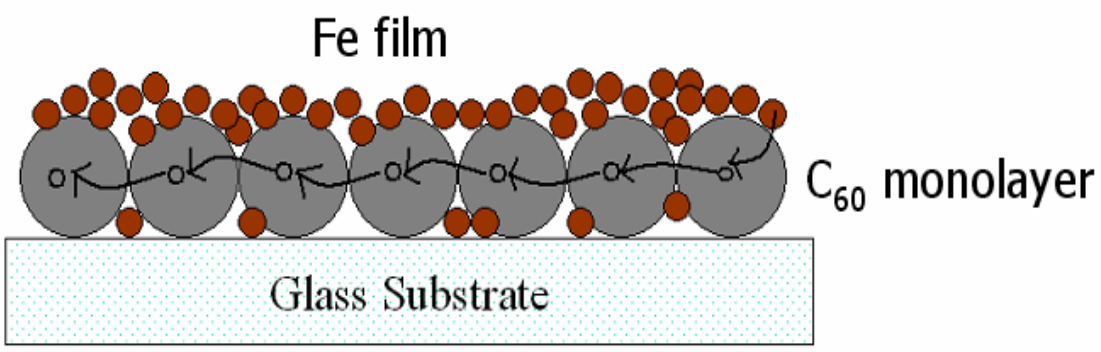

Figure 6-12:A cartoon of iron/C_{60} bilayer samples. Big circles represent C_{60} molecules and the small brown circles represent iron atoms. The small open circles represent electrons transferred from the iron film to C_{60} ,which can move freely in the monolayer.

We grew two Fe/C_{60} films with sheet resistances R_o=1600Ω and 4100Ω, which are well within the range of iron films grown on bare glass and compared their transport properties with iron films having similar resistances. The AH resistance at T=5K was found to be R_{xy}^{AH} =64Ω and 81Ω respectively, which is what one would expect from monolayer of iron on glass. These films also showed RR scaling behavior similar to that seen in low resistance iron films where both $R_{xx}(T)$, and $R_{xy}^{AH}(T)$ obeyed a logarithmic temperature dependence at low temperatures, with the logarithmic prefactors $A_R \approx A_{AH} \approx 1$. These observations demonstrate that the underlying C_{60} layer does not alter the transport properties of iron. However, an important point to note is that it takes less iron to grow a film of certain resistance when grown on C_{60} rather than bare glass, because of the shunting path provided by the C_{60} monolayer.

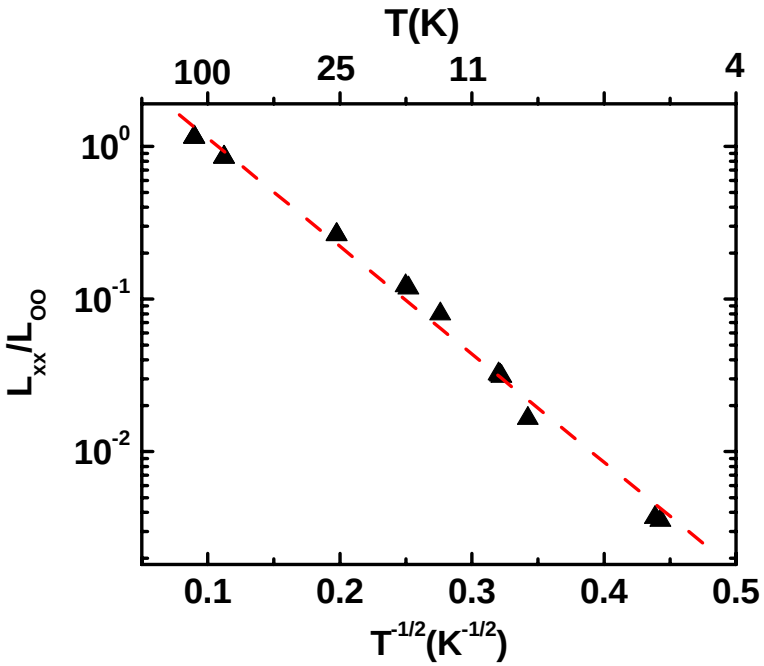

Figure 6-13:Plot of conductivity showing hopping transport in a Fe/C_{60} sample as given by equation (6-10).

We now focus our attention on iron/C_{60} films that are in the strongly disordered regime. Figure 6-13 shows $R_{xx}(T)$ at B=0 for such a film with resistance at T=5K, $R_o \approx 20\text{M}\Omega$. We observe that this film does not show the logarithmic temperature dependence of conductivity. Instead the longitudinal conductance fits to the following functional form as predicted [44] by theories of hopping conduction in granular metallic films:

$$L_{xx}(T) = L_{xx}^{O} \exp(-(\frac{T_\xi}{T})^{-1/2}) \qquad (6\text{-}10)$$

where L_{xx}^{0} and T_ξ are characteristic resistance and energy scales in a two dimensional system with localized electronic states. The fit in Fig. 6-13 yields T_ξ=266K and $L_{xx}^{O} = 1.754 L_{OO}$. Table 6-1 summarizes the fitting results for all the strongly disordered films under consideration. We note that the T_ξ is directly related to the Coulomb

energy[44] $E_C \sim e^2/\langle d \rangle$ associated with the charging of grains when an electron hops from one grain to another, <d> being the average grain size. Our data as shown in table 6-1, reveal that T_ξ increases with increasing R_o indicating that for high resistance samples the average grain size is smaller.

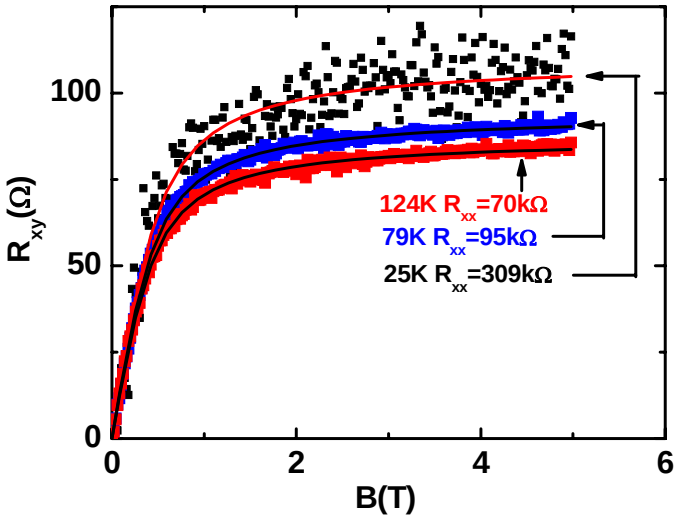

Figure 6-14: The AH effect in strongly disordered Fe/C_{60} sample at three different temperatures. Legend quotes resistances at given temperatures corresponding to the hall curves of same color. The solid lines represent fits to the Langevin function.

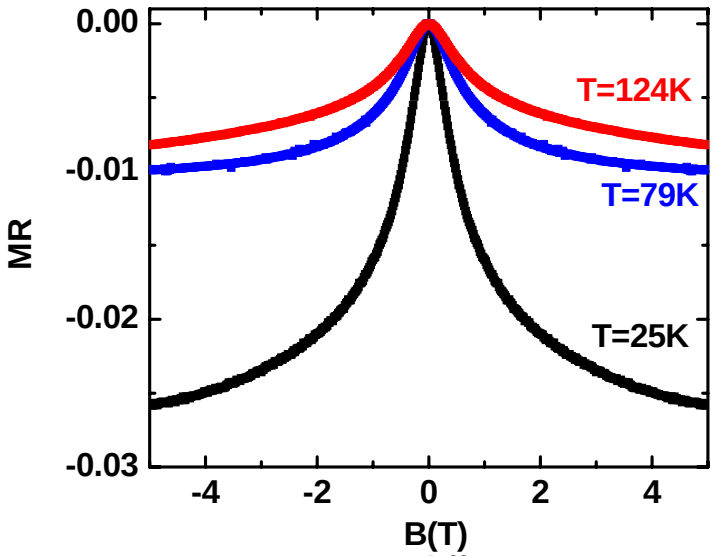

Figure 6-15:Magnetoresistance curves at different temperatures for the Fe/C_{60} sample shown in Figs. 6-13 and 6-14. The curves do not show sharp saturation at a particular field as seen in iron films (Figure 6-7).

The resistance of the particular sample shown in Fig. 6-13 is high so that the Hall signal was much less than the longitudinal potential due to the misalignment of transverse leads. Thus for this sample we could extract Hall curve accurately only for temperatures at and above T=25K as shown in Fig. 6-14. The film still exhibits anomalous behavior in the Hall curves, indicating the presence of finite local magnetic moments at such high resistances. However, the AH curves do not exhibit a sharp "knee" like saturation at any definite applied field similar to that seen in iron films (Figure 6-5); instead there is a smooth and gradual cross over to a high field saturated value of Hall resistance. The sample also exhibits negative magnetoresistance (Figure 6-15), but in this case also we do not observe a sharp saturation at any characteristic field as seen for thicker iron samples (Figure 6-7). These are possible indications of the absence of long range ferromagnetic coupling between the grains comprising the films. However, an important observation is that for samples exhibiting hopping transport behavior, the resistance increases dramatically with decreasing temperature, but the corresponding AH curves do not change significantly. As deduced from the legend of Fig. 6-14, for the resistance increases by 440% while the AH resistance increases only by 33%.

An important feature of the high resistance Fe/C_{60} samples is that the AH curves could be fitted with very high accuracy to the Langevin function

$$L(x) = \coth(x) - 1/x \tag{6-11}$$

which describes the magnetization of a paramagnetic system consisting of non interacting particles or clusters of magnetic moment μ, as follows

$$M(B,T) = M_s L(\mu B / k_B T) \tag{6-12}$$

where M_s is the saturation magnetization and μ is the magnetic moment of an individual magnetic entity. The motivation behind fitting the AH curves to Langevin functions is based on the expectation that the magnetization response of a film consisting of weakly coupled isolated iron grains will be similar to that of superparamagnetic system. Since AH resistance is proportional to the magnetization (equation 6-2) of the film, we fit our data to the following functional form:

$$R_{xy}^{AH}(T,B) = R_s(T)M(T,B) = R_{xy}^{0}(T)(\coth(\gamma(T)B) - \frac{1}{\gamma(T).B}) \qquad (6\text{-}13)$$

where γ and R_{xy}^{o} are fitting parameters and are functions of temperature. The solid lines in Fig. 6-14 show Langevin fits to the AH curves at different temperatures.

For the ideal case of non-interacting magnetic grains one expects a paramagnetic response so that $\gamma(T) = n\mu_B / k_B T$ and $R_{xy}^{o}(T) = n\mu_B R_s(T)$ where n is the average number of Bohr magnetons μ_B in each grain. Ideally, in a system with paramagnetic response, the magnetization curves at different temperatures collapse onto a single curve when plotted as a function of *B/T*. Accordingly, since AH resistance is proportional to magnetization, one might expect the *B/T* scaling to hold for the AH curves also. However we failed to observe the *B/T* scaling behavior in any of our Fe/C_{60} samples. Thus the assumption that the ferromagnetic grains are non-interacting and act independently of each other does not hold in our samples. We already have evidence of electrons tunneling between grains in the temperature dependence of resistance and expect the magnetic response to be modified by these transport processes. However, to the best of our knowledge we are not aware of any theoretical treatment of AH response to an applied field in the strongly disordered hopping regime.

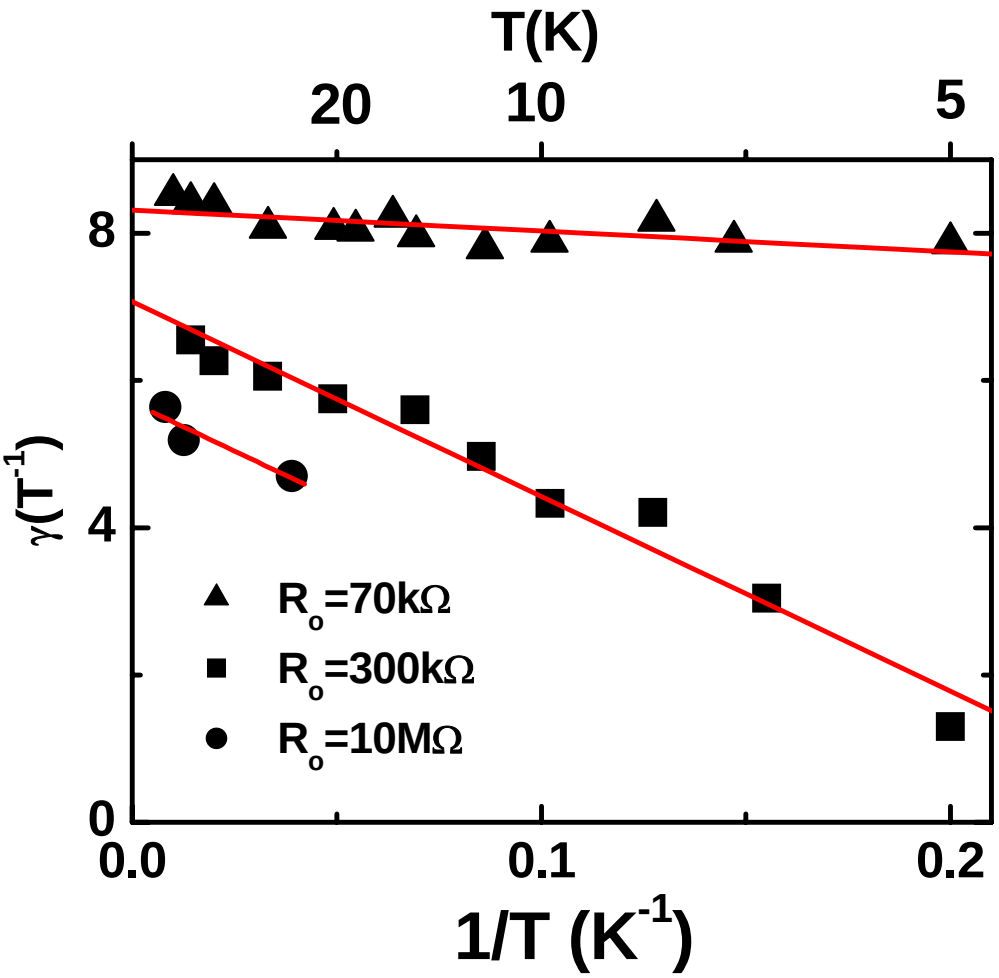

Figure 6-16:Plot of γ (see equation 6-13) as a function of inverse temperature for three different Fe/C_{60} samples. Solid lines represents linear fits given by equation 6-14.

In Fig. 6-16 we have plotted the extracted fitting parameter γ used in equation (6-13), as function of corresponding inverse temperatures for three different Fe/C_{60} samples. We note that for the case of an ideal non-interacting paramagnetic response with *B/T* scaling behavior one would expect the data for γ as a function on T^{-1}, to fit a straight line with positive slope going through the origin. Surprisingly our data show a negative slope and finite positive intercept as shown by the solid lines in Fig. 6-16. This result leads us to propose the following phenomenological expression:

$$\gamma(T) = \frac{n\mu_B}{k_B}\left(\frac{1}{T_J} - \frac{1}{T}\right) \qquad (6\text{-}14)$$

where T_J and n are fitting parameters. Table 6-1 summarizes the results of the fit to equation (6-14) for data on the three samples shown in the Fig. 6-16. The observed values of T_J indicate a new and much weaker energy scale compared to the charging energy of grains as measured by T_ξ listed in Table 6-1, or the long range ferromagnetic exchange as measured by the Curie temperature T_c listed in Table 6-2. The important point to note is that as T approaches T_J, γ approaches zero. Thus, as $T \to T_J$ from above, one has to apply increasingly strong enough magnetic fields B, so that the AH resistance reaches its saturation value R_{xy}^o. We note here that for the ferromagnetic samples the AH resistance for $B>B_s$, is independent of the applied magnetic field. This is not true for a paramagnetic sample, where the magnetization and hence AH resistance depend on the applied field. At a particular temperature the AH resistance reaches its saturation value R_{xy}^o for the argument $\gamma B>>1$. However, according to the experimentally determined dependence of equation (6-14), extrapolation to a temperature $T=T_J$ with corresponding resistance $R_{xx}=R_J$, the parameter $\gamma=0$ which in turn implies that the AH resistance $R_{xy}^{AH} = 0$ irrespective of the applied field. Thus, the dependence of γ as a function of temperature points to a phase transition at $T=T_J$, whre the AH effect disappears. This behavior is similar to that observed for the case of AH resistance with localized moment [32, 33], when R_{xy}^{AH} approaches zero as temperature is reduced because of decreasing spin disorder at lower temperature.

The fitting parameter R_{xy}^o in equation (6-13) represents the saturation AH resistance at a given temperature and is considered as R_{xy}^{AH}. Surprisingly, for these strongly disordered iron/C_{60} samples, R_{xy}^{AH} showed a logarithmic decrease with

increasing temperatures (Figure 6-17), which is a very weakly varying function compared to the exponential rise of longitudinal resistance. Thus one would expect the temperature dependence of the AH conductivity to be same as that of the longitudinalconductivity as expressed by the equation:

$$L_{xy} \approx \frac{R_{xy}}{R_{xx}^2} \approx L_{xy}^0 \exp(-(\frac{T_{\xi 1}}{T})^2) \qquad (6\text{-}15)$$

Figure 6-18 shows the temperature dependence of AH conductivity for two Fe/C_{60} samples with R_o =70kΩ and 300kΩ, fitted to the functional form as predicted by equation (6-15). The result of the fits of conductivity to equation (6-10) and AH conductivity to equation (6-15) are summarized in Table 6-1.

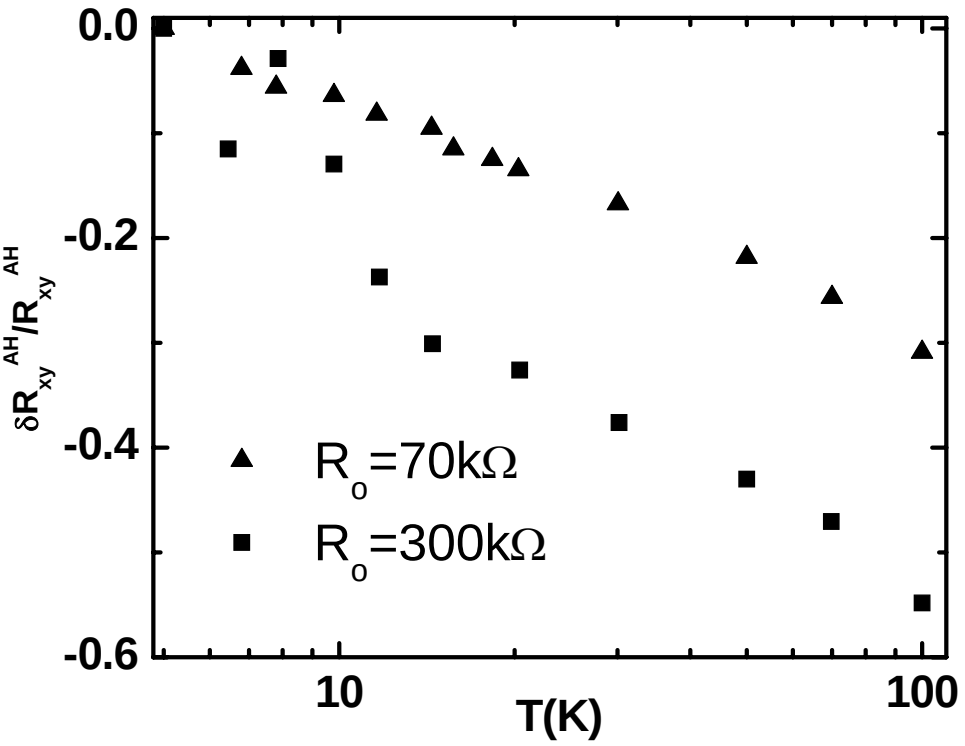

Figure 6-17: Logarithmic temperature dependence of AH resistance of Fe/C_{60} samples in the strongly disordered regime.

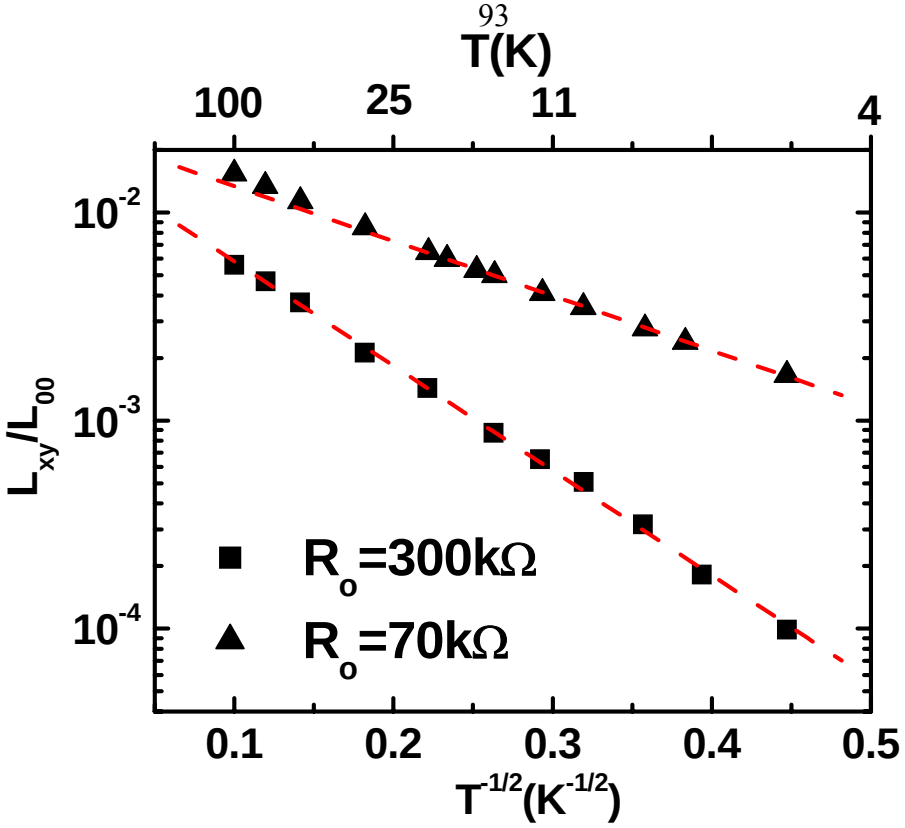

Figure 6-18:Temperature dependence of AH conductivity of Fe/C_{60} samples.

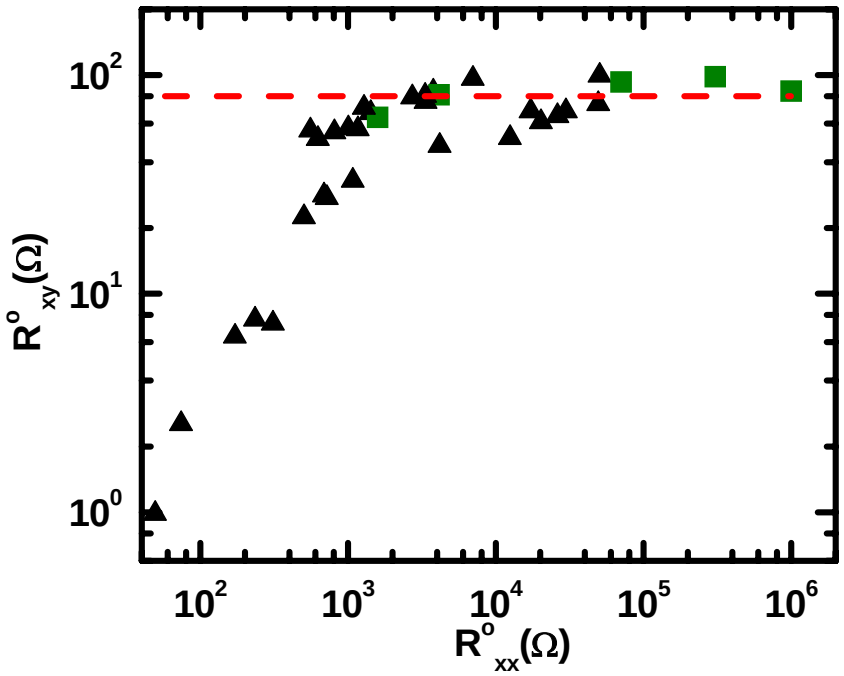

Figure 6-19: AH resistance for Fe/C_{60} samples (green square points) as a function of sheet resistance, superimposed on the data for iron samples shown in previously in Fig. 6-6. The dashed line represents the average value of AH resistance of 80Ω in the high resistance limit.

Table 6-1:Summary of the results for three different Fe/C60 samples.

R_o	L_{xx}^0	T_ξ	L_{xy}^0	$T_{\xi 1}$	T_J	R_J	n
70kΩ	5 .03L_{00}	11K	0.025 L_{00}	36.7K	0.34K	4.76MΩ	4
300kΩ	5.15 L_{00}	47K	0.019 L_{00}	133.9K	3.7K	0.56MΩ	40
10MΩ	5.78 L_{00}	266K	0.014 L_{00}	652.4K	4.6K	28MΩ	39

We now discuss how the AH resistance for the strongly disordered Fe/C_{60} films compare with that of the weakly disordered iron films discussed earlier. In Figure 6-19 we have superimposed the R_{xy}^{AH} for several Fe/C_{60} films on the data on pure iron films, already shown in Figure 6-6. We observe that not only the dependence of AH resistance for the Fe/C_{60} samples on R_o follows the same trend as that of pure iron, but also the magnitudes of AH resistances R_{xy}^{AH} are within the experimentally observed scatter, determined for the iron films. Thus these results consolidate the argument that in the Fe/C_{60} bilayers, the underlying monolayer of C_{60} does not affect the magnetism due to the iron film as measured by AH resistance. The central and significant result of our investigation is that the AH resistance for iron and iron/C_{60} films attains a constant magnitude of the order of 80Ω and is unaffected by increasing resistance as seen experimentally up to 1MΩ. At higher resistances, extrapolations show that R_{xy}^{AH} collapses to zero.

Experiments on Cobalt Films

To understand whether the results obtained for iron samples are typical of other itinerant ferromagnetic materials grown under similar conditions, we decided to investigate the behavior of AH conductivity in thin films of cobalt. Figure 6-20 shows an AH curve for a cobalt film with R_o=3200Ω at T=5K, which has two important distinction from that of an iron film of similar resistance (Figure 6-5b). The high field saturation

value of AH resistance for this particular cobalt film is close to 6Ω, which is one order of magnitude less than that of an iron film of similar resistance that had an AH resistance around 80Ω. Moreover, the slope of the Hall curve in the high field region is negative unlike iron, which had a positive slope. These findings are in agreement with existing data on bulk material [22], where iron and cobalt are known to exhibit hole-like and electron-like carriers respectively. The magnitude of the AH coefficient R_s [22] in bulk iron is about one order of magnitude higher than that of cobalt as shown in Table 6-2.

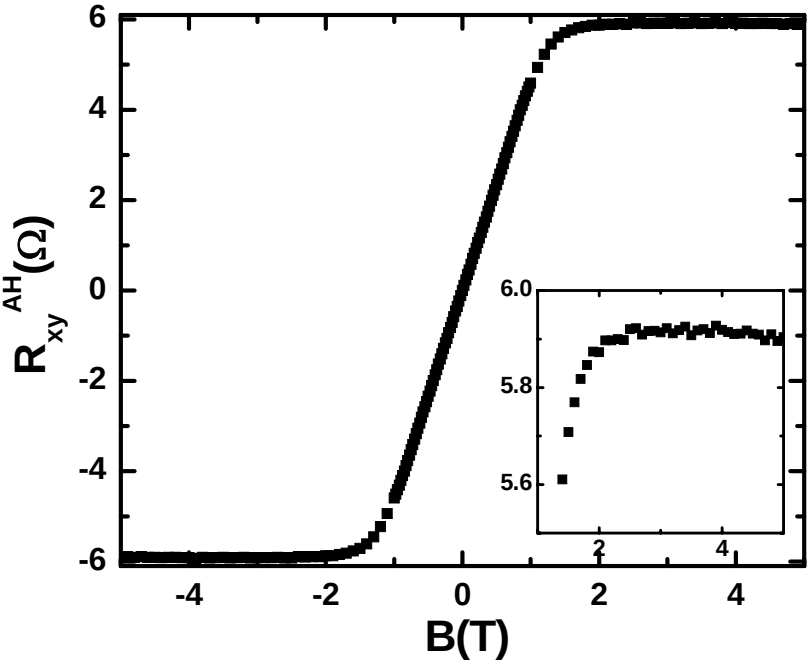

Figure 6-20:AH effect in a cobalt film with R_o=3200Ω at T=5K. Inset is a magnification of the high field region to emphasize the negative slope for the normal Hall effect.

Next we investigate the scaling behavior of R_{xx} and R_{xy}^{AH} for a particular film with varying temperature. For a cobalt film with R_o=756Ω, we found RR scaling behavior with logarithmic temperature dependence of R_{xx} and R_{xy}^{AH} with slopes $A_R \approx A_{AH} \approx 1$. For another cobalt film with R_o=3185Ω, we observed deviation from RR scaling with $A_R \approx 0.69$ and $A_{AH} \approx 0.391$, so that the logarithmic coefficient of AH conductivity

$2A_R - A_{AH} \approx 0.985$. We note that the above behavior is in agreement with our observations of the high resistance iron samples, where the prefactor A_R of the longitudinal conductivity deviates from unity as R_o increases beyond 3kΩ, but the prefactor ($2A_R$-A_{AH}) for AH conductivity does not change appreciably.

We measured the AH resistance of several cobalt films at $T=5K$ to find the dependence on R_o. Figure 6-21 shows a monotonic increase in R_{xy}^{AH} for $R_o<1000\Omega$, followed by a saturation at constant average value of R_{xy}^{AH} ~5.8Ω for R_o in the range of 1000-15000Ω. This leads to the important result that for both iron and cobalt polycrystalline films, the AH resistance ceases to increase and attains a constant value as the sheet resistance increases beyond some characteristic value of the order of $\hbar/e^2$≈4100Ω. However, we found that the value of the AH resistance in the high resistance regime depends on the material itself.

Table 6-2 quotes some important properties of bulk samples of iron and cobalt [22]. The anisotropy energy K_1, which is related to spin-orbit coupling strength in the material is about one order of magnitude higher for cobalt and than iron. Interestingly, the observed values of saturation of R_{xy}^{AH} in our experiments in the high resistance (ultra-thin) regime, is higher for iron(~80Ω) by about one order of magnitude than that of cobalt(~6Ω). The reported values of anomalous Hall coefficients R_s for bulk samples are also in agreement with the trend mentioned above. We note that the moments per atom [22] in bulk iron and cobalt are very close. These data emphasizes that although the AH resistance is proportional to magnetization, it is a magnetotransport property that depends

strongly on the spin-orbit coupling which in turn depends on band structure and other material dependent parameters.

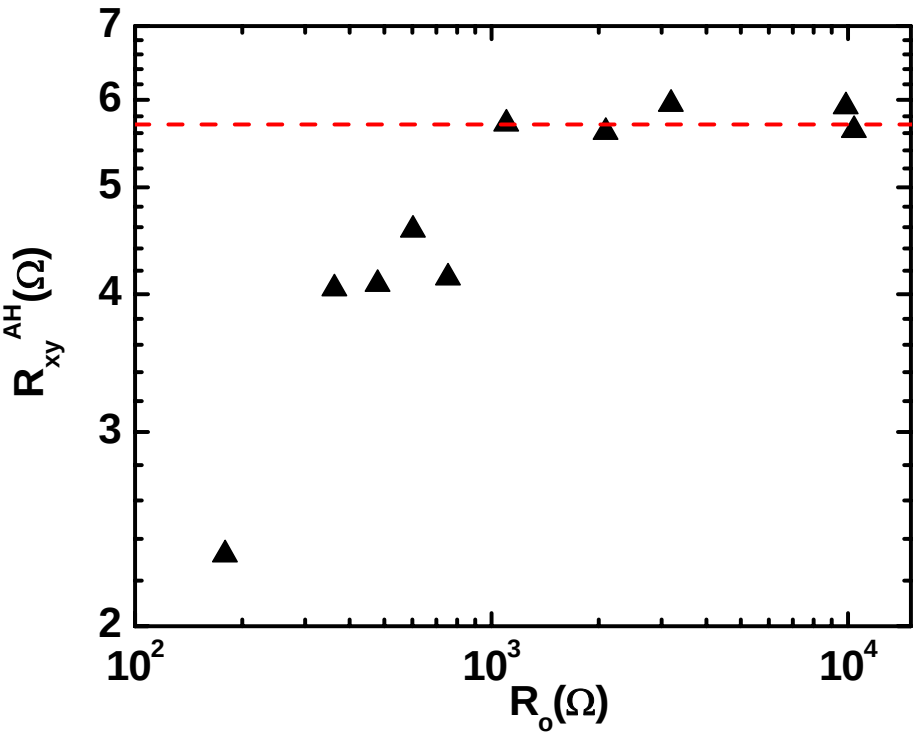

Figure 6-21:AH resistance for cobalt films as a function of R_o. The dashed line represents the average value for the AH resistance in the limit of high resistances.

Table 6-2:Comparison of some properties of bulk iron and cobalt. The last row quotes our results of AH resistance in ultra-thin films

	Iron	**Cobalt**
Moments per atom, M	$2.12\mu_B$	$1.72\mu_B$
Curie temperature, T_c	1043K	1404K
Anisotropy energy, K_1	$4.8X10^5$erg/cm^3	$41.2X10^5$ erg/cm^3
Anomalous Hall coefficient, R_s	$7.22X10^{-12}\Omega$cm/G	$0.24X10^{-12}\Omega$cm/G
Anomalous Hall resistance, R_{xy}^{AH}	80Ω	6Ω

Discussion of Experimental Results

Absence of Quantum Corrections to Hall Conductivity

We begin with the discussion of the previous experiment [48] by Bergmann and Ye, which focused on the low temperature quantum corrections to AH conductivity. The samples in this case are believed to have a different morphology compared to those grown for our experiments. Freshly grown antimony films around 10 atomic layers thick kept at liquid He temperature, were used as substrates, and iron films were then condensed on top by e-beam evaporation. The arriving adatoms on the cold substrate do not have enough energy to diffuse and form crystalline grains. They simply stick to the surface where they land. Hence, these quench-condensed films were believed to be amorphous, homogeneous and highly disordered. These films could not be heated above 20K because of irreversible transformations into crystalline form. The films reported in the experiments were in the thickness range of 2 to 10 atomic layers with corresponding sheet resistances R_o varying from 1900Ω to 500Ω. The magnitude of AH resistance was found to be higher than what we find for our polycrystalline films of similar resistance. For example, a film with R_o=1910Ω the AH resistance was reported to be of the order of 110Ω, almost double the value for our polycrystalline films with the same R_o.

The longitudinal conductivity L_{xx} of the quench condensed films showed a logarithmic decrease with temperature with the normalized prefactor A_R close to unity, in agreement with the results of our experiments on polycrystalline films with R_o<3000Ω. However, the important finding of Bergmann and Ye's investigation was that the logarithmic slope for the AH resistance $R_{xy}^{AH}(T)$ was twice the slope of the longitudinal resistance $R_{xx}(T)$. In terms of our notation this implies A_{AH}/A_R=2. This in turn implies

that the AH conductivity L_{xy}^{AH}, does not have a logarithmic temperature dependence because the prefactor ($2A_R$-A_{AH})=0. This is a consequence of inverse relationship between conductivity and resistivity tensor and is illustrated as follows:

$$\begin{aligned} & L_{xy}^{AH} \approx \frac{R_{xy}^{AH}}{R_{xx}^2} \Rightarrow \\ & \ln(L_{xy}^{AH}) = \ln(R_{xy}^{AH}) - 2\ln(R_{xx}) \Rightarrow \\ & \frac{\delta L_{xy}^{AH}}{L_{xy}^{AH}} = \frac{\delta R_{xy}^{AH}}{R_{xy}^{AH}} - 2\frac{\delta R_{xx}}{R_{xx}} \end{aligned} \qquad (6\text{-}16)$$

The above is a general relation, which is true under all circumstances. Thus experimental observation for the quench-condensed films that the slope of relative changes in $R_{xy}^{AH}(T)$ is twice the slope of the relative changes in $R_{xx}(T)$ directly implies the absence of temperature dependence in L_{xy}^{AH} as shown below,

$$\frac{\delta R_{xy}^{AH}}{R_{xy}^{AH}} = 2\frac{\delta R_{xx}}{R_{xx}} \Rightarrow \delta L_{xy}^{AH} = 0 \qquad (6\text{-}17)$$

It is known that in non-magnetic metals, the normal Hall conductivity does not have any finite quantum corrections due to electron interactions alone [36]. Thus, having ruled out the weak localization effects (explained below) it was concluded that the quantum corrections to the longitudinal conductivity L_{xx} arise due to electron interactions but the corresponding quantum corrections to L_{xy}^{AH} are zero. This is a surprising result that both the anomalous and the normal Hall effect behave similarly although they originate from different physical mechanisms.

Motivated by Bergmann and Ye's experimental results, theoretical calculations [47] were performed to include the effect of quantum corrections to L_{xy}^{AH}. The effect of weak

localization that arises from interference of coherent electronic wavefunctions was neglected in these systems because of the presence of strong spin-orbit scattering that destroys the phase coherence of electrons. The logarithmic temperature dependence of conductivity was attributed to the Coulomb anomaly that arises from interaction between conduction electrons in the presence of disorder. Many body calculations were carried out to include the exchange corrections to AH conductivity due to the short range electron-electron interaction, and the sum of all contributions, turned out to be zero, in agreement with the experimental findings. The corresponding Hartree terms were not included in the calculations as they are important only for the long range interaction. Thus the scaling behavior observed in quench-condensed films [48] was explained within the framework of short range electron interactions [47].

Finite Quantum Corrections to Hall Conductivity

For our polycrystalline films with R_o<3000Ω, which is the range of resistance for the quench-condensed films, we observed the relative resistance (RR) scaling behavior (Figure 6-8) for T<20 K where the relative changes in $R_{xx}(T)$ and $R_{xy}^{AH}(T)$ are exactly equal and using equation (6-16) it follows,

$$\begin{aligned} &\frac{\delta R_{xy}^{AH}}{R_{xy}^{AH}} = \frac{\delta R_{xx}}{R_{xx}} \Rightarrow \\ &\frac{\delta L_{xy}^{AH}}{L_{xy}^{AH}} = -\frac{\delta R_{xx}}{R_{xx}} = \frac{\delta L_{xx}}{L_{xx}} \end{aligned} \tag{6-18}$$

Thus we have a finite logarithmic temperature dependence of AH conductivity $L_{xy}^{AH}(T)$ and the relative changes in $L_{xy}^{AH}(T)$ equal in magnitude and sign to that of longitudinal conductivity $L_{xx}(T)$. According to present understandings of quantum theory of transport,

finite quantum corrections to normal Hall conductivity [36] can arise only from weak localization effects while the corrections due to electron interactions are zero. The weak localization theory predicts that the normal Hall coefficient R_n and hence the Hall resistance at a given field $R_{xy} = R_n B$ should be temperature independent. Hence, relative change in Hall conductivity should be twice that of the relative changes in conductivity itself, as explained earlier in chapter 5. The finite logarithmic slope for L_{xy}^{AH} in our samples raises the possibility of existence of weak localization corrections in AH effect.

We discussed earlier the case of short range interactions between conduction electrons in the presence of disorder, which gives rise to a logarithmic temperature dependence of conductivity for weak disorder and does not lead to any corrections to anomalous Hall conductivity [47]. We revisited the issue of effect of electron interactions to AH conductivity in the light of the new results obtained in our experiments, with the help of our theoretical collaborators [52]. We realized that in the earlier calculations [47] both impurity scattering and electron-electron interaction strength were considered only as first order perturbations. In good metals like iron, impurity scatterings are considered to be weak due to screening effects by other electrons, and first order perturbation theory turned out to be a good approximation. However, in the polycrystalline samples used in our experiments, scattering from grain boundaries and inter-grain tunneling processes dominates over the ordinary impurity scattering. The AH conductivity was recalculated [53] by treating the impurity scattering in all orders (strong scattering) with short range electron interactions. These calculations reveal that in the strong scattering limit, the coupling constants that determine the strength of potential and spin-orbit scattering are renormalized thus modifying the expression of AH conductivity for both skew scattering

and side jump mechanisms. However the surprising result[52] was that by including the effect of a short range electron interactions in the presence of strong impurity scattering to calculate the temperature dependent quantum corrections to the residual values of AH conductance, the sum of all contributions was found to be zero, just like the weak scattering scenario. Although some details still have to be worked out, the calculations suggest the existence of a profound gauge symmetry associated with electron interactions that leads to zero corrections to diagonal conductivity under all conditions. The Hartree terms are not considered as they are important only for long range interactions that are ruled out in good metals like iron. This is supported by the fact that the experimentally observed numerical prefactor for longitudinal conductivity A_R~1 over a wide range of resistances from 50-2000Ω, which is thought to be the universal exchange correction that does not depend on the details of interaction strength or sign, as discussed in chapter 5.

The quench-condensed films of Bergmann and Ye [48] were amorphous in nature and considered to be highly disordered with mean free path of the order of few angstroms. The phase relaxation time τ_φ due to spin-flips may be comparable to elastic scattering time τ ; thus completely quenching the weak localization effects. However having ruled out electron interactions as a source of the finite quantum corrections to AH conductivity we revisited the possibility of weak localization effects in our samples.

Assuming that the grains comprising our samples are good metals with crystalline structure and the overall resistance is determined by the tunnel barriers between grains. Even in the ideal limit of no impurities inside the grains, the electrons can undergo a diffusive motion due to specular scattering from grain boundaries. It was shown that in granular media [42] at low temperatures, $T < g_T \delta$, electrons can move coherently over

several grains where δ is the mean energy level spacing in the grains and g_T is a dimensionless inter-grain tunnel conductance. Thus it is possible for weak localization effects to be important in granular films. However, our films are ferromagnetic in nature and hence there exists a strong internal magnetic induction B_{int}~10^4T that is responsible for the polarization of conduction electrons giving rise to ferromagnetism. This B_{int} is a fictitious field that aligns spins but does not affect the orbital motion of the electrons and therefore should not affect the weak localization effects. In fact it was shown for the case of homogeneous itinerant ferromagnetic systems that the presence of strong internal magnetic field nullifies the effect [38] of strong spin-orbit scattering responsible for spin flip processes that lead to the so called "weak anti-localization". The results of these theoretical calculations [38] lead to weak localization corrections to conductivity similar to that in non-magnetic systems but modified to include two bands of up and down spin electrons.

With the above picture in mind, the interference corrections are calculated for strong impurity scattering with spin-orbit coupling and a finite correction to AH conductivity is obtained [52] with the numerical prefactor of the logarithmic temperature dependence close to unity . The weak localization correction to AH conductivity is further supported by the high temperature behavior (T>20K) as shown in Fig. 6-8, where the AH conductivity rapidly deviates from logarithmic behavior, probably due to phase relaxation of electrons from inelastic processes, like phonon scattering, that destroy interference effects. However, the resistance $R_{xx}(T)$ continues to exhibit a logarithmic behavior over a longer temperature range (Figure 6-8) , raising the possibility that the

mechanism for quantum corrections to longitudinal conductivity is different from that of AH conductivity.

Theoretically it is believed that the effect of weak localization and electron interactions are additive [35] and since both effects predict logarithmic temperature dependence, the numerical prefactor is simply the sum of individual prefactors. However, this fact has not been established with certainty in any experimental investigation. For example, in a previous magneto-transport study on palladium thin films [54], the normal Hall resistance was found to be independent of temperature, which according to current understanding indicates dominance of localization effects over interaction effects. This observation is made over the same temperature range where the resistance varies logarithmically with temperature. However such a conclusion was found to be inconsistent with the apparent need to include interaction effects to explain the zero field temperature dependence of resistance as in palladium spin-orbit scattering is known to be strong. We note that the films used in this investigation were grown on glass substrates at room temperatures by e-beam evaporation. We believe that these palladium films have a granular morphology similar to those in our experiments and arguments regarding the separation of quantum corrections for longitudinal and Hall conductivity is also applicable in this case.

We propose a novel mechanism to explain consistently the temperature dependence of both the longitudinal conductivity and the AH conductivity. We emphasize that the important feature of granular films is that the conductivity of each grain is much larger compared to tunneling conductivity between grains and hence the later dominates the longitudinal transport properties. However the AH conductivity is a property that arises

from the ferromagnetic nature of the grains and is affected by scattering processes within the grains and not the inter grain tunneling process. Thus if we track an electron in a granular film, the AH voltage is developed due to electron motion within the magnetic grains, while the longitudinal voltage drop that determines the resistance is predominantly across the tunnel barriers between the grains. The transverse Hall voltage in equilibrium (no current in transverse direction), is due to accumulation of static charges at the sample boundary and is unaffected by granular morphology.

Thus we propose that for the samples that exhibit RR scaling behavior, so that the relative change in longitudinal resistance R_{xx} and the AH resistance R_{xy}^{AH} are equal over the temperature range T=5-20K, the underlying mechanism responsible for the quantum corrections are different. The quantum corrections for longitudinal conductivity are due to electron interaction in granular metallic system as discussed in chapter 5, which is cutoff by temperature above a characteristic value on the order of $g_T\delta$. This temperature could be large for low resistance samples. The AH conductivity assumes quantum corrections that are due to weak localization effects associated with the diffusive motion of electrons within each grain and are destroyed either by inelastic processes like phonons at higher temperatures or by the inter-grain tunneling process depending on the tunnel resistance for that sample. For $R_o < \hbar / e^2$, and at low temperatures when phonon scatterings are quenched, conduction electrons can move coherently over several grains and loose their phase information due to electron interaction processes that determine the quantum corrections to longitudinal, thus resulting in RR scaling behavior. As temperature is raised, phonons inside the crystalline grains might destroy the phase coherence of electrons within the grain. Hence the weak localization corrections in AH

resistance are cutoff at characteristic temperatures due to phonons. The correction to longitudinal conductivity depends on the coherence of several tunneling processes, which are cutoff at characteristic temperatures that depend on the average grain sizes and tunnel barrier height given by the product $g_T\delta$.

The above explanation is also consistent with the data on high resistance samples with R_o>3000Ω. As shown in Fig. 6-11the relative change in AH resistance is unaffected by increasing resistance. In this situation the coherent motion of electrons that contribute to weak localization effects is confined to individual grains. Since the intrinsic nature of the iron grains does not change significantly with increasing R_o, the relative change in AH resistance is unaffected. However, with increasing resistance the average grain size <d> and the tunneling conductance becomes smaller. Thus the effect associated with charging of grains $E_C \sim -e^2/\langle d \rangle$ becomes increasingly important for the thinner films. We speculate that the charging effect of grains might introduce an unscreened long range Coulomb force in the system and thus the Hartree term in the expression for conductivity [35] given by $(1-\ln(1+F_0^\sigma)/F_0^\sigma)$, becomes important, where F_0^σ is the interaction parameter. A finite negative value of F_0^σ gives rise to a negative contribution from the Hartree terms and reduces the value of the coefficient from unity due to the exchange term [35]. This is a possible explanation of the deviation of A_R from unity at high resistances shown in Fig. 6-9a. We note that the effect of Coulomb forces due to charging of grains becomes prominent in the strongly disordered Fe/C_{60} samples where the conductivity rapidly diverges as given by equation (6-10) as predicted by theoretical calculations [44] that explicitly takes into account the effect of charging energy as an electron hops from one grain to another. The onset of the so called Coulomb blockade

happens for resistances of the order of $\hbar/e^2$ and results in the decrease in the value of A_R with increasing R_o and eventually reaches the hopping regime. However, the surprising observation is that even in the strongly disordered samples the AH resistance R_{xy}^{AH}, continues to vary logarithmically with temperature (Figure 6-17) and further consolidates our argument for a separation of inter and intra grain mechanisms affecting the longitudinal and AH resistances respectively.

We note here the results of a previous experiment on quench-condensed copper films [55] with resistance varying from 100Ω to 40000Ω, where the prefactor A_R was found to be close to unity over the entire range. These films are homogeneous and amorphous and exhibit the universal exchange correction to conductivity. The deviation of A_R from unity for our polycrystalline films at high resistances is probably due to granular morphology of the films where the Hartree terms could be important, as explained above.

We also note here that the deviation of A_{AH} from unity (Figure 6-9b) for the high resistance iron samples is due to the definition of normalized relative change in equation (6-6), where one divides the relative change in AH resistance by the low temperature resistance. Thus even though the relative change in the AH resistance does not change (Figure 6-11), A_{AH} decreases with increasing R_o.

Dependence of Anomalous Hall Conductivity on Disorder

So far we have discussed the scaling of longitudinal conductivity L_{xx} and AH conductivity L_{xy}^{AH} with respect to varying temperatures. Next we discuss another surprising result shown in Fig. 6-19, which exhibits the dependence of the magnitude of the low temperature (T=5K) value of AH resistance in our polycrystalline films on R_o. We observe an important crossover behavior near R_o~2000Ω. In the low resistance

regime, we observed a monotonic increase in the AH resistance with increasing R_o. However in the high resistance regime with R_o varying over a wide range from 2000Ω to 1MΩ, the magnitudes of the corresponding AH resistances attain a constant value $R_{xy}^{AH} = 80 \pm 10\Omega$. We emphasize that Fig. 6-19 is on a log-log scale and spans a considerably wide range of resistances starting from R_o~2000Ω where the samples are weakly disordered iron films with logarithmic temperature dependence to R_o~1MΩ where the Fe/C_{60} samples are strongly disordered exhibiting hopping transport behavior. A similar behavior was also observed in cobalt Fig. 6-20, where the AH resistance was found to saturate at $R_{xy}^{AH} = 6 \pm 1\Omega$ as R_o varied from 1000Ω to 10000Ω.

Our observation that R_{xy}^{AH} attains a constant value while R_o increases can be expressed in terms of conductivities as shown in Fig. 6-22 for iron and Fig. 6-23 for cobalt. In both figures we have plotted on log-log scale the AH conductivity L_{xy}^{AH} as a function of longitudinal conductivity L_{xx} in units of the quantum of conductance L_{00}. We found that for both iron and cobalt films, as L_{xx} of the films decreases (resistance increases), the corresponding L_{xy}^{AH} also decreases and the data fit to a straight line as shown by dashed lines. The corresponding slopes (shown in inset) for both iron and cobalt are found to be close to 2. Thus we conclude that, in the limit of decreasing conductance of the sample i.e. $L_{xx} \to 0$, the AH conductance also decreases $L_{xy}^{AH} \to 0$, but the approach to zero happens at different rates so that

$$L_{xy}^{AH} \propto L_{xx}^2 \Rightarrow R_{xy}^{AH} = \frac{L_{xy}^{AH}}{L_{xx}^2} = const. \qquad (6\text{-}19)$$

The behavior described in the equation (6-19) has been discussed theoretically [56] and verified experimentally in two dimensional electron gas [57] in the context of quantum Hall effect and is known as a "Hall Insulator". We note that in the measurement of the quantum Hall effect one is measuring the normal Hall effect in very high magnetic fields. Our AH measurements on disordered itinerant ferromagnets reflect distinctly different physics. We denote the behavior described by equation (6-19) as the "anomalous Hall insulator".

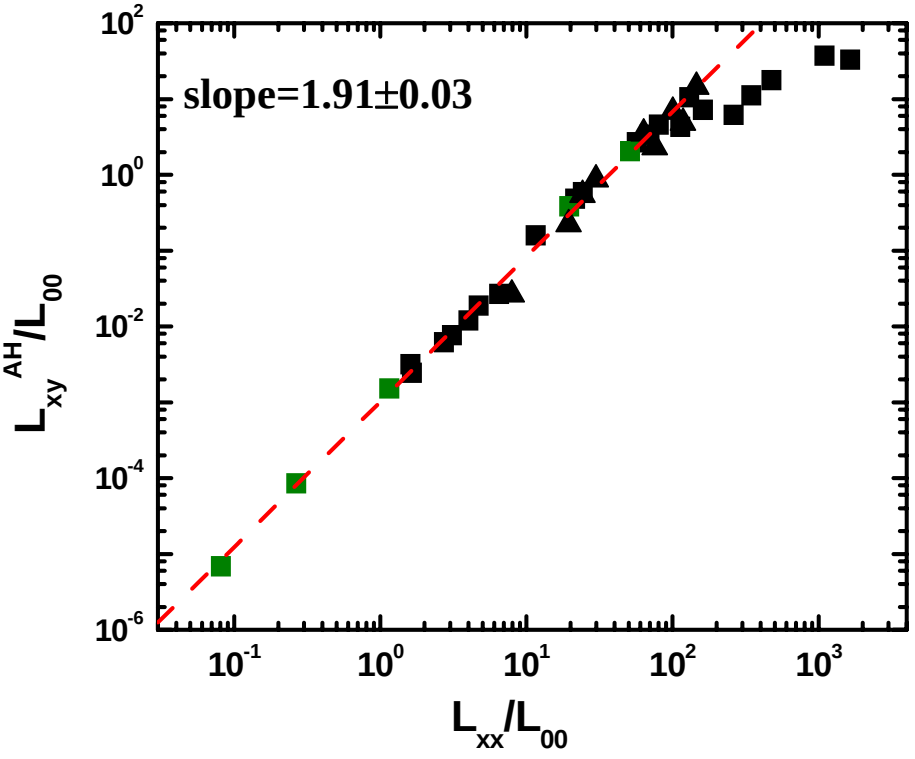

Figure 6-22:The anomalous Hall conductivity vs longitudinal conductivity in units of quantum of conductance L_{00} for iron films on a log-log plot. Triangular data points represents ion-milled iron films. Green square points represents Fe/C_{60} samples. The red dashed line represents the linear fit for the high resistance samples with slope =1.92 ±0.03 and intercept ~80±10Ω.

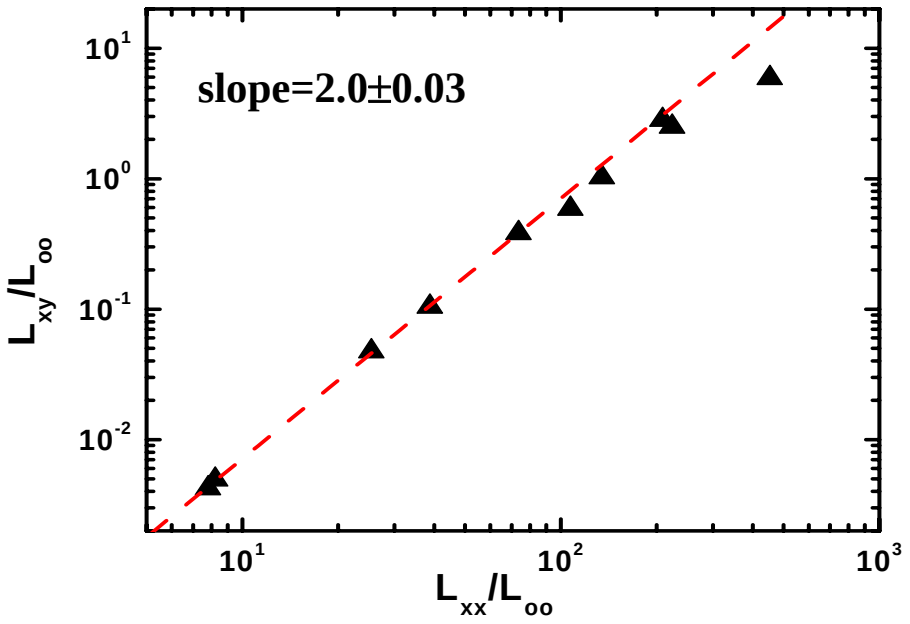

Figure 6-23: The anomalous Hall conductivity vs longitudinal conductivity in units of quantum of conductance L_{00} for cobalt films on a log-log plot. The red dashed line represents the linear fit for the high resistance samples with slope =2.0±0.03 and intercept =6±1Ω.

The various microscopic mechanisms for AH effect discussed in chapter 4 assume that at low temperatures, when impurity scattering is the dominant mechanism, each impurity is responsible for both potential scattering and skew scattering due to spin-orbit scattering. These theories predict a monotonic dependence of the AH resistance on the sheet resistance of the form $R_{xy}^{AH} \sim R_{xx}^{\alpha} M$, where $\alpha = 1,2$. However, as we have discussed in the previous section, granular films provide a unique situation where the dominant scattering mechanism determining resistance and AH resistance are different especially at high resistances. The fact that R_{xy}^{AH} assumes a value independent of the resistance is a manifestation of the fact that with increasing R_o, the average inter-grain coupling gets weaker, but the intrinsic ferromagnetic nature of the grains comprising the films does not change significantly.

A refined theoretical model for the residual AH conductivity [53] that might be relevant in granular samples would be to consider two sets of scattering centers in the system: one is the normal potential scattering centers that do not give rise to skew scattering with concentration N_n and the other is the set of scattering centers that gives rise to skew scattering with concentration N_m. In the limit that the skew scattering is weak and the normal scattering is strong and hence determines the mean free path, it was shown by Muttallib and Wolfle [53] that the AH conductivity for skew scattering mechanism is given by

$$\sigma_{xy}^{AH(SS)} \sim \frac{N_m}{N_n^2} \tag{6-20}$$

and for side jump mechanism

$$\sigma_{xy}^{AH(SJ)} \sim \frac{N_m}{N_n} \tag{6-21}$$

The longitudinal conductivity in this model is not affected by the weak skew scattering processes and has the usual Drude kind of dependence due to the potential scattering centers and is given by

$$\sigma_{xx} \sim 1/N_n \tag{6-22}$$

The above dependences for AH conductivity on the impurity concentrations are different from those obtained earlier in the framework of skew scattering [25] and side jump mechanism [27]. In our model of granular ferromagnetic films, we assume that the properties of individual grain do not change with increasing resistance. This is equivalent to saying that N_m remains unchanged as resistance increases. Thus it follows from equations (6-20) and (6-21) that for skew scattering mechanism, the scaling behavior $\sigma_{xy}^{AH} \sim \sigma_{xx}^2$ appears naturally implying that R_{xy}^{AH} is independent of R_{xx}.

Now we briefly discuss a previous experiment by Lee *et.al*. [58] on metallic ferromagnetic copper-chromium selenide spinel $CuCr_2Se_4$ that addresses an important issue of whether the AH current due to the Berry phase mechanism[28] is dissipationless, i.e. independent of impurity concentration. The magnetic moments in this spinel compound are localized on the chromium atoms and the coupling between the moments is due to superexchange along Cr-Se-Cr bonds. A series of these spinel compounds were grown by chemical vapor deposition and Se atoms were systematically substituted by Br atoms to form $CuCr_2Se_{4-x}Br_x$, without significantly changing the saturation magnetization. However, as *x* varies from 0 to 0.85, the low temperature resistivity increases by factor of 270, which was attributed predominantly due to increase in impurity scattering rate $1/\tau$ and partly due to a decrease in the hole density. It was shown that by varying the resistivity ρ_{xx} of the samples over several decades, the AH resistivity ρ_{xy}^{AH} at *T*=5K for each of the samples normalized by the hole density n_H obeys the relation $\left|\rho_{xy}^{AH}\right| / n_H \sim \rho_{xx}^2$, implying that the normalized AH conductivity σ_{xy}^{AH} / n_H at *T*=5K is independent of impurities and probably has an origin of a topological nature[28].

The above result is different from our results where we find the AH conductivity tends to zero with increasing resistance. We note the important distinctions between Lee *et. al*. experiment and ours. The spinel compounds are not itinerant ferromagnets unlike our iron films. The resistance in the spinel samples was varied by changing the impurity concentration, whereas in our experiments we are changing the inter grain tunnel resistance without significantly changing the intrinsic grain properties like impurity concentration. Moreover we note that the resistivity of the spinel samples were less than

200μΩcm, which is close to the Mooij limit [50], unlike our samples where the resistivity is inferred to be much higher than 100μΩcm.

Anomalous Hall Response in Fe/C_{60} Films

So far we have discussed experimental evidence for a crossover in the magneto-transport properties in granular ferromagnetic films around a sheet resistance of the order of $\hbar/e^2$. The crossover is a manifestation of granular morphology of our films that results in a separation of intra-grain mechanism that affect the AH resistance from the inter grain processes that affect the longitudinal resistance. This leads to the anomalous Hall insulating behavior, where the AH resistance R_{xy}^{AH} remains constant while the sheet resistance of the samples varies over a wide range from the weakly disordered regime to the strongly disordered hopping regime. Although the anomalous Hall insulating behavior is found to hold for films resistances up to 1MΩ, the question remains open whether this behavior holds for arbitrarily high resistances or breaks down at some characteristic resistance much larger than $\hbar/e^2$. This question is related to our initial motivation to understand the nature of magnetism in itinerant ferromagnets in the limit of zero conductivity. We wanted to find out if the Stoner criterion [6] for the occurrence of band ferromagnetism breaks down in the limit of high resistance when the conduction electrons are increasingly localized as in a strongly disordered samples and conduction is via hoping between localized states.

The existence of a superparamagnetic response in thin ferromagnetic systems consisting of weakly interacting magnetic clusters has been established in several investigations [59-61], using SQUID measurements. The magnetization curves at a given temperature as a function of applied magnetic field *B* exhibit a Langevin dependence,

obey the characteristic *B/T* scaling behavior and show no hysteresis below a characteristic blocking temperature T_B related to the volume of individual magnetic grains. The conventional view of a paramagnetic response is that lowering temperature or increasing the magnetic field should increase the magnetic order in the system. This is the basis of *B/T* scaling behavior in paramagnetic systems where the magnetization curves at different temperatures collapse onto one curve when plotted as function of *B/T*.

Our high resistance (>50kΩ) Fe/C_{60} films consist of isolated weakly coupled ferromagnetic grains as supported by data on transport and magnetoresistance properties. In our experiments we could not measure directly the magnetization of the films using SQUID or any equivalent method, which are thermodynamic measurements of volume magnetization. Instead we have performed AH measurements, which are essentially a transport measurement where, by introducing a charge current through the sample and relying on the spin-orbit coupling between the itinerant electrons and volume magnetization *M*, we measure a transverse voltage that is proportional to *M*.

The AH curves for our strongly disordered Fe/C_{60} samples, as a function of applied field fit to a high degree of accuracy to Langevin function (equation 6-12) as shown by the solid lines in Fig. 6-14, further supporting the picture of isolated magnetic particles and absence of long range ferromagnetic order. However in a strongly disordered film, as temperature is lowered, in addition to increasing magnetic order between isolated magnetic grains, there is an opposing process of the quenching of itinerancy of conduction electrons which leads to a rapid increase in the resistance. This manifests itself in the systematic analysis of the Langevin coefficient γ defined in equation (6-13), which is found to decrease linearly with inverse temperature as described by equation (6-

14). As temperature is lowered and approaches a characteristic temperature T_J, the coefficient γ also decreases, which implies that one needs to apply a stronger magnetic field to saturate the AH response. However at $T=T_J$, the AH response will always be zero irrespective of the applied magnetic field, thus signaling a possible phase transition. We note that to demonstrate the anomalous Hall insulating behavior in the Fe/C_{60} samples we have used the AH resistance as the phenomenological fitting parameter R_{xy}^{o}, which is independent of applied field. We emphasize that this is a valid procedure as long as $T>T_J$. Thus our results suggest that the anomalous Hall insulating behavior holds only for resistances lower than R_J determined by extrapolating equation (6-10) to T_J. R_J is a new resistance scale and as shown in Table 6-1 has values much larger than $\hbar/e^2 \approx 4100\Omega$. For higher resistances $R>R_J$ there will be no AH effect. We note that the trend of decreasing γ with decreasing temperature starts at relatively high temperatures of the order of 100K, thus allowing us to estimate T_J even from high temperature measurement, where the Hall signal can be measured with greater accuracy.

CHAPTER 7
SUMMARY AND FUTURE WORK

In this dissertation we address an unsettled issue regarding itinerant ferromagnetic exchange known to exist in the transition metal elements (iron, cobalt, nickel) and investigate the nature of magnetic ordering in ultrathin films of these materials as the conduction electrons are progressively localized due to increasing disorder. We have presented a systematic *in situ* magnetotransport study on a series of Fe, Co and Fe/C_{60} films with sheet resistances varying over a wide range of 100Ω to 1MΩ. These films are believed to consist of polycrystalline metallic grains of very low resistance and the sheet resistance in these films is a measure of average inter-grain tunneling resistance. We investigate the magnetic properties of these films by monitoring the anomalous Hall (AH) effect, which is the transverse potential proportional to the volume magnetization in response to a longitudinal charge current. Our results provide strong evidence that due to the granular morphology of the films, the microscopic scattering mechanisms that affect the electrical conduction and band ferromagnetism are different and lead to unusual properties that may seem counterintuitive in the light of existing theories on homogeneous systems.

The temperature dependence of longitudinal electrical conductance in iron films exhibits a crossover in behavior around a sheet resistance of the order of $\hbar / e^2 \approx 4100\Omega$. For resistances below the crossover value, the films show weakly disordered behavior with logarithmic temperature dependence and a universal prefactor of unity arising from the exchange interaction between conduction electrons. For resistances above the

crossover, the logarithmic prefactor was found to systematically decrease from unity. We propose that as the inter-grain coupling becomes progressively weaker with increasing resistance of the sample, the electrostatic energy associated with the charging of grains as an electron hops from one grain to another assumes an unscreened long-range character. This leads to a finite contribution from the Hartree term in the expression for conductivity which is opposite in sign to that of the exchange correction, thus explaining the decrease in the value of logarithmic prefactor from unity due to the universal exchange correction. The high resistance iron samples (>50kΩ) were grown on a monolayer of C_{60} to increase film stability and exhibited Coulomb blockade with an exponential of $T^{1/2}$ increase in resistance.

The granular morphology of the films manifests itself in the relative scaling behavior of the longitudinal resistance (R_{xx}) and AH resistance (R_{xy}^{AH}) as temperature is varied in the range 5-20K. For resistances less than $\hbar / e^2$, we find a unique scaling behavior in which the relative changes in R_{xx} and R_{xy}^{AH} are equal with logarithmic prefactors close to unity. However for temperatures above 20K, R_{xy}^{AH} deviates from logarithmic behavior and decreases at a faster rate compared to R_{xx}, which continues to exhibit logarithmic behavior to higher temperatures. We propose a model in which the AH resistance derives from quantum corrections arising from weak localization effects associated with the diffusive motion of electrons inside the grains. These contributions are suppressed at higher temperatures by inelastic process such as phonon scattering. The longitudinal resistance, on the other hand, is dominated by Coulomb interaction effects

associated with charging of grains due to inter-grain tunneling processes, which are cut off at relatively higher temperatures that depend on grain size and tunnel resistance[42].

For resistances higher than $\hbar / e^2$, the scaling behavior described above breaks down. The striking observation in this regime is that the temperature dependent relative changes in R_{xy}^{AH} for different samples do not show any significant differences from each other while the residual resistance R_{xx} at T=5K varies over a wide range of 3kΩ to 50kΩ and the corresponding relative changes in R_{xx} systematically increase. We argue that the increasing residual resistance is due to the weakening of coupling between grains. While the grain sizes may be smaller for a thinner film with higher resistance, the intrinsic ferromagnetic properties of individual grains that determine the AH resistance do not change significantly. This argument is also consistent with our data on the dependence of the AH resistance on the residual resistance as discussed below.

The AH resistance at T=5K for iron samples was found to increase monotonically with increasing resistance until around 2kΩ when the AH resistance ceases to increase any further. In the high resistance regime $R_o >> \hbar / e^2$ including the strongly disordered Fe/C_{60} films, the AH resistance is found be constant with an average value near 80Ω, while the longitudinal residual resistance is varied over several decades from 3kΩ to 1MΩ. Similar observations have been made in cobalt films where the AH resistance remains constant around 6Ω while the longitudinal resistance varies from 1kΩ to 10kΩ. This is the "anomalous Hall insulating" behavior where the Hall resistance remains finite in the limit of conductivity approaching zero. The fact that the iron and cobalt samples saturate at different values of the AH resistance reveals an important aspect of our AH

measurements, that is, although the AH effect is proportional to volume magnetization, the proportionality constant is a transport property depending on the strength of the spin-orbit coupling in each material. The magnitudes of the magnetization per atom of iron and cobalt as measured in SQUID magnetometers are found to be very close to each other. However the anisotropy energy K_1 for cobalt is one order of magnitude higher than that of iron. Both K_1 and the AH effect are related to spin orbit coupling in the material which explains the difference in the magnitude of R_{xy}^{AH} for iron and cobalt.

Although the Hall insulating behavior is found to hold for strongly disordered samples with resistances as high as 1MΩ, the question remains open whether these trends will continue to be obeyed for films with arbitrarily low conductance where they become indistinguishable from insulators. To shed some light on this possibility, we performed a detailed analysis of the dependence on field and temperature of the AH curves for strongly disordered Fe/C_{60} films. At each temperature, the AH curves as a function of magnetic applied field B, were found to obey the classical paramagnetic response described by the Langevin function $R_{xy}^{0}(\coth(\gamma B) - 1/\gamma B)$, indicating the presence of isolated magnetic clusters and the absence of ferromagnetic coupling between them. However the argument of the Langevin function γ extracted from the fits showed a linear decrease with inverse temperature and points toward a characteristic low temperature T_J where the coefficient will be zero. This trend is opposite to that expected in the magnetization response of a paramagnetic or superparamagnetic system, where the coefficient of the Langevin function is known to increase linearly with inverse temperature. The extrapolation of the coefficient γ to zero at some characteristic low temperature $T = T_J$ implies that the AH resistance will be identically zero irrespective of

the applied magnetic field. Thus for a sample characterized by given grain sizes and tunneling resistance, there is a certain temperature and hence resistance when the magnetic order as measured by AH resistance is destroyed. The anomalous Hall insulating behavior will only hold for resistances less than an extrapolated resistance R_J determined by the temperature T_J. An important point is that the trend towards vanishing γ begins at relatively high temperature and one can therefore make an estimate of T_J and R_J from high temperature measurements. The existence of a sample-dependent resistance R_J that is orders of magnitude higher than $\hbar/e^2$ and which delineates a pronounced disappearance of ferromagnetism as measured by the AH effect is unexpected and to our knowledge has not been anticipated for highly disordered itinerant ferromagnets.

We have presented new results on the magnetotransport properties of thin ferromagnetic films and provided preliminary explanation of several apparent unusual behaviors by taking into account the granular nature of the samples. Transport properties of granular media have drawn considerable attention in recent times, although a complete and well-established theoretical understanding is yet to be achieved. A simple way to test the validity of our arguments based on granularity of the sample is to perform a similar experiment on films that are homogeneous and reproduce the results previously reported by Bergmann and Ye [48]. This can likely be achieved by choosing suitable substrates and/or different growth conditions. A popular method of growing homogeneous films is to maintain the substrate at very low temperatures during growth, during which the arriving atoms simply condense onto the substrate without having enough energy to diffuse and form crystalline grains. In our experimental set up it is difficult to cool down the sample receiver efficiently for growing samples via quench-condensation. However

one can also choose a different material that can be grown in both granular and homogeneous forms with similar properties. For example, depending on the substrate temperature, manganite materials [62] with ferromagnetic properties can be grown in both granular and homogeneous forms. The manganites have the added advantage of not being air sensitive like iron or cobalt; hence they can be easily measured and differences in the properties, if any, in the two cases can be attributed to morphology.

In this dissertation we tried to understand how band ferromagnetism is affected by increasing disorder by reducing the film thickness. Another important route to address this question is by changing the density of charge carriers in the films by the field effect and monitor the changes in AH resistances. The field effect experiments are performed in a capacitor geometry, where conducting "gate" electrode is separated from the film under observation by a layer of dielectric. By applying a potential across the gate and film one can change the carrier density in the films, the induced charge density being limited by the breakdown voltage of the dielectric. Field effect experiments are prominent only in low conductivity systems where carrier density can be modulated significantly with experimentally achievable induced charges. As a possible low carrier density material, we propose the use of iron/C_{60} bilayers that exhibit prominent magnetic ordering as measured by the AH effect. Using degenerately doped silicon as the gate electrode, the native silicon oxide as the dielectric, and the Fe/C_{60} bilayer as the top layer, a simple field effect device suitable for experiments can be realized. It will be quite interesting to investigate how the AH effect varies as the carriers are systematically depleted from the film.

Another interesting experiment would be to systematically study the AH effect in ferromagnetic metals with localized moments, e.g., gadolinium, and look for a similar high resistance scale where the AH resistance disappears. The exchange mechanisms for band ferromagnets like iron and Heisenberg ferromagnets like gadolinium are quite different and might yield additional results that will shed more light on the microscopic origin of magnetism in metals.

LIST OF REFERENCES

[1] G.A. Prinz, Science **282**, 1660 (1998).

[2] C.M. Hurd, *The Hall effect in metals and alloys* (Plenum Press, New York, 1972).

[3] J.E. Hirsch, Physical Review Letters **83**, 1834 (1999).

[4] Y.K. Kato, R.C. Myers, A.C. Gossard, and D. D. Awschalom, Science Express, 1105514 (2004).

[5] P. Zhang, J. Shi, D. Xiao, and Q. Niu, condmat 0503505 (2005).

[6] E.C. Stoner, *Magnetism and matter* (Methuen, London, 1934).

[7] A.R. Gonzalez-Elipe, F. Yubero, and J.M. Sanz, *Low energy ion assisted film growth* (Imperial College Press, distributed by World Scientific Publishing Co, 2003).

[8] M. Ritter, M. Stindtmann, M. Farle, and K. Baberschke, Surface Science **348**, 243 (1996).

[9] S. Rusponi, G. Costantini, F.B. de Mongeot, C. Boragno, and U.V.Valbusa, Applied Physics Letters **75**, 3318 (1999).

[10] T.M. Mayer, E. Chason, and A.J. Howard, Journal of Applied Physics **76**, 1633 (1994).

[11] J. Erlebacher, M.J. Aziz, E. Chason, M.B. Sinclair, and J.A. Floro, Physical Review Letters **84**, 5800 (2000).

[12] S.O. Demokritov, C. Bayer, S. Poppe, M. Rickart, J. Fassbender, B. Hillebrands, D.I. Kholin, N.M. Kreines, and O.M. Liedke, Physical Review Letters **90**, 097201/1 (2003).

[13] D. Stein, Li Jiali, and J.A. Golovchenko, Physical Review Letters **89**, 276106/1 (2002).

[14] L.J. van der Pauw, Phillips Technical Review **26**, 220 (1958).

[15] G.T.Kim, J.G. Park, Y.M.Park, C. Muller-Schwanneke, M. Wagenhals, and S. Roth, Review of Scientific Instruments **70**, 2177 (1999).

[16] P.Mitra and A.F.Hebard, Applied Physics Letters **86**, 063108 (2005).

[17] K. Fuchs, Proceedings Cambridge Philosophical Society **34**, 100 (1938).

[18] E.H. Sondheimer, Advances Physics **1**, 1 (1952).

[19] B.N.J. Persson, Physical Review B. **44**, 3277 (1991).

[20] S.G.Mayr and R.S. Averback, Physical Review B (Condensed Matter and Materials Physics) **68**, 75419 (2003).

[21] A. F. Hebard, R. R. Ruel, and C. B. Eom, Physical Review B **54**, 14052 (1996).

[22] E.P. Wohlfarth, *Ferromagnetic materials* (North-Holland, Amsterdam, 1980).

[23] B.D. Cullity, *Introduction to magnetic materials* (Addision-Wesley, New York, 1972).

[24] V.K. Dugaev, A. Crepieux, and P. Bruno, Physical Review B, 104411 (2001).

[25] J. Smit, Physica (Amsterdam) **21**, 877 (1955).

[26] J. Smit, Physical Review B **8**, 2349 (1973).

[27] L. Berger, Physical Review B **2**, 4559 (1970).

[28] R. Karplus and J.M. Luttinger, Physical Review **95**, 1154 (1954).

[29] M. Onada and N. Nagaosa, Journal of Physical Society of Japan **71**, 19 (2002).

[30] G. Sundaram and Q. Niu, Physical Review B **59**, 14915 (1999).

[31] T. Kasua, Progress in Theoretical Physics(Japan) **16**, 45 (1956).

[32] J. Kondo, Progress in Theoretical Physics(Japan) **27**, 772 (1962).

[33] F.E. Maranzana, Physical Review **160**, 421 (1967).

[34] P.A. Lee and T.V. Ramakrishnan, Reviews of Modern Physics **57**, 287 (1985).

[35] B.L. Altshuler and A. G. Aronov, edited by A. L. Efros and M. Pollok (North-Holland, Amsterdam,1985).

[36] B.L. Altshuler, D. Khmel'nitzkii, A.I. Larkin, and P.A. Lee, Physical Review B **20**, 5142 (1980).

[37] S.Hikami, A.I. Larkin, and y.Nagaoka, Progress in Theoretical Physics Letters **63**, 707 (1980).

[38] V.K. Dugaev, P. Bruno, and J. Barnas, Physical Review B **64**, 14423 (2001).

[39] G. Zala, B.N. Narozhny, and I.L. Aleiner, Physical Review B **64**, 214204 (2001).

[40] C. Castellani, C. DiCastro, P.A. Lee, and M. Ma, Physical Review B **30**, 527 (1984).

[41] B.L. Altshuler and A.G. Aronov, Solid State Communication **46**, 429 (1983).

[42] I.S. Beloborodov, K.B. Efetov, A.V. Lopatin, and V.M. Vinokur, Physical Review Letters **91**, 246801 (2003).

[43] V. Ambegaokar, U. Eckern, and G. Schon, Physical Review Letters **48**, 1745 (1982).

[44] P. Sheng, B. Abeles, and Y. Arie, Physical Review Letters **31**, 44 (1973).

[45] J.S. Helman and B. Abeles, Physical Review Letters **22**, 1429 (1976).

[46] H. Fukuyama, Journal of Physical Society of Japan **49**, 64 (1980).

[47] A. Langenfeld and P. Wolfle, Physical Review Letters **67**, 739 (1991).

[48] G. Bergmann and F. Ye, Physical Review Letters **67**, 735 (1991).

[49] L.I. Maissel and R. Glang, *Handbook of thin film technology* (McGraw Hill Book Company, New York, 1970).

[50] J.H. Mooij, Phys. Status Solidi A **17**, 521 (1973).

[51] C.C. Tsuei, Physical Review Letters **57**, 1943 (1986).

[52] K. Muttalib, Private communication (2005).

[53] P. Wolfle and K. A. Muttalib, condmat 0510481 (2005).

[54] W.C. McGinnis and P.M. Chaikin, Physical Review B **32**, 6319 (1985).

[55] H. White and G. Bergmann, Physical Review B **40**, 11594 (1989).

[56] S. Kivelson, D.H. Lee, and S.C. Zhang, Physical Review B **46**, 2223 (1992).

[57] M. Hike, D. Shahar, S.H. Song, D.C. Tsui, Y.H. Xie, and D. Monroe, Nature **395**, 675 (1998).

[58] W. Lee, S. Watauchi, V.L. Miller, R.J. Cava, and N. P. Ong, Science **303**, 1647 (2004).

[59] A. Frydman, T.L. Kirk, and R.C. Dynes, Solid State Communication **114**, 481 (2000).

[60] C. Binns and M.J. Maher, New Journal of Physics **4**, 85.1 (2002).

[61] Y. Park, S. Adenwalla, G.P. Felcher, and S.D. Bader, Physical Review B **52**, 12779 (1995).

[62] A. Biswas, Physical Review B **61**, 9665 (2000).

BIOGRAPHICAL SKETCH

The author is the first child of Mr. Prabhat Kumar Mitra and Mrs. Ratna Mitra, born on 8th May 1976 in the great city of Calcutta, located in the eastern part of India. He grew up in his 150 years old ancestral house in a small town called Halisahar, around 40km north of Calcutta. Just like most small town kids the author had his own share of climbing trees, fishing, swimming, biking and several other cherished memories. At a very young age his father introduced him to the wonderful world of books during a visit to the Calcutta book fair. By the time the author was in high school he was the proud owner of a small library of science books, many of which were from Russia. He went to school in the neighboring town of Kalyani where he used to bike everyday and made many friends. His father was the only tutor he had on all subjects, till his tenth standard. He got interested in physics in particular among other science subjects during his high school days and where he found a wonderful physics teacher, Mr. Misra. He joined Jadavpur University in Calcutta in 1993 for undergraduate studies and graduated with a Bachelor of Science degree with honors in physics in the summer of 1996. The author showed keen interest in the laboratory classes and was well known among his friends for his ability to troubleshoot. During his final year at J.U., he took a course on advanced condensed matter physics, where he was exposed to various topics in contemporary physics like superconductivity, superfluidity, NMR, etc. and decided to pursue advanced studies in this field. He then joined the Physics Department of the Indian Institute of Science for post–graduate studies after being selected for the Integrated PhD program.

He received the Master of Physical Sciences degree in 1999 with a thesis on experimental soft condensed matter under Prof. Ajay Sood. The education and research experience at IISc were extremely fruitful and gave the author confidence to explore new and better career opportunities outside of India. He joined the graduate program at the University of Florida in the Fall of 2000 for pursuing a PhD degree in physics. During a casual “meet the faculty session” followed by a lab tour, the author came in touch with Prof. Art Hebard and found a kindhearted gentleman as supervisor and one of the most resourceful labs and a very enthusiastic group in the department. During the summer of 2004 fate brought him to close to a wonderful and friendly soul, Mahasweta, and eventually they got married in the winter of same year. The author is considered to be very quiet and taciturn person and believes in using his ears more than his voice. He is also particularly interested in cooking and watching movies.